Morphological and functional characterisation of non-fast spiking interneurons in layer 4 microcircuitry of rat barrel cortex

Von der Fakultät für Mathematik, Informatik und Naturwissenschaften der RWTH Aachen University zur Erlangung des akademischen Grades einer Doktorin der Naturwissenschaften genehmigte Dissertation

vorgelegt von

Master of Science

Vishalini Sivarajan

aus Chennai, Indien

Berichter: Universitätsprofessor Dr.rer.nat. Dirk Feldmeyer

Universitätsprofessor Dr.rer.nat. Björn Kampa

Tag der mündlichen Prüfung: 22. February 2017

துன்பம் உறவரினும் செய்க துணிவாற்றி
இன்பம் பயக்கும் வினை.
However great the hardship, Pursue with firmness the act that yields bliss.

- Thiruvalluvar, Kural (Verse 669), circa 200 BCE

To my family

Contents

1. Introduction

1.1. The mammalian neocortex

The neocortex is one of the distinctive features of the mammalian brain that consists of six distinguishable layers. The neocortex is the evolutionarily newest part of the cerebral cortex, which constitutes 90% of the cerebral cortex in humans *(Nieuwenhuys R et al. 1998)*. The evolution of neocortex in mammals is regarded as a paramount development that promoted the higher cognitive function *(Baumgartner G 1983; Mountcastle V 1995; Northcutt RG and JH Kaas 1995; Smart IH 2008)*.

Parcellation of the neocortex

A key feature of the mammalian neocortex is that it is sub-divided into multiple areas. The delineation of the cortical areas was observed in preparations stained for cell bodies (Nissl technique *(Nissl F 1894)*) and the distribution pattern of myelinated fibres in preparations stained for myelin sheath (Weigert technique *(Weigert C 1885)*). Among several maps of the human cortex based on the parcellation of the neocortex, Brodmann's map by Korbinian Brodmann became the most famous parcellation, which sub-divides the human cerebral cortex into 52 areas *(Brodmann K 1909)* **(Fig. 1.1)**. Despite many advances in the field of neuroscience, Brodmann's map is still widely used to designate functional regions in the cortex *(Loukas M et al. 2011)*. Regions in the neocortex with

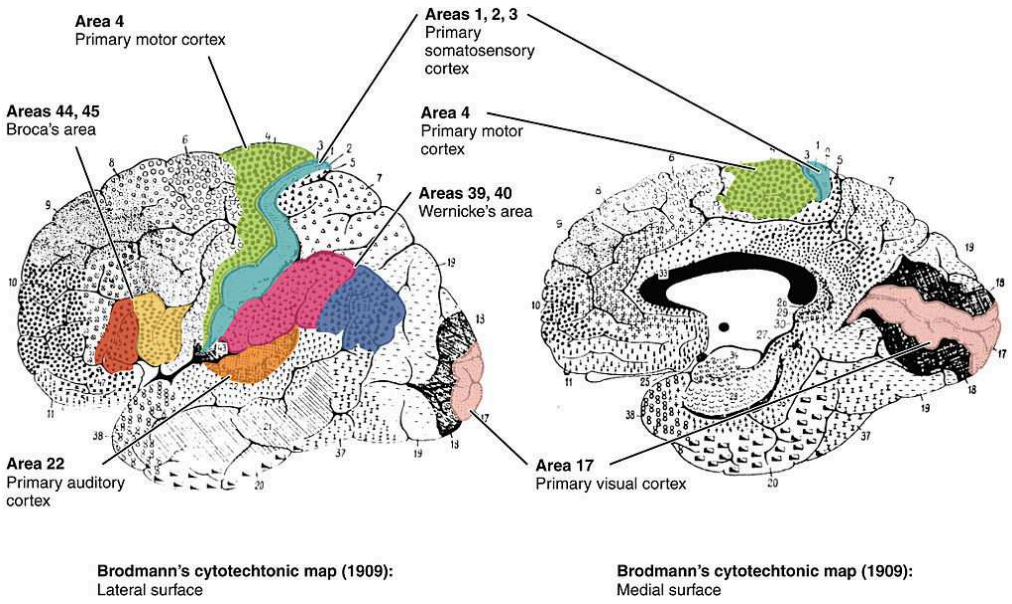

Fig. 1.1. Brodmann map. *Lateral (left) and medial (right) view of functionally distinct regions of the cortex based on its cytoarchitecture at a microscopic level (adapted from Brodmann, 1909)*

distinct cytoarchitectural properties tend to have a specific function. Abnormal function of the neocortex is, in turn, often associated with several psychiatric illnesses such as autism, epilepsy, mental retardation, and schizophrenia *(Kaufmann WE and HW Moser 2000; Luna B et al. 2002; Mueller SG et al. 2009; Lewis DA et al. 2011)*.

Cytoarchitecture of the neocortex

The neocortex is a sheet of cells, about 3.4 mm thick, and is organised into horizontal layers and vertical columns, which receive or transmit information to or from adjacent cells or distant regions of the brain *(Kaas and Krubitzer 1991)*.

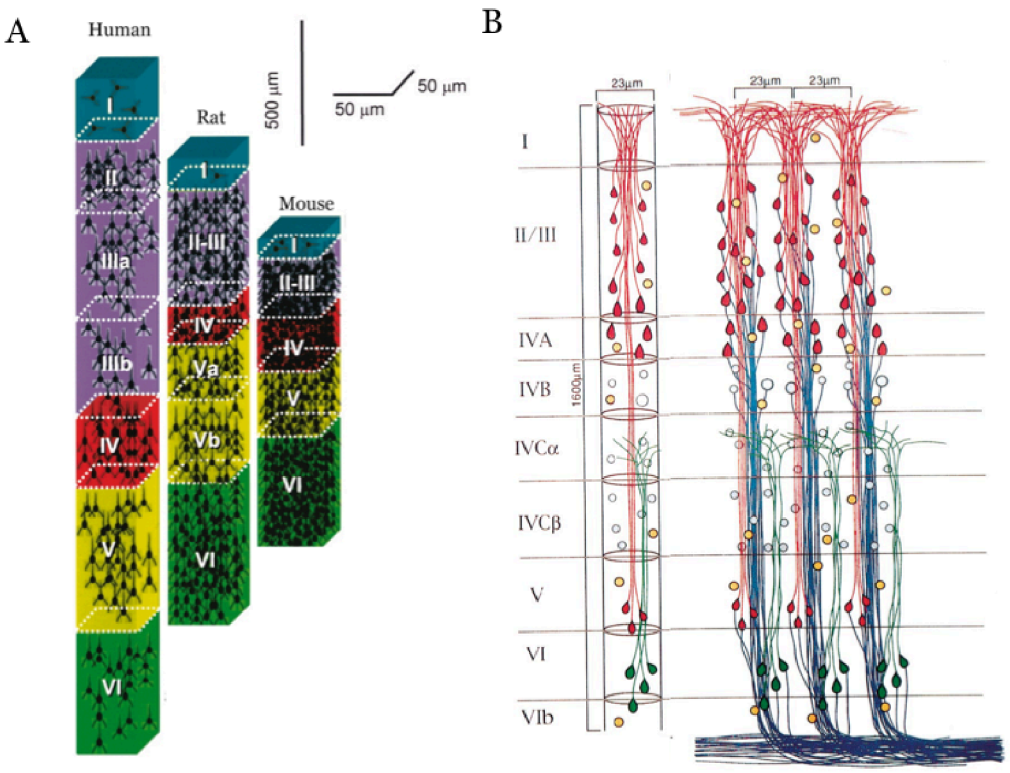

Fig. 1.2. Laminar and columnar organization of the neocortex. *(A) Comparison of the thickness of layers, and number of neurons within cubes of cortical tissue (50 x 50 µm) from the pial surface to the white matter in the human (left, temporal cortex), rat (middle, barrel cortex), and mouse (right, barrel cortex). Adapted and modified from DeFelipe, 2011 (Defelipe, 2011). (B) Schematic representation of cortical neurons in vertical modules of the striate cortex of the macaque monkey. A drawing to represent the columns showing the arrangement of dendrites and axons (Mountcastle, 1997).*

Neocortical layers can be distinguished by techniques that stain cell bodies of neuron, myelin and the processes of neurons. Each layer of the neocortex is defined primarily by the presence, absence, and density of distinctive cell types. Accordingly, the neocortex is grouped into six main layers, from outside (pial surface) to inside (white matter).

Another prominent feature of the neocortex is its vertical columnar organization called 'Cortical Columns'. A seminal observation by Vernon Mountcastle half a century ago led to the discovery of cortical columns *(Mountcastle VB 1957)*. Mountcastle hypothesised that the cortical columns are elementary units of organization in the somatosensory cortex that is made up of a vertical group of cells extending through all the cell layers **(Fig. 1.2)**. Neurons within a column tend to have similar response properties, possibly because they form local processing network *(Kandel ER 2013)*. However, the concept of cortical columns remains highly controversial in recent years. Skeptics argue that the vertical groups of cells are mere by-product of ontogenetic development without functional significance *(Horton JC and DL Adams 2005)*. To understand the functional properties of cortical areas, it is crucial to identify the connectivity profiles of the different neuronal cell types in the local microcircuits. The rodent barrel or somatosensory cortex is one of the best-studied models of cortical microcircuitry.

1.2. The rodent barrel/somatosensory cortex

Rodents are nocturnal animals. They live underground and inhabit tunnels. They primarily use their whiskers for navigation, rather than depending on vision per se. Rodent whiskers are highly sensitive to mechanical stimulation and allow them to orientate themselves in their natural environment *(Brecht M et al. 1997)*. Because of their strong dependence of whiskers, rodents developed a highly specialized somatosensory (barrel) cortex with a one-to-one representation of whiskers *(Woolsey TA and H van der Loos 1970)*. Tactile information from the whiskers on the rodents' snout is processed in the contralateral barrel cortex. A cross section of layer 4 (L4) of the barrel cortex shows 'barrel'-like structure that are arrangement in a somatotopic fashion, similar to the whiskers of the whisker pad. Whiskers are an important sense organ for rodents, just like hands for humans and other primates. In the cortical 'homunculus', which is a physical representation of the human body, hands and lips are over-represented, meaning that our hands are a lot more sensitive to touch than the rest of the body. In a similar way, the 'ratunculus' or the 'musculus' shows over-representation of the whiskers, which reflects the high degree of innervation of the whisker follicles. Unlike the continuous distribution of thalamic afferents to L4 in humans, the barrel cortex receives discrete clumps of afferents from the thalamus, largely separated on all sides by gaps with sparse thalamocortical afferent branches *(Woolsey TA and H van der Loos 1970; Land PW and SL Erickson 2005)*. The gaps that separate the barrels are called *septa*, which are characterised by a low

cell density and shows slow responsiveness to stimuli *(Brecht M and B Sakmann 2002)*. A single barrel receives its sensory input predominantly from one whisker, known as principal whisker *(Welker C 1976)*. Tangential sections of the barrel cortex show the barrel morphology and organization in the S1 cortex, which can also be visualised in the living, unstained brain slices. The barrels are arranged in 5 rows A-E, with each row having 4-7 arcs. The four large caudal whiskers are represented by four corresponding barrels spanning the first arc, and are designated by Greek letters α, β, γ, and δ. This arrangement exactly reflects the arrangement of whiskers in the snout on the contralateral side. A barrel column can be defined as an extension of barrel borders in L4 throughout all the cortical layers **(Fig. 1.3)**. This one-to-one representation of whiskers and anatomical correlate of a cortical column makes it possible to characterise single neocortical neurons and cortical microcircuitry using anatomical and functional techniques. The whisker-barrel system has also emerged as an excellent model to study the molecular mechanisms underlying the

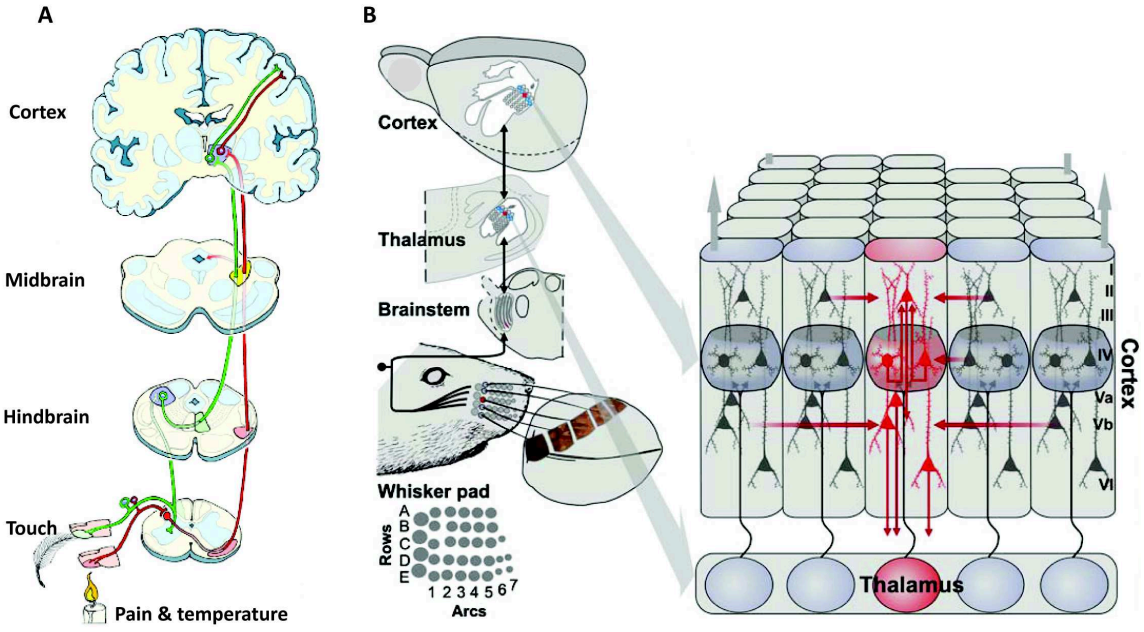

Fig. 1.3. Human and rodent somatosensory cortex. *(A) Simplified schematics of human somatosensory pathway. Afferent sensation such as pain, temperature, touch and proprioception ascends the spinal cord, passes through the midbrain and finally reaches the somatosensory cortex through thalamus. (B) Touch sensations by the whiskers on the snout, which are arranged in arcs and rows, carry sensory information through brainstem and thalamus, which is finally processed in the somatosensory cortex. At each level of the pathway, an isomorphic arrangement of neuronal cell groups, in the form of barrelettes in the brain stem, barreloids in the thalamus, and barrels in the somatosensory cortex, reflecting the layout of the whisker on the snout can be found (adapted and modified from Schubert et al. 2007).*

cortical circuit development, and experience-dependent plasticity *(Feldman DE and M Brecht 2005; Inan M and MC Crair 2007; Petersen CCH 2007; Feldmeyer D et al. 2013)*.

Sensory afferent pathways in rodents

The primary afferent fibres that innervate whisker follicles using several specialized end organs, including *Merkel* cells, lanceolate- and club-shaped ending, and free nerve endings transduce sensory information *(Ebara S et al. 2002)*. The first station on the ascending pathway, which integrates information from multiple whiskers, is the brain stem trigeminal nuclei (TN), which consist of principal nucleus (PrV) and three spinal nuclei (oralis, SpVo; interpolaris, SpVi and caudalis, SpVc) *(Veinante P et al. 2000)*. The sensory signals are topographically separated in barrelettes, structures equivalent to cortical barrels, with each barrelette representing predominantly one whisker *(Ma PM and TA Woolsey 1984; Henderson TA and MF Jacquin 1995)*. Important tactile processing such as the integration of signals across whiskers, computation of direction selectivity, and response adaptation takes place at the level of TN *(Minnery BS and DJ Simons 2003)*.

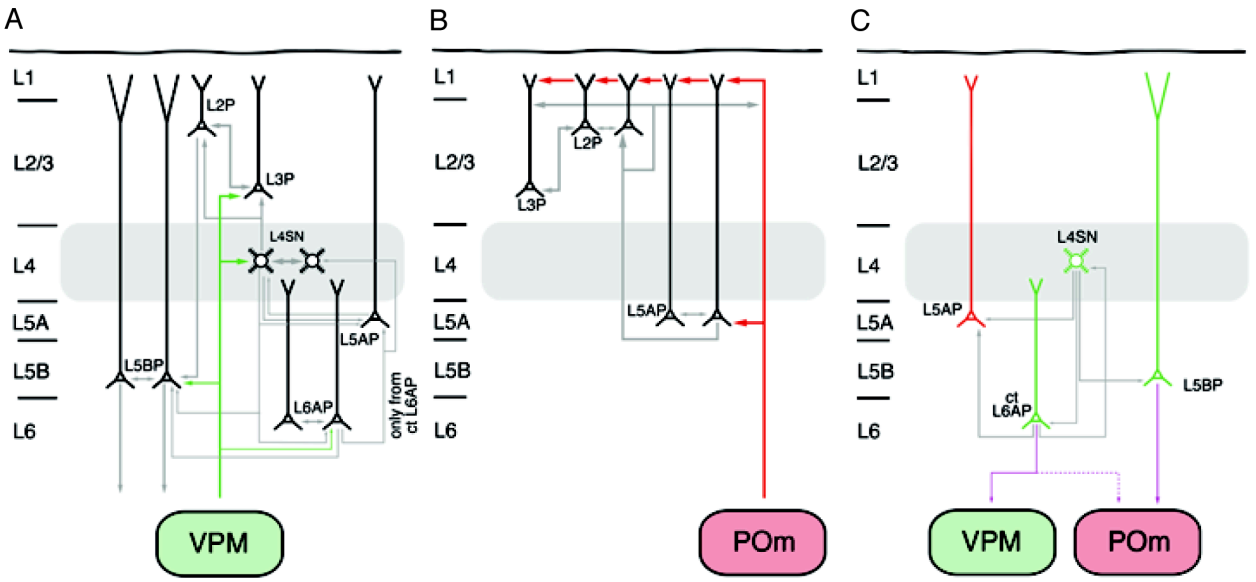

Fig. 1.4. Simplified schematics of parallel cortical microcircuits in the barrel cortex. *(A) Synaptic connections receiving input from the ventroposterior medial nucleus (VPM) of the thalamus (lemniscal). (B) Synaptic connections receiving input from the posterior medial thalamic nucleus (POm) of the thalamus (paralemniscal). (C) Synaptic connections involved in the corticothalamic feedback loop. Note that VPM and POm inputs interdigitated at several different stations, for e.g., L5A neurons receives direct input from the POm and indirect input from the VPM (via L4 spiny neurons), and L5B neurons receive input from the VPM and project to the POm (modified and adapted from Radnikow et al., 2015)*

The flow of sensory information is conveyed via four separate pathways that originate from different trigeminal nuclei: two 'lemniscal' pathways, an 'extralemniscal' pathway and a 'paralemniscal' pathway *(Ahissar E et al. 2000; Pierret T et al. 2000; Yu C et al. 2006)*. These pathways pass through different whisker-related, thalamic nuclei, the ventro-posterior-medial nucleus (VPM) and medial part of the posterior nucleus (POm; *(Chmielowska J et al. 1989)*. VPM contains histological compartments called 'barreloids' associated with individual whiskers and is subdivided into a 'head', 'core', and 'tail' region, each relaying different ascending pathways *(van der Loos H 1976; Urbain N and M Deschenes 2007)*. Finally, thalamic afferents from either VPM or POm project to different cortical layers in the somatosensory barrel field, with predominant projections to L4, making it the major input layer of the barrel and of other sensory cortices *(Woolsey TA and H van der Loos 1970; Lu S-M and RCS Lin 1993; Pierret T et al. 2000; Oberlaender M et al. 2011)*.

The *first lemniscal pathway* originates from single whisker neurons in PrV, is relayed via the core region of VPM barreloid and terminates predominantly in L4, and basal L3, and to a lesser extent in L5B and L6 of the barrel columns *(Henderson TA and MF Jacquin 1995)*. The *second lemniscal pathway* arising from multi-whisker neurons in PrV is transmitted via the head of barreloids in VPM and terminates exclusively in septal columns *(Veinante P and M Deschenes 1999)*. The *extralemniscal pathway* from multi-whisker neurons in rostral SpVi is conveyed via the barreloid tail and terminates in dysgranular S1 and in S2 *(Pierret T et al. 2000)*. The *para-lemniscal pathway* from multi-whisker neurons in the caudal part of SpVi is sent via the anterior POm and terminates in L1 and L5a *(Wimmer VC et al. 2010; Ohno S et al. 2012)* **(Fig. 1.4)**. There are several hypotheses about the function of each of these pathways. For instance, one hypothesis proposes that the lemniscal neurons convey detailed whisking and touch information, extralemniscal neurons encode contact timing, and para-lemniscal codes information about whisking kinematics *(Yu C et al. 2006; Diamond ME et al. 2008)*.

1.3. Major groups of cortical neurons

The barrel cortex consists of excitatory neurons and interneurons. Excitatory neurons are called principal neurons since they represent the majority of cortical neurons throughout all layers except L1. They are also termed pyramidal cells because of their characteristic triangular cell body and possess a prominent apical dendrite pointing

towards the pial surface. The dendrites of excitatory neurons are studded with spines, which acts as the main excitatory synaptic input region *(Peters A and IR Kaiserman-Abramof 1970)*. Another kind of excitatory neuron is the spiny stellate neuron, which constitutes 70-80% of the excitatory neurons in L4 *(Feldmeyer D et al. 1999)*. Following the release of the neurotransmitter glutamate, excitatory neurons generate excitatory postsynaptic potentials (EPSP) in the postsynaptic neurons.

Although inhibitory interneurons constitute only a minor fraction of neurons in the neocortex, they provide the main source of inhibition by releasing γ-amino butyric acid (GABA) at their postsynaptic terminal. The dendrites of interneurons are typically sparsely spiny or non-spiny. Synaptic contacts are made onto the dendritic shafts of interneurons, unlike excitatory neurons where synaptic contacts are made in the dendritic spines.

Origin of cortical neurons

During cortical development, excitatory neurons and interneurons are generated from neural progenitors located in dorsal and ventral telencephalon respectively *(Rakic P 1990; Parnavelas JG 2000; Kriegstein AR and SC Noctor 2004; Lodato S and P Arlotta 2015)*. Cortical neurogenesis starts at embryonic day 11 (E11) and ends at E19 in mice, and from E13 to E21 in rats *(Angevine JB and RL Sidman 1961; Berry M and AW Rogers 1965; Caviness VS 1982; Bayer SA and J Altman 1991; Marin O and JLR Rubenstein 2001)*. All cortical neurons originate from neuroepithelial cells (NEC), which forms the lining of neural plate. Before the onset of neurogenesis, they undergo symmetric proliferative division to expand the progenitor pool both in lateral and radial dimensions *(Fish JL et al. 2008)*. After the onset of neurogenesis, between E10 and E12 in mice, NECs give rise to distinct cell types, such as radial glial cells (RGCs) and intermediate precursor cells (IPCs) *(Noctor SC et al. 2004)*. RGCs undergo multiple rounds of cell division in the ventricular zone (VZ), which consists of specialized epithelial tissue that lines the lateral ventricles. A small fraction of cortical pyramidal neurons (10-20%) is generated by RGCs when they undergo terminal asymmetric, neurogenic division *(Kowalczyk T et al. 2009)*. IPCs are generated from RGCs via symmetric, proliferative divisions. They undergo mitotic division and generate a new germinal zone called subventricular zone (SVZ), where a substantial fraction of cortical pyramidal neurons (80%) are produced *(Haubensak W et al. 2004; Kowalczyk T et al. 2009; Hansen DV et al. 2010; Taverna E et al. 2014; Vasistha NA et al. 2014)*. Early-born neurons or pioneer neurons at E12.5 (mice) migrate

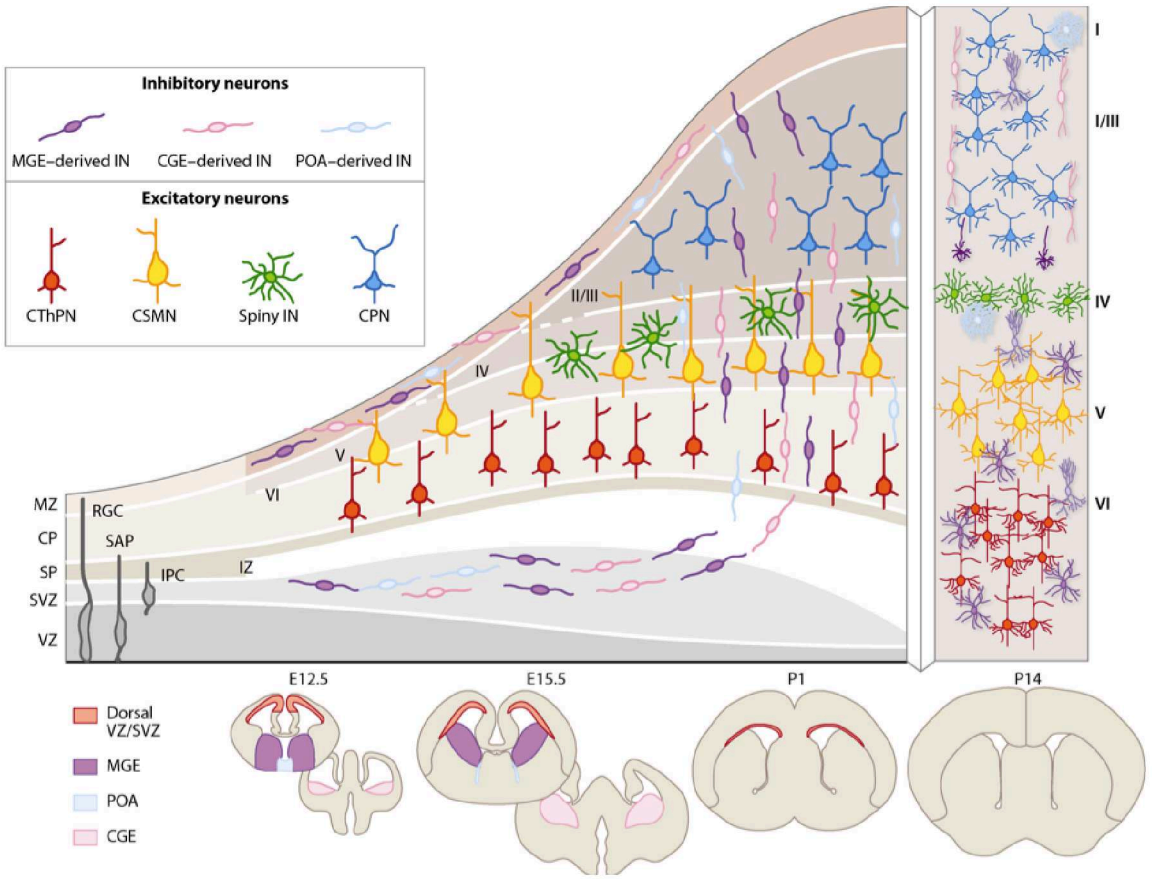

Fig. 1.5. Neurogenesis of excitatory and interneurons. *Excitatory neurons originate from pallium/dorsal telencephalon and they migrate radially to the overlying cortical plate, whereas cortical interneurons originate from subpallium/ventral telencephalon and they migrate tangentially over long distances to reach the cortical plate, where they migrate radially to acquire their laminar positions. Interneurons originate mainly from medial ganglionic eminence (MGE), caudal ganglionic eminence (CGE), and preoptic area (POA) of the ventral telencephalon. Abbreviations: CP, cortical plate; CPN, callosal projection neuron; CSMN, corticospinal motor neuron; CThPN, corticothalamic projection neuron; E, embryonic; IPC, intermediate precursor cell; IZ, intermediate zone; MZ, marginal zone; P, postnatal; RGC, radial glial cells; SAP, subapical progenitor; SP, subplate; SVZ, subventricular zone; VZ, ventricular zone (Lodato & Arlotta 2015).*

to form the first layer during mammalian corticogenesis, known as cortical primordial plexiform layer, or preplate *(Marin-Padilla M 1971)*. Subsequently, the preplate is split into peripheral marginal zone (MZ) and subplate (SP) by newly born neurons at E14 that migrate along radial glial cells from the VZ. They occupy a new layer between these two zones to form the cortical plate (CP), which is the final plate formed in corticogenesis, where lamination of cortical layers forms in an inside-out fashion, i.e., L6 is formed first, followed by L5 and so on *(Bayer SA and J Altman 1991; Allendoerfer KL and CJ Shatz 1994; Marin-Padilla M 1998)*. Earlier born neurons occupy deeper layers in the cortex, while later born neurons bypass earlier-born neurons to occupy superficial layers

(Angevine JB and RL Sidman 1961) **(Fig. 1.5)**. In rodents, the superficial L4 and L2/3 are formed postnatally.

Excitatory neurons are generated from the proliferative zones of the *pallium*, and they migrate radially to the overlying cortical plate in an 'inside out' fashion *(Berry M and AW Rogers 1965; Rakic P 1974)*. Inhibitory interneurons, on the other hand, are generated from the proliferative zones of the *subpallium*. They migrate tangentially over long distances to reach their destination in the neocortex, where they migrate radially to acquire their laminar positions and integrate in an 'inside out' fashion *(Nadarajah B and JG Parnavelas 2002; Hevner RF et al. 2003; Marin O and JLR Rubenstein 2003; Guillemot F 2005)*.

Distinct interneuron types are generated in spatially and temporally distinct regions in the ventral telencephalon. The ventral telencephalon consists of ganglionic eminences (GE) and preoptic area (PoA) *(Wonders CP and SA Anderson 2006; Gelman DM and O Marin 2010)*. The GEs are present only in the embryonic and fetal stages of neural development that guide cell and axon migration *(Encha-Razavi Fr and P Sonigo 2003)*. They are found between the thalamus and caudate nucleus. The PoA lies ventral to the GEs. The GEs in the ventral telencephalon are further subdivided into medial (MGE), lateral (LGE), and caudal (CGE) ganglionic eminences based on their location within the subventricular zone (SVZ) *(Fishell G 1997)*. Virtually all cortical GABAergic interneurons are generated from the MGE and the CGE and, to a small extent, from PoA *(Wonders CP and SA Anderson 2006; Gelman DM et al. 2009)*. GABAergic interneurons are generated between embryonic days E11-E17 in mice *(Sultan KT et al. 2013)*.

1.4. Single-cell electrophysiology

To characterise individual neurons and to find the synaptic connectivity between different neurons in a cortical microcircuitry, electrophysiological methods have been used extensively in the recent decades. The most accurate way for recording ionic currents involving action potential (AP) activity was made possible by the development of the voltage clamp technique. Experiments by Hodgkin and Huxley in 1950s on squid giant axons with 400 – 500 µm diameter were performed using voltage clamp methods to study the ionic mechanism involved in nerve excitation *(Hodgkin AL and AF Huxley 1952)*. However, this technique had a limitation insofar that it could be performed only on large

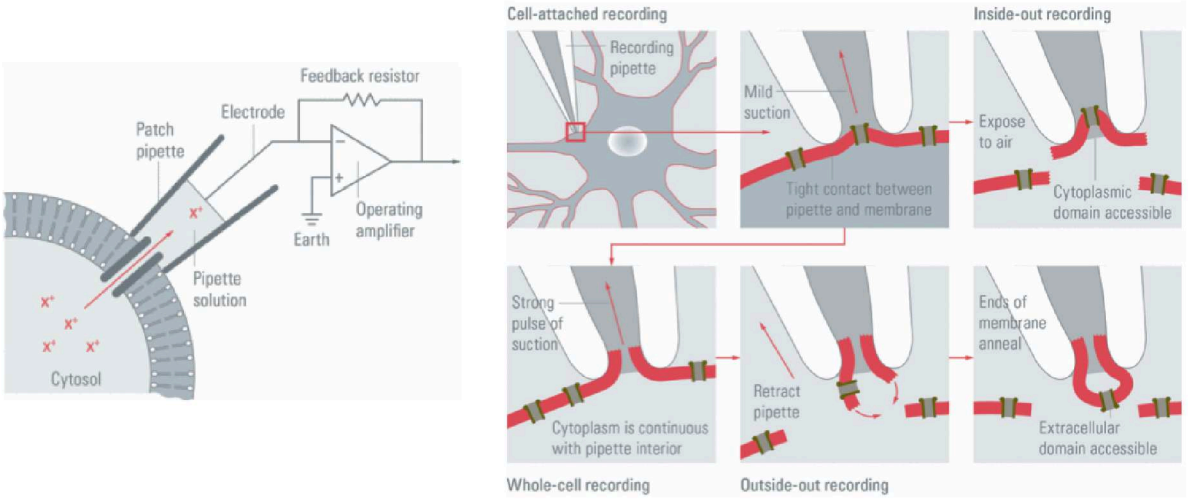

Fig. 1.6. General principle of patch-clamp recording and recording methods. *(Left) A patch pipette with electrolyte solution is tightly sealed onto the cell membrane, which causes the cell membrane to rupture upon quick suction. Thus the inside of the cell becomes continuous with the pipette, which can be recorded by an electrode that is connected to an amplifier. This gives access to changes in current and voltage within the cell. The four recording methods for patch clamp are cell-attached mode, inside-out mode, whole-cell recording mode, and outside-out mode (Source: Leica Systems).*

cells as sharp microelectrodes were used to penetrate the membrane. A scientific breakthrough was achieved by Erwin Neher and Bert Sakmann in 1976 who received Nobel Prize for their development of patch clamp technique *(Neher E et al. 1978)*. This technique revolutionised modern cellular electrophysiology by providing the possibility to access single ionic channels with high resolution. Neher and Sakmann were able to successfully patch cell membranes to record whole-cell currents and single-channel currents and showed versatility in recording from any kind of cells *(Hamill OP et al. 1981)*.

General principle of the patch-clamp technique

The patch clamp technique is a variation of voltage clamp. In this technique, a thin glass pipette is pressed against a cell's surface. The pipette is fitted with a chlorided silver wire and filled with a electrolyte solution. Suction is applied to the inside of the pipette, which results in a high resistance seal between pipette tip and cell membrane, commonly referred to as *giga seal* or *gigaohm seal* because the resistance reaches the gigaohm range. This is one of the crucial steps in patch clamp technique, which highly improves the quality of recording by increasing the signal-to-noise ratio. After establishing the giga seal, negative pressure is applied to break the patched cell membrane, which allows continuity between the inside of the cell and the cell interior. By achieving this, all ions attached to the patched membrane flows into the pipette, which are then recorded by a chlorinated silver electrode connected to an electronic amplifier. This gives access to changes in

current and voltage within the cell. In voltage-clamp mode, the voltage is held constant by which the ionic currents could be studied. In current-clamp mode, the membrane potential changes can be studied by holding the current. This configuration of recording is called whole-cell patch clamp technique, where it is possible to study the single cell properties, such as passive membrane properties and action potential properties. Based on the research question, three other configurations can be employed, such as cell-attached mode, inside-out mode, and outside-out mode. In cell-attached mode, the cell membrane is not disrupted, whereas in the other two configurations, the cytoplasmic domain or extracellular domain of a membrane 'patch' is accessible following the retraction of pipette *(Sakmann B and E Neher 1984)* **(Fig. 1.6)**.

Application of the patch clamp technique

For correlated functional and morphological studies, intracellular markers such as biocytin are used. Biocytin was added to the electrolyte solution, by which the patched neurons were stained by post-hoc histological procedures and the morphology of stained neurons were revealed *(Horikawa K and WE Armstrong 1988)*. By visualising and tracing the morphology of patched neuron with the help of bright-field microscope and Neurolucida software, it was possible to generate three-dimensional neuronal morphologies *(Marx M et al. 2012)*.

To identify the presence of certain molecular markers in patched neurons, either fluorescent dyes were added to the electrolyte solution, or the cell contents were aspirated in the recording pipette. Immunostaining methods or single cell PCR made it possible to identify the expression of certain molecular markers *(Kawaguchi Y et al. 1989; Cauli B et al. 1997)*. Recent development combines patch-clamp recording with single-cell RNA sequencing to reveal the morphology, physiology and molecular expression of single neurons simultaneously *(Qiu S et al. 2012; Cadwell CR et al. 2016)*.

The patch-clamp technique combined with intracellular labelling during recording is the only reliable method available to date to characterise the morphological and functional properties of identified, synaptically connected neurons. The method that allows the identification of both pre- and postsynaptic neurons is called paired-recording, which is generally combined with the intracellular injection of biocytin during recording so that the morphology of both pre- and postsynaptic neuron can be identified *(Qi G et al. 2015)*.

Therefore, the paired recording technique continues to be a powerful tool in the study of neuronal microcircuitry.

1.5. Excitatory and inhibitory cortical networks

Cortical network formed of excitatory neurons are linear and highly predictable. For example, a chain of connected excitatory neurons would excite each other at every step, resulting in an avalanche of excitation without global stability. They excite each other, independent of factors, like time, or strength of excitation. On the other hand, an inhibitory network behaves entirely different. Following similar example, activation of an inhibitory neuron in a chain would suppress its target inhibitory neuron, which might induce inhibition to the third neuron resulting in increased activity of the third neuron. Therefore, inhibitory circuits are hard-to-predict and show non-linearity.

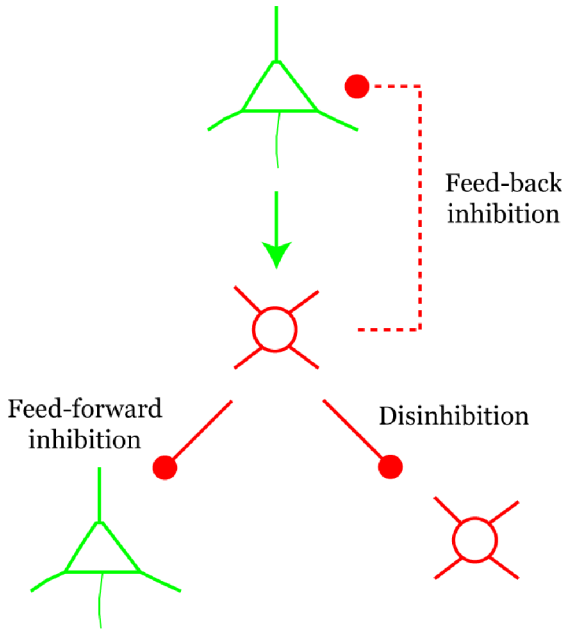

Fig. 1.7. Types of neural inhibition. *Recruitment (green arrow) of an interneuron (red) by an excitatory neuron (green) may cause inhibition (red line) to one of the three targets – excitatory neuron upstream (feed-back), excitatory neuron downstream (feed-forward), or another interneuron (disinhibition).*

In a cortical circuit involving excitatory and inhibitory interneurons, the firing patterns depend on the exact details of wiring connections and synaptic strength. Inhibitory connection can be subdivided into three main types. In a feed-forward inhibition system, recruitment of an interneuron by direct thalamic input or via excitatory neurons causes decreased activity of other excitatory neurons **(Fig. 1.7)**. This kind of

inhibition can substantially increase the temporal precision of firing, by narrowing the temporal window of discharge probability of excitatory neurons *(Buzsaki G 1984)*. Inhibition of an interneuron is called disinhibition, because the target neuron is released from inhibition.

In a recurrent or feedback inhibitory circuit, excitatory neuron activates an interneuron, which in turn, inhibits the same excitatory neuron. Such kind of inhibition provides stability by negative feedback. An extension of feedback inhibition is lateral inhibition. This occurs when an interneuron is recruited by an excitatory neuron, which, in turn, suppresses the activity of surrounding excitatory neurons. Lateral inhibition provides contrast enhancement by suppressing the similarly activated surrounding neurons ('winner take all').

1.6. Neuronal diversity in the neocortex

Excitatory neurons, though present in abundance, show relatively stereotypical characteristics in their morphology, electrophysiology, and molecular identities. To balance the excitatory effects generated by the majority group of principal cells, the minority inhibitory interneurons compensate by their massive diversity with respect to molecular, structural and functional properties *(Gupta A et al. 2000; Ascoli GA et al. 2008; DeFelipe J et al. 2013)*. Such diversity suggests that different groups of interneurons are involved in different functions and synaptic inhibition acts in different ways *(Burkhalter A 2008)*. However, identification of synaptic connections of interneurons is very difficult due to its diversity, which makes classification of interneurons pivotal in determining their functional role in the barrel cortex microcircuitry.

PETILLA Nomenclature

Due to the discrepancies in the naming and classification of different interneuron subtypes, an international group of researchers specialising in development, anatomy and/ or physiology collaborated for a general agreement regarding a universally acceptable nomenclature and classification of neocortical interneurons (Petilla Interneuron Nomenclature Group; *(Ascoli GA et al. 2008)*). Several features, such as laminar projections, columnar projections, and positioning were used to classify a large sample of inhibitory interneurons and statistical tools were used to group them into different subtypes. Only those neuronal types that are more easily identifiable with their unique

axonal morphologies such as chandelier and Martinotti cells reached a high degree of consensus (*(DeFelipe J et al. 2013)* see following text).

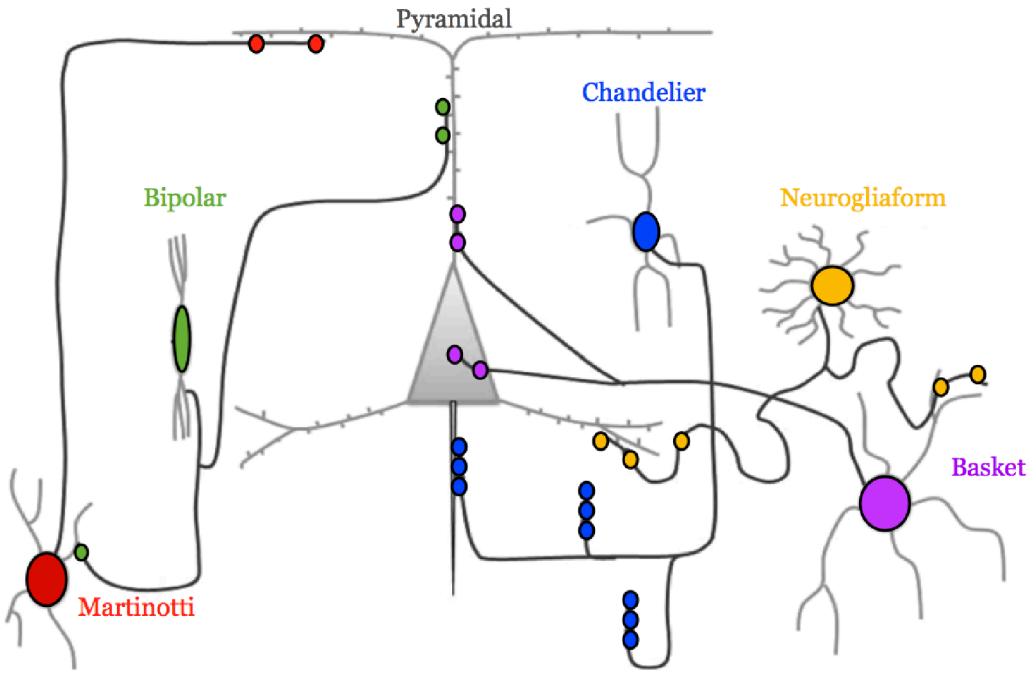

Fig. 1.8. Morphological subtypes of interneurons. *Schematics illustrating different subtypes of GABAergic interneurons and their subcellular target to pyramidal cells in neuronal networks of the rodent barrel cortex (Adapted and modified from Zaitsev, 2013).*

Morphological criteria

Morphological diversity can be observed at the levels of subcellular target domains and axonal projection pattern. Based on subcellular postsynaptic target innervation, there are mainly three subtypes – axon-targeting, soma-targeting, and dendrite-targeting cells **(Fig. 1.8)**. Axonal projection pattern has a critical influence on the intra- and inter-columnar processing and they reflect the maximum 'inhibitory territory' of a neuron, and they determine the functional compartments the neuron will receive or transmit synaptic information *(Helmstaedter M et al. 2009b; Merchant H et al. 2012)*. Accordingly, the axonal projections could be local, lateral, or translaminar *(Helmstaedter M et al. 2009a; DeFelipe J et al. 2013)*.

Electrophysiological criteria

The whole-cell patch clamp technique was used to study the active and passive membrane properties of recorded neurons, using brief pulse of hyper- and depolarising current injections. Subthreshold electrical parameters of the neuron such as resting

potential, input resistance, sag, membrane time constant, and rheobase were used to characterise the passive membrane properties. Action potential properties such as threshold, amplitude, half-width, afterhyperpolarisation, and firing properties such as inter-spike-interval, adaptation, and maximum firing frequency were used to characterise interneurons.

Interneurons show very diverse types of firing pattern, such as, fast-spiking, regular-spiking, burst-spiking, irregular spiking, and late-spiking *(Ascoli GA et al. 2008; DeFelipe J et al. 2013)*. In a simplified way, interneurons could be either fast-spiking (FS) or non-fast spiking (nFS), where the latter include all the firing patterns except FS. Action potential properties of nFS interneurons such as AP half-width, AHP amplitude, and firing frequency fall between FS interneurons and excitatory neurons **(Fig. 1.9)**.

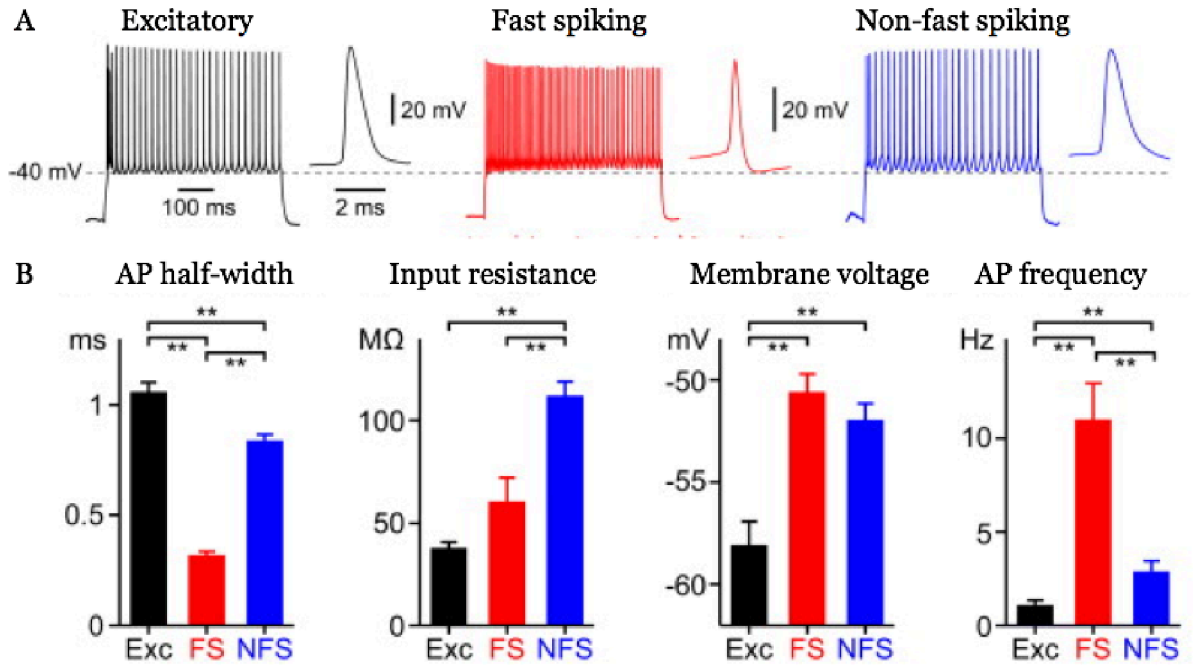

Fig. 1.9. Membrane and firing properties of excitatory and inhibitory neurons. *(A) Firing pattern of excitatory (black), fast spiking interneuron (red), and non-fast spiking interneuron (blue) in response to depolarising current injection. (B) Differences in action potential duration, input resistance, membrane voltage and firing frequency elicited by three groups of neurons (adapted from Gentet et al., 2010).*

Molecular criteria

One of the most widely used ways of classify interneurons in the recent years is by the molecular features of interneurons. Interneurons differ in their molecular fingerprint, i.e. in the expression of transcription factors, neuromodulatory peptides, calcium-binding proteins, and of receptors. The discovery of these markers was mostly possible by the use

of immunostaining, conventional transgenic methods, Cre-transgenic mouse lines that express a particular protein by conditional gene targeting approaches, qPCR for single-cell gene profiling, modified RT-PCR, RNA-seq and more recently Patch-seq, which is a modification of RNA-seq. A recent study by Rudy et al., 2011 suggested that nearly 100% of all neocortical GABAergic interneurons belong to one of the three non-overlapping groups defined by the expression of calcium-binding protein parvalbumin (PV) (40%), the neuromodulatory peptide somatostatin (SOM) (30%) and the ionotropic serotonin receptor 5HT3$_a$R (30%) *(Rudy B et al. 2011)*. However, a recent study using RNA-seq shows that interneuron classes are extremely diverse and at least 16 different subclasses of interneurons were identified *(Zeisel A et al. 2015)* **(Fig. 1.10)**.

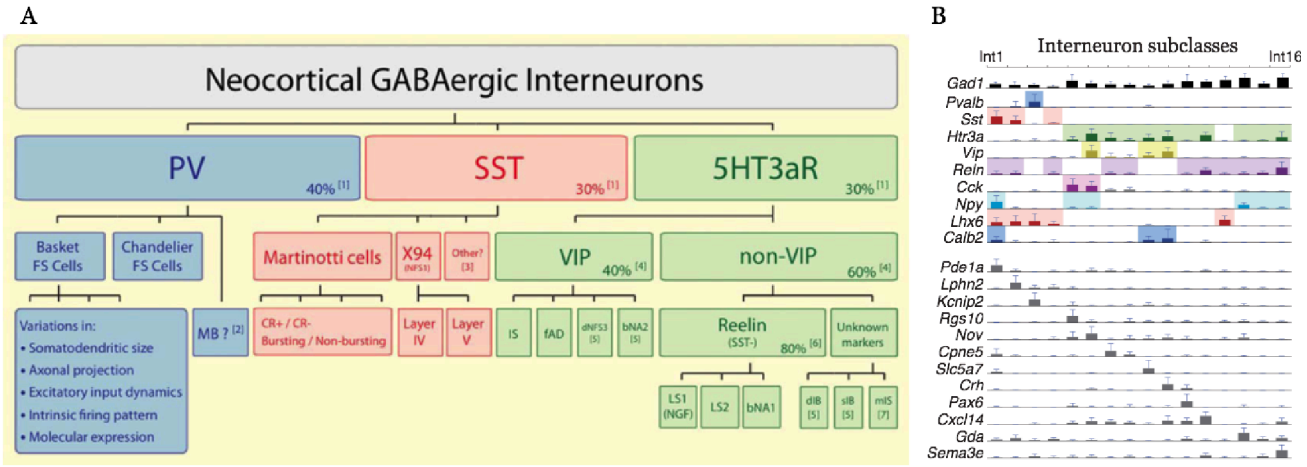

Fig. 1.10. Classification of neocortical interneurons based on their molecular expression. *(A) Nearly 100% of all neocortical interneurons belong to one of the three groups of molecular markers (Adapted from Rudy et al., 2011). (B) A recent study (Zeisel et al., 2015) showing that interneuron classes are extremely diverse and at least 16 different subclasses were identified based on the expression of molecular markers.*

Based on the above-mentioned criteria, several classes of interneurons were identified in rat barrel cortex. The best-studied interneuron classes are listed in the table below.

Cell types	Targets	Layers	Morphological features	Firing properties	Molecular markers	Synaptic properties
Chandelier cells	Axon initial segments of pyramidal cells	Mostly found in L2 and L6	Terminal axonal branches resemble candlestick appearance of the chandelier	Fast-spiking action potential	Parvalbumin	Depolarise pyramidal cells
Basket cells	Soma and proximal dendrites	All layers except L1	Locally confined axon, multipolar dendritic arbor	Fast-spiking action potential	Parvalbumin	Strong synaptic depression
Martinotti cells	Distal dendrites of pyramidal cells	Abundant in L5, present in all layers except L1	Axon projects vertically to form terminal branches in L1, sends horizontal collaterals across columns	Low-threshold firing/ non-fast spiking	Somatostatin	Weak synaptic facilitation
Neurogliaform cells	Synaptic and volume transmission	Present in all layers	Dense axonal arbor, multipolar dendrites	Late spiking, broad AP half-width	5HT3aR and Reelin	Electrical synapse with other interneurons.
Bipolar/Bitufted cells	Interneurons	Predominant in L2/3	Bipolar dendrites, axon spans through many layers, confined to home column	Adapting, bursting or irregular firing	VIP	Preferentially inhibit somatostatin interneurons

1.7. Shortcomings in the current method of classification

Due to the recent advances in molecular and genetic methods, it is now possible to tag, and manipulate specific neuronal populations. In recent years, several studies aimed at interneuron classification by identifying a specific group of interneuron using transgenic animals expressing fluorescent protein or using Cre-recombinase technique. It is questionable whether these kinds of classifications completely describe the function of an interneuron subtype in the cortical network. A recent study by Linnarson and colleagues on classification on neurons using large-scale single-cell RNA sequencing (RNA-seq) identified 15 subclasses of neocortical interneurons based on the expression of molecular markers. PV was the only non-overlapping group expressed by only one interneuron type, whereas SOM was expressed by 3 interneuron subgroups, with varied degrees of co-expression of Reelin, NPY, Lhx6, Calbindin2, and so on. Interestingly, 5HT3aR was expressed by almost 11 interneuron subclasses, with co-expression of multiple molecular markers *(Zeisel A et al. 2015)*. However, PV is known to be expressed by two distinct groups of interneurons, such as basket cells and chandelier cells, which clearly have

distinct morphology, electrophysiology and connectivity profiles *(Kawaguchi Y and S Kondo 2002)*. Therefore, it is of paramount importance to choose unbiased and reliable criteria, which give a clear functional relevance for the interneuron subtypes. For a complete identification of the inhibitory network in the barrel cortex, it is essential to characterise interneuron subtypes based on axonal and dendritic morphology because they determine the structural and functional connectivity.

1.8. Aim of this study

Only few studies on the quantitative classification of structural and functional properties of neocortical GABAergic interneurons are currently available *(Karagiannis A et al. 2009; McGarry LM et al. 2010; Muralidhar S et al. 2013; Perrenoud Q et al. 2013; Koelbl C et al. 2015)*. L4 of rat barrel cortex shows the least dense population of interneurons with only 8.1%, out of which PV expressing FS interneurons are present in abundance *(Meyer HS et al. 2011)*. The other interneuron population - nFS interneurons were described in previous studies as low threshold spiking (LTS) and/or regular spiking non pyramidal cells (RSNP) in L4 of rodent barrel cortex *(Gibson JR et al. 1999; Porter JT et al. 2001; Sun QQ et al. 2006)*. However, to date no quantitative characterisation of nFS interneurons in L4 of rat barrel cortex is available.

The aim of this study is to investigate the electrophysiological, morphological and molecular properties of nFS interneurons and their synaptic connections with other excitatory and inhibitory neurons in L4 of rat barrel cortex. This study was performed using single and paired whole-cell patch clamp recordings, with simultaneous biocytin fillings, morphological 3D reconstructions using Neurolucida® tracing software and immunohistochemistry to quantitatively characterise nFS GABAergic interneurons and their role in the neuronal micro-circuitry of the neocortex. The quantitative classification was based mainly on the axonal innervation domains of nFS interneurons with reference to cortical layers and columns, which helps in determining the function or type of presynaptic neurons, and can also be used as a predictor of synaptic connectivity. In addition, classification based on electrophysiological properties was also performed to identify the heterogeneity of nFS interneurons firing patterns.

2. Materials and methods

2.1. Slice preparation

All experiments were performed in accordance with the guidelines of the Federation of European Laboratory Animal science Association (FELASA) and the German animal welfare act. The animals used for this study were Wistar rats (Charles River, either sex) aged 17-21 postnatal days (P17-21). The experimental procedure was adopted from Agmon and Connors with minor modifications *(Agmon A and BW Connors 1991)*. The rats were anaesthetised using isoflurane, decapitated and their brains transferred to ice cold (~4° C) preparation solution with a high magnesium and low calcium concentration (i.e. 4 mM $MgCl_2$ and 1 mM $CaCl_2$) to minimise overall synaptic activity. The solution was bubbled continuously with carbogen gas (95% O_2 and 5% CO_2) to maintain adequate oxygenation and physiological pH level. Oblique coronal slices of somatosensory cortex were cut at an angle of 45° to the midline *(Chmielowska J et al. 1989; Feldmeyer D et al. 1999)* **(Fig. 2.1)**. The tissue caudal to the cut was glued on to an ice-cold metal stage of a vibrating microtome (HM 650 V, Microm) with the cut surface glued to the metal stage. The tissue was totally immersed in ice-cold preparation solution, which was bubbled with carbogen gas. The initial sections were discarded until the brain surface with striatum and hippocampus started to appear. Brain slices of 350 µm thickness were made at a high vibration frequency and at a slow speed. The brain slices were incubated for about an hour at room temperature (21-24 °C) in preparation solution.

2.2. Solutions

During whole-cell voltage recordings, slices were continuously perfused (perfusion speed ~5 mL/min) with an artificial cerebrospinal fluid (ACSF) containing (in mM): 125 NaCl, 25 D-glucose, 25 $NaHCO_3$, 2.5 KCl, 2 $CaCl_2$, 1.25 NaH_2PO_4 and 1 $MgCl_2$, bubbled with carbogen gas and maintained between 30-33 °C. Patch pipettes (4-8 MΩ) were pulled from thick-wall borosilicate glass capillaries (outer diameter, 2.0 mm; inner diameter 1.0 mm) and filled with an internal solution containing (in mM): 135 K Gluconate, 4 KCl, 10 HEPES, 10 Phosphocreatine, 4 Mg-ATP and 0.3 GTP (pH 7.4, 290-300 mOsm). Biocytin was added to the internal solution at a concentration of 4 mg/ml to label the patched neurons during recording.

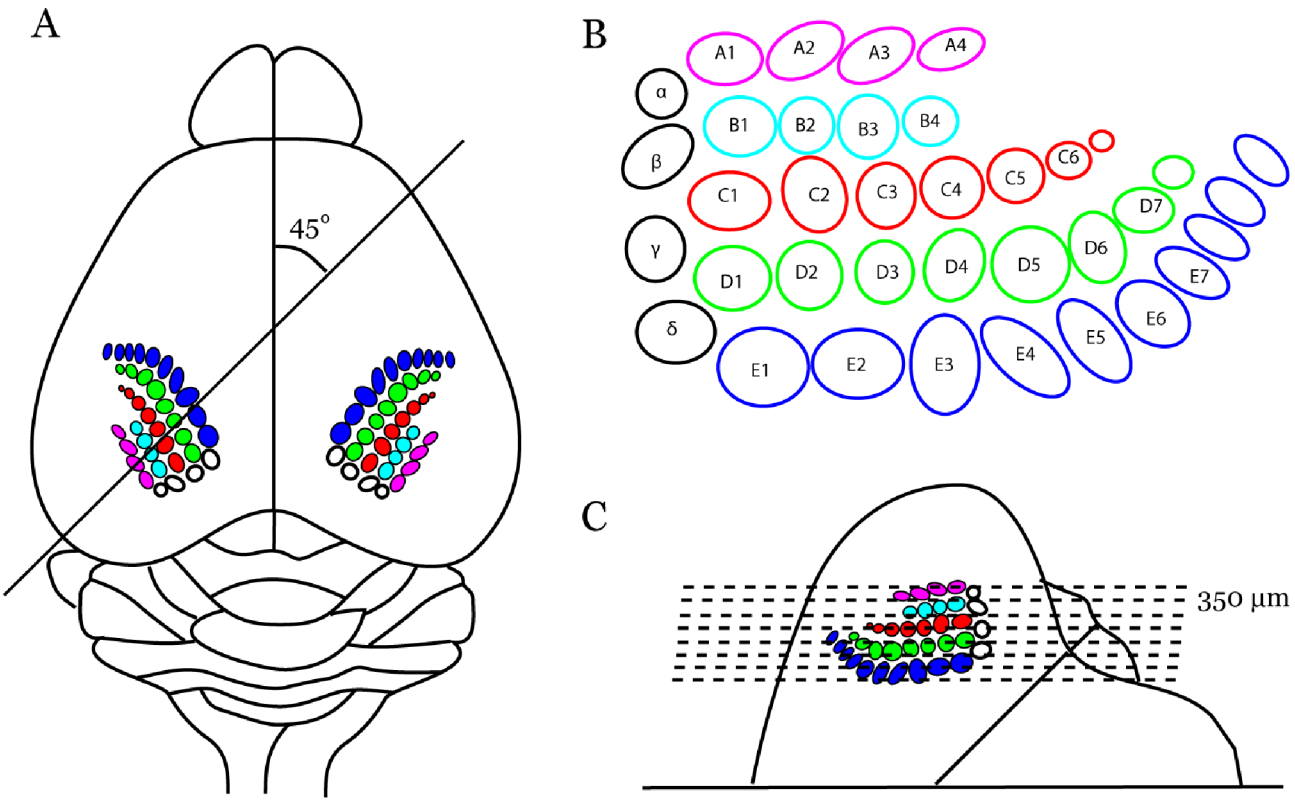

Fig. 2.1. Slice preparation. ***(A)*** *Dorsal view of rat brain with barrel structures shown in colours. Oblique coronal cut was made at an angle of 45° to the midline.* ***(B)*** *Schematic representation of whiskers in the barrel cortex. The barrels are arranged in 5 rows A-E labeled in different colours, with each row having 4-7 arcs. The four large caudal whiskers are represented by four corresponding barrels mounting the first arc, and are designated by Greek letters α, β, γ and δ, labeled in black.* ***(C)*** *The cut end of the brain was glued to the metal stage and brain sections were made at a thickness of 350 µm using vibrating microtome.*

2.3. Whole-cell patch clamp technique

Identification of non-fast spiking interneurons in L4 of rat barrel cortex

Slices were placed in the recording chamber under an upright microscope, fitted with 4x/ 0.13 numerical aperture and 40x water immersion/0.80 numerical aperture objectives (Olympus, Tokyo, Japan) with the hippocampus on the right side. Under bright-field illumination at low magnification, L4 can be visualised as light hollow barrel-like structures with narrow dark stripes in between *(Feldmeyer D et al. 1999)*. Even though barrel structures were present in 6-8 slices, a continuous band of barrels were visible only in the last 2-3 slices. Under infrared differential inference contrast (IR-DIC) microscopy, individual L4 neurons were visualised at 40x magnification *(Dodt H-U and W Zieglgänsberger 1990; Stuart GJ et al. 1993)* **(Fig. 2.2A)**. Interneurons could be distinguished from excitatory neurons by their large, ovoid shaped soma with no clearly

visible apical dendrite like structure *(Simons DJ and TA Woolsey 1984; Koelbl C et al. 2015)* **(Fig. 2.2B)**. Another feature of interneurons in L4 is that they never form clusters, unlike excitatory neurons *(Lubke J et al. 2000)*. However, the soma morphology does not allow a clear distinction between FS and nFS interneurons. We used intrinsic firing patterns recorded in current clamp mode to reliably differentiate nFS interneurons from other neuron types. Interneurons of the nFS type display a firing pattern intermediate to excitatory neurons and FS interneurons **(Fig. 2.2C)**. They show broad AP and AHP compared to FS interneurons, low firing frequency at highest current injection and high spike frequency adaptation *(Beierlein M et al. 2003)*.

Single cell recordings

Whole cell patch-clamp recordings were performed using patch pipettes of 5-7 MΩ resistance pulled of thick borosilicate glass capillaries (outer diameter, 2.0 mm; inner diameter 1.0 mm). Pipettes were filled with internal solution and biocytin to label the patched neuron. Infrared video microscopy was used for the visualisation of neurons in barrel cortex. Neurons were selected based on their large, ovoid shaped soma with no clearly visible apical dendrite and those that are located at the barrel borders *(Ma Y et al. 2006; Daw MI et al. 2007)*. Stimulation protocols were programmed using "Patch master" software (Heka Elektronik). Signals were recorded by the recording electrode which is a chloride silver electrode connected to a pre-amplifier, which sends signal to another amplifier (EPC10, HEKA, Lambrecht, Germany) and finally to the computer. A ground electrode was used to set the zero level. Micromanipulators were used to control the movement of pipettes with high precision in three-dimensional planes. A slight positive pressure was applied to the pipette to prevent any blockage before patching. Upon contact with the soma, a small dimple could be visible due to the positive pressure from the pipette, which causes slight increase in resistance. Suction was applied to facilitate the increase in resistance up to gigaohm range – also known as gigaseal. Resistance values of 1 GΩ or more within seconds guaranteed a good signal-to-noise ratio. To break the cell membrane attached to the pipette, further suction was applied which formed a direct connection between the neuronal cytoplasm and the patch pipette.

Dual recordings

GABAergic interneurons show high connectivity with other neuron types *(Koelbl C et al. 2015)*. Therefore we followed a procedure called 'dual' or 'paired' recording to find

connections between neurons. nFS interneurons were patched in whole-cell mode as the pre-neuron and a prospective post-synaptic neuron was also patched within the same barrel in whole-cell mode. Membrane potential of the post-neuron was set to a holding potential of -55 mV to increase driving force for Cl^- thereby facilitating the identification of inhibitory connections. An action potential was elicited in the pre-neuron and the inhibitory response of post-synaptic neuron was monitored for a possible post-synaptic potential. If a connection was found between pre- and post-neuron, we continued recording the response of post-synaptic neuron by eliciting action potentials in the pre-synaptic neurons.

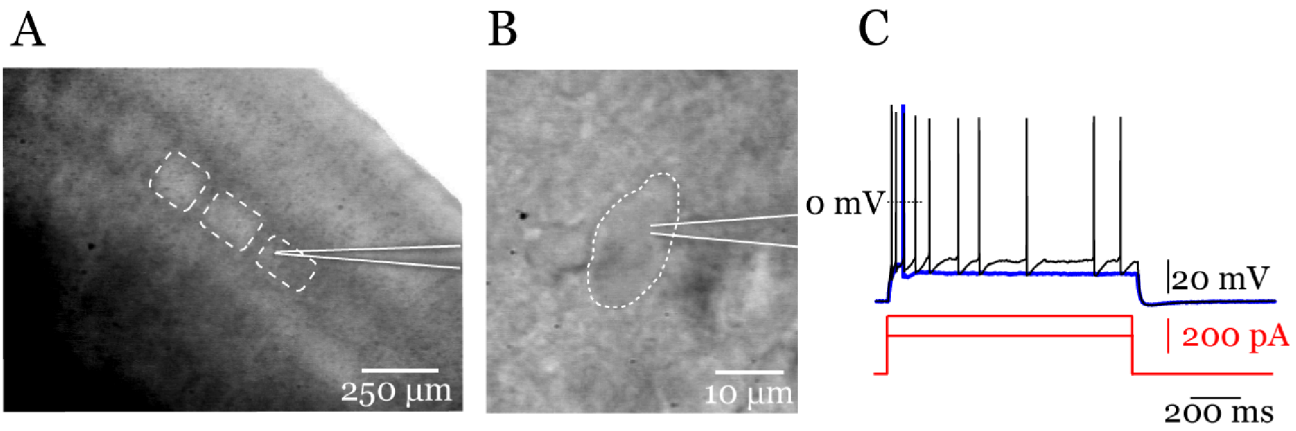

Fig. 2.2. nFS interneuron identification. ***(A)*** *Photograph of an acute thalamocortical brain slice showing the light-hollow barrels in L4 and the patch pipette .* ***(B)*** *IR-DIC image of a L4 nFS interneuron during patching with patch pipette (Scale bar: 10 µm).* ***(C)*** *Identification of nFS shown in A was confirmed by the firing pattern. Injection of rectangular current pulse is shown in red traces and the corresponding voltage response in blue (first spike) and black (10 spike train).*

Immunohistochemical staining

For the identification of molecular markers expressed by GABAergic interneurons, we prepared brain slices at a thickness of 200 µm using vibratome. The brain slices were immediately fixed with 4% PFA in 0.1 M phosphate buffer (PB) solution (pH 7.4) for at least 24 hour at 4°C. Slices were then permeabilised in 0.5% Triton X-100 in 0.1 M PB with 1% milk powder for 1 hour at room temperature. Primary and secondary antibodies were diluted with the permeabilisation solution with 0.5% Triton X-100 and 0.1 M PB. The primary antibodies used were against PV (mouse monoclonal, 1:500, P3088, Sigma-aldrich), SOM (rabbit polyclonal, 1:500, sc-13099, Santa Cruz Biotechnology, Heidelberg, Germany), 5HT3aR (goat polyclonal, 1:500, ab51950, Abcam), and Prox-1 (goat polyclonal, 1:100, AF2727, R&D systems). After incubating in primary antibodies overnight at 4 °C,

the slices were rinsed thoroughly with 0.1 M PB which was followed by incubating the slices with secondary antibodies for 2-3 hrs at room temperature in dark. The secondary antibodies used were Alexa Fluor® 647 (1:500), Alexa Fluor® 594 (1:500), and Alexa Fluor® 488 (1:500, all Invitrogen) conjugated with goat, mouse or rabbit. Controls were also performed with the absence of secondary antibody. After final rinsing with 0.1 M PB for several times, the slices were embedded in Moviol and viewed using Epifluorescence microscope. The fluorescence images were taken using CellSans system from Olympus Life Sciences.

In some experiments, to identify the molecular markers expressed by nFS interneurons, we added Alexa Fluor® 594 biocytin salt (1:500, Invitrogen, Darmstadt, Germany) to the internal solution (composition as described before) to identify the patched neurons in the post-hoc antibody labeling methods. After recording, the slices were fixed in 4% paraformaldehyde (PFA) in 0.1 M phosphate buffer (PB) solution (pH 7.4) for at least 24 hour at 4 °C and repeated the same procedure as mentioned before. The position of the biocytin stained neuron could be visualised by the conjugated Alexa dye, which would then be verified for the presence of a specific molecular marker. After collecting the fluorescence data, the slices were incubated in 0.1 M PB overnight, which was later followed by biocytin processing to get the morphological data.

2.4. Analysis of electrophysiological parameters

Passive membrane properties

Resting membrane potential (RMP) was measured immediately after breaking in through the cell membrane. The series resistance was also measured, which corrects the membrane voltage errors under conditions of high access resistance between pipette and cell interior. Only neurons with a stable RMP between -50 and -75 mV and with a series resistance of less than 40 MΩ were included for data analysis to guarantee a high recording quality. Membrane properties such as input resistance, membrane time constant and voltage sag were measured. The recorded data was analysed using custom-written macros (courtesy of Dr. Karlijn van Aerde) in Igor Pro 6 (Wavemetrics).

Active properties

Action potential (AP) was elicited using rectangular current pulse injection for 1 s, at varied current steps. A smaller increase in step size of 10 pA was used to identify the first

AP. The properties of single AP such as AP threshold, AP half-width, AP time, AP amplitude, and after-hyperpolarisation (AHP) amplitude were measured at the first ever elicited AP, since this ensures lowest variance due to the fact that it is not influenced by sustained stimulation and it is very close to the native threshold.

A larger increase in step size of 25 pA was used to identify the firing properties. The first AP train with a minimum of ten spikes was used to measure the inter-spike interval (ISI), and spike frequency adaptation.

Electrophysiological data analysis

The input resistance (R_{in}) was calculated by plotting the relation between changes in voltage and the injected current. The values lying in the range between -50 and 50 pA current injection were fitted using a linear regression and the slope of the linear fit was measured as the input resistance **(Fig. 2.3A)**.

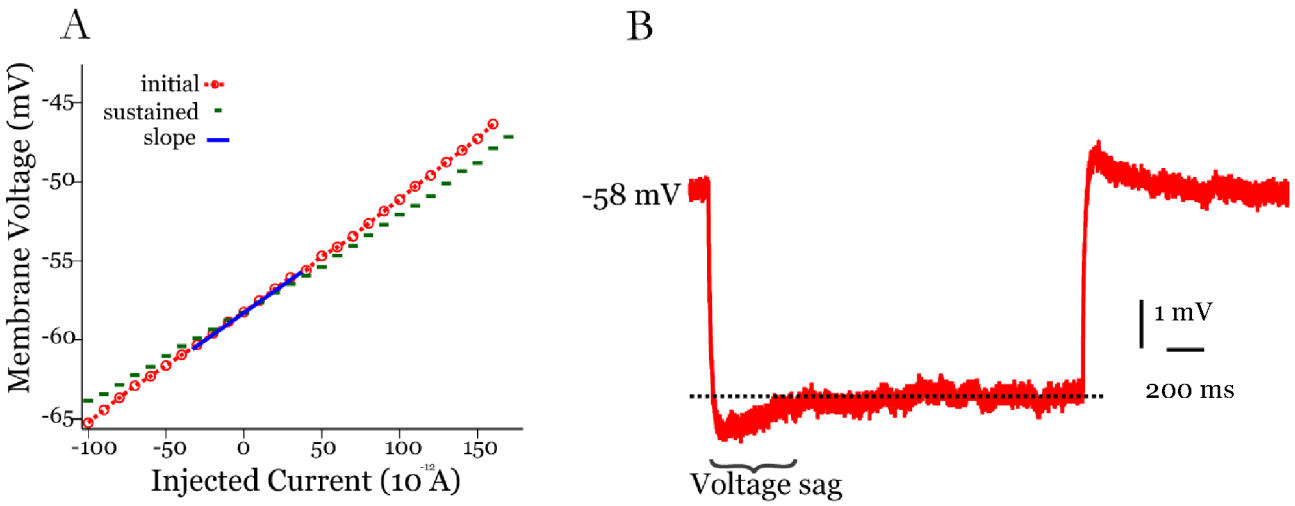

Fig. 2.3. Passive membrane properties. (A) *The initial (red circle) and sustained (green line) membrane voltage was plotted against the injected current. The linear slope fitted between -50 and 50 pA was measured as input resistance.* ***(B)*** *Voltage sag seen during hyperpolarizing potential.*

The membrane time constant tau τ (ms) indicates the time for the membrane potential to fall from the resting membrane potential to 1/e (~63%) of its final value in the changing curve during the application of a small negative current pulse. The shorter the time constant, the faster the membrane potential is fully polarised.

A voltage 'sag' is sometimes seen at hyperpolarising potentials, which is mediated by **h**yper polarisation activated, **c**yclic-**n**ucleotide gated (HCN) channels. The voltage sag was quantified by the sag index, which was calculated as the difference between the most hyperpolarised voltage and the steady-state voltage deflection, divided by the steady-state deflection **(Fig. 2.3B)**.

AP threshold (mV), AP time (ms), and rheobase (pA) were measured as the minimum voltage, time and current respectively, which were required for the initiation of first spike **(Fig. 2.4A)**. AP amplitude (mV) was measured by calculating the voltage difference between the maximum and the threshold during depolarisation. AP half-width (ms) was determined as the time difference between rising phase and decaying phase of the AP at half-maximum amplitude. AHP amplitude (mV) was calculated as the difference voltage difference between minimum and the threshold during hyperpolarisation **(Fig. 2.4B)**. AP accommodation is measured as the difference between the first three AP peak and the last three AP peak on a 10-spike train. AHP accommodation is measured as the difference between the first and the last AHP peak on a 10-spike train.

Since the excitability of a neuron depends on multiple properties, like RMP, AP threshold and R_{in}, an index was used to measure the excitability of a neuron *(Lazarus MS and ZJ Huang 2011)*.

Excitability index (EI) = (RMP-AP threshold)/R_{in}.

The **i**nter-**s**pike **i**nterval (ISI) (ms) is defined as the time taken between individual spikes and was calculated as an average during 10-spike train. The spike frequency adaptation ratio was calculated as the ratio of the mean of first three ISIs and the last three ISIs in a 10-spike train **(Fig. 2.4C)**. Value close to 1 would mean no adaptation, and close to 0 would mean very high adaptation. Since not all neurons could be injected with similar highest current value as this might lead rapid saturation in some but not in all neurons, it was not possible to measure the highest firing frequency based on a specified highest current injection. Therefore, the average firing frequency of the neuron was assessed measuring multiple firing frequency responses following current injections ranging from 0 to 300 pA. The values lying in the linear range were fitted using a linear regression and the average firing frequency per 100 pA of the neuron was calculated **(Fig. 2.4D)**.

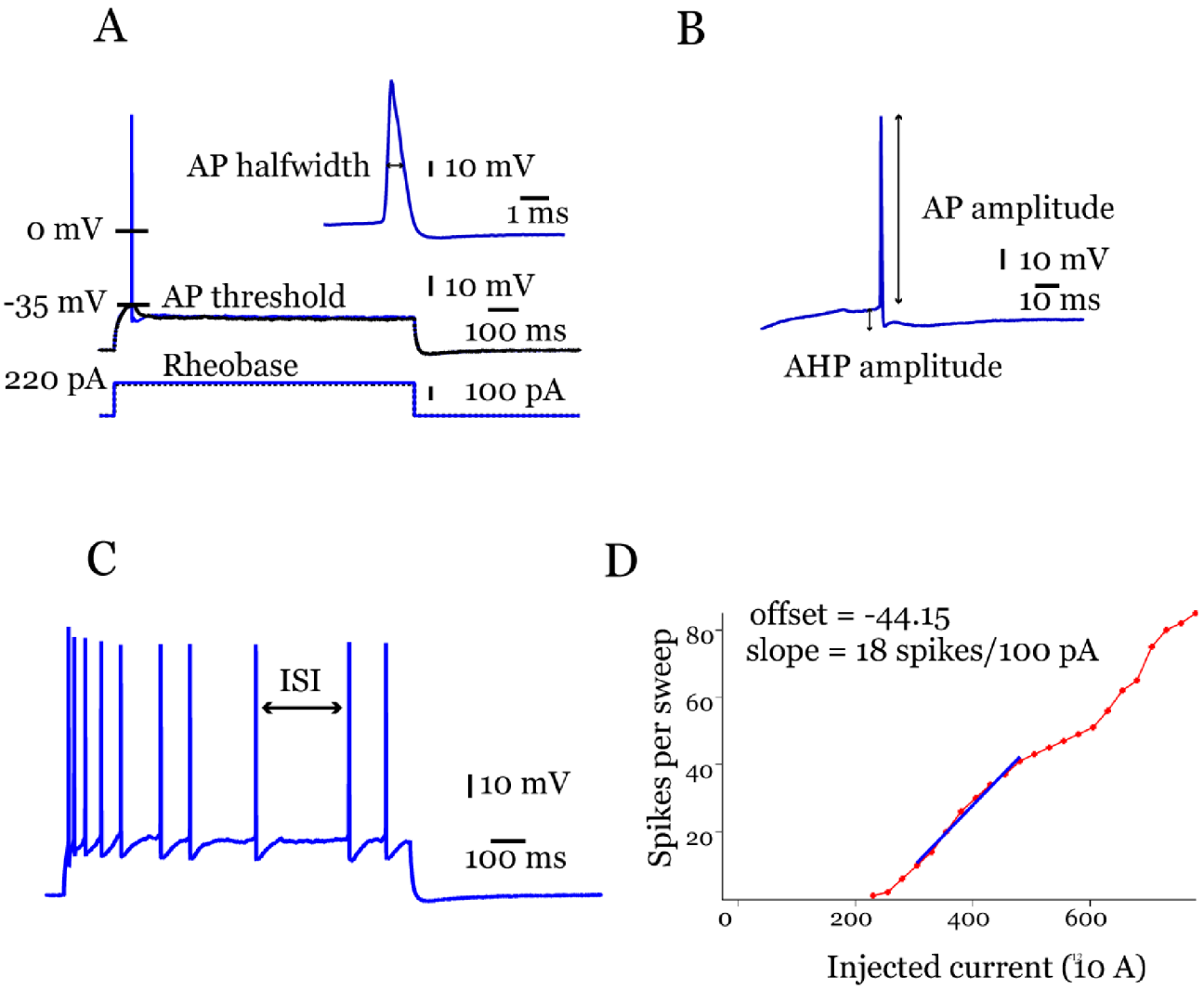

Fig. 2.4. Active membrane properties. ***(A)*** *Action potential (AP) threshold was measured as the minimum voltage required for the initiation of first spike. Rheobase was measured as the minimum current required to generate the first spike. Blue trace corresponds to threshold current and voltage. Black trace corresponds to pre-threshold current and voltage. Inset: AP halfwidth was measured as the time difference between rising and decaying phase of the AP at half-maximum amplitude.* ***(B)*** *Calculation of AP amplitude and AHP amplitude are shown.* ***(C)*** *Inter-spike interval (ISI) was calculated as an average of time taken between individual spikes in a ten-spike train.* ***(D)*** *Average firing frequency was calculated by plotting number of spikes against injected current. The slope of linear fit corresponds to the average firing frequency per 100 pA current injection.*

Synaptic physiology

Synaptic parameters such as PSP amplitude, latency, rise time and decay time were analysed as described in previous studies *(Feldmeyer D et al. 1999)*. The recorded data were analysed using custom-written algorithms (Igor Pro; Wavemetrics, Lake Oswego, OR). First, an average sweep was generated after aligning the individual sweeps to their corresponding presynaptic AP peaks. The PSP peak amplitude, Vpeak, was calculated as

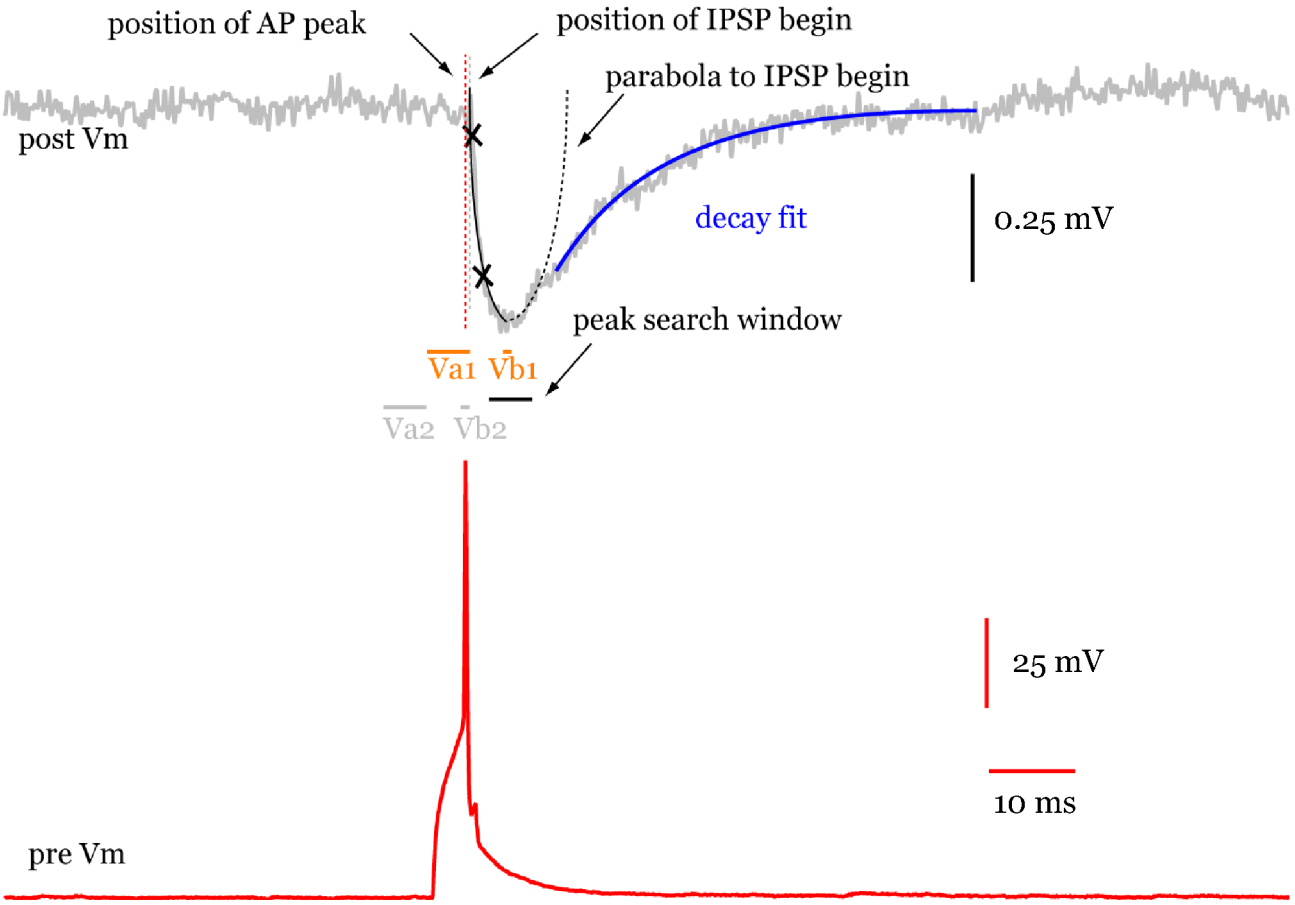

Fig.2.5. Analysis of synaptic properties (latency, amplitude, noise, rise time, and decay time). *Paired recording was performed between a L4 non-fast spiking interneuron (bottom) and a L4 spiny neuron (top) (Vm, membrane potential). The latency was defined as the time interval between the peak of presynaptic AP and the onset of the IPSP (dashed vertical lines). IPSP amplitude, Vpeak, was calculated as the difference between maximum voltage, Vb1, and the mean baseline amplitude, Va1. Vnoise was calculated as the difference between Vb2 and Va2 (refer text for details). Rise time was calculated as the mean time to rise from 20% to 80% (two crosses) of the peak amplitude. The onset of the IPSP was obtained using a parabolic fit of the IPSP rising phase to the baseline. The decay of IPSP was fitted with exponential fit to the falling phase of the IPSP (blue line).*

the difference between maximum voltage and mean baseline amplitude. The maximum voltage, Vb1, was measured within a 'peak search window' of 5 ms as a mean over 0.5-1 ms. The mean baseline amplitude, Va1, was measured in a baseline region of 5 ms just preceding the PSP. The PSP noise amplitude, Vnoise, was calculated in a similar manner as Vpeak, where a second maximum voltage, Vb2, and a second baseline amplitude, Vb1, were measured in a similar duration as Vb1 and Va1, and were separated by the same interval. Rise time was calculated as the mean time to rise from 20% to 80% of the peak amplitude as determined from the number of trials (linear fit). The latency was calculated as the time interval between the peak AP amplitude and the onset of the PSP. The decay time constant

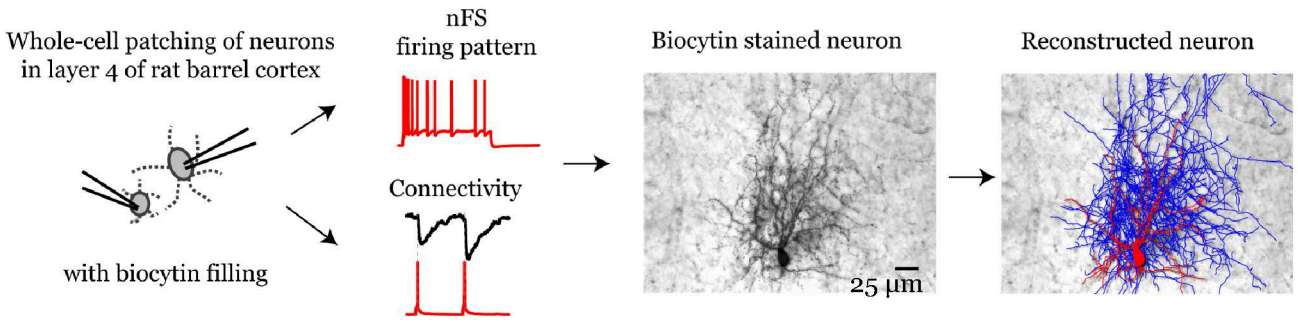

Fig. 2.6. Schematic representation of experimental approach. *Single neurons and paired neurons were recorded using whole-cell patch clamp technique and were filled with biocytin. nFS interneurons were identified using their firing pattern. After recording, biocytin labelling was processed using immunohistochemical methods, which allowed us to identify the morphology of patched nFS interneurons. Later, the stained neurons were reconstructed using Neurolucida software to get the complete 3D morphology of patched neurons. Axon is labeled in blue, soma and dendrites in red.*

was measured using single exponential fits to the decay phase of both individual and averaged responses. The background noise of the recordings was calculated by the standard deviation (s.d.) of Vnoise **(Fig. 2.5)**. The coefficient of variation (c.v.) of PSP amplitudes was calculated by subtracting the variance of the baseline noise from the variance of the PSP peak amplitude. Failures were defined as events with amplitudes less than 1.5 times the s.d. of the noise.

2.5. Morphological 3D reconstructions and analysis

Histological procedures

Slices containing biocytin filled neurons were later fixed in 4% PFA in 100 mM PB solution for at least 24 hour at 4 °C. The slices were then incubated in about 2 mL of H_2O_2 solution for about 20 min to block any endogenous peroxidase activity. After rinsing the slices several times using 100 mM PB solution, they were incubated in 1% avidin-biotinylated horseradish peroxidase (Vector ABC staining kit, Vector Lab. Inc.) containing 0.1% Triton X-100 for 1 hr at room temperature. It was followed by chromogen reaction by adding 3,3-diaminobenzidine (Sigma-Aldrich, USA) until the biocytin filled neurons with clear axonal and dendritic branches were clearly visible. The slices were again rinsed with 100 mM PB solution several times, followed by slow dehydration using ethanol and xylene. Finally the slices were mounted on gelatinised slides and embedded using Eukitt medium (Otto Kindler GmbH) *(Marx M et al. 2012)*.

Morphological 3D reconstructions

Biocytin labelled neurons in L4 were morphologically reconstructed using Neurolucida software (MicroBrightField, USA) and Olympus BX61 microscopy at 1000 X magnification (100x objective and 10x eyepiece). Only slices with clear neuron labelling and low background staining were considered for reconstruction **(Supplementary Fig. 1,2)**. During single-cell reconstruction, axons were always labeled in blue, soma and dendrites in red **(Fig. 2.6)**. For synaptically coupled neurons, interneurons were labeled blue and red,whereas, excitatory neurons were labeled black for axon and green for soma and dendrites. Along with the neuronal reconstructions, demarcation between different layers, barrel borders, pial surface, and white matter were labeled. After reconstruction, the image was rotated such that the pial surface is aligned at the horizontal plane. Tissue shrinkage, which could be observed during biocytin processing, was corrected in all axes (factor 1.1 in the x and y axes, factor 2.1 in the z axes) *(Marx M et al. 2012)*. Analysis of 3D reconstructed neurons was done with Neuroexplorer software (MicroBrightField, USA). Morphological properties of neurons such as the length and the distribution of axon and dendrites across different layers and adjacent barrels were analysed *(Helmstaedter M et al. 2009b)*.

2.6. Quantitative classification methods

Principal component analysis

The dataset of neurons were represented in the form of a matrix, where rows of the matrix correspond to individual neurons and the columns to variables. The dataset was then standardised, since not all the parameters used were in the same unit, especially electrophysiological parameters. The standardised data set having mean 0 and standard deviation 1 retained the properties of the original dataset. Principal Component Analysis (PCA) was used to analyse the interrelation between variables and to reduce the dimensionality of the dataset while still preserving the maximum variability. PCA reduces the redundancy of the dataset by eliminating correlated variables that might double weigh the variables. PCA produces linear combinations of the original variables to generate new axes, also known as principal components (PC) that are orthogonal and therefore, uncorrelated.

The variances explained by each PC are represented as eigenvalues. To determine the number of PCs to retain for cluster analysis, we used Kaiser's rule, which is one of the

most widely used criterion. Kaiser's rule is an objective way to determine the number of clusters by leaving all components with eigenvalues less than one. Since the dataset is standardised, the variables have an eigenvalue of one, and therefore PCs with eigenvalue greater than one describe more of the data's variance than an original variable. To visualise the percentage of variance explained, we used Pareto charts, which give a graphical representation of the variance explained by each PCs.

Hierarchical unsupervised cluster analysis

Quantitative classification was performed using agglomerative hierarchical unsupervised Cluster Analysis (CA) that quantifies how different, or how similar two neurons are. CA was performed on the dataset in PC space using Euclidean distances to calculate the linkage distance. Ward's minimum variance method was used for combining clusters at each stage, which minimises the total within-cluster variance *(Ward Jr JH 1963)*. To have a visual representation of the distance at which clusters are combined, a dendrogram was used where the vertical lines show joined clusters. The position of the line indicates the distance at which clusters are joined. The number of optimal clusters was determined using Thorndike procedure, where the linkage step with maximum linkage distance was used for cutoff *(Thorndike RL 1953)*.

K-means clustering

K-means is an alternative clustering tool, where the number of clusters, K is predefined. In this study, K-means clustering was performed, with K equal to the number of clusters from hierarchical clustering. The K-means method first randomly identifies centroids for each cluster. Each dataset is grouped to the nearest centroid to form a set of temporary clusters. The mean point of the temporary cluster is then assigned as the new centroids, the data points are rearranged, and the process continues until there is no change in the clusters.

Silhouette analysis

Silhouette analysis measures the quality of the clustering by calculating the separation between the resulting clusters *(Rousseeuw PJ 1987)*. The silhouette plot shows a measure of how close each dataset in one cluster is to the neighbouring clusters. This measure ranges between -1 to 1. Silhouette value near 1 means that the dataset in one

cluster is far separated from the neighbouring clusters. A value of -1 indicates that the dataset might be wrongly assigned.

2.7. Axonal and dendritic density maps

3D maps of axonal and dendritic length density were made using computerised 3D reconstructions, where the axonal and dendritic tree length per unit volume of 50 × 50 × 50 μm^3 was calculated. The soma centre of each neuron was given the co-ordinates of X, Y, Z = (0, 0, 0), and the relative co-ordinate of the beginning and endpoint of each segment in the tracing were obtained using the segment points analysis in Neurolucida Explorer. Further steps were carried out in Matlab using custom-written software (courtesy of Dr. Guanxiao Qi and Dr. Haijun Wang). 3D density maps were constructed for each reconstructed neuron from a single cluster, and then were averaged to get the 3D density map for this cluster. Individual density maps were aligned with respect to the barrel centre where the cell body is located. Barrel borders were identified in the low magnification (4× objective) bright-field photomicrographs made during patch-clamp recording. The averaged density map for each cluster was smoothed using the 3D smooth function in Matlab with a Gaussian kernel (s.d. = 50 μm). Isosurfaces were calculated at the 80-percentile for the smoothed density maps. Finally, axonal and dendritic density maps were visualised in blue and red, respectively.

2.8. Statistical Analysis

Data are represented as mean±standard deviation. For datasets with 3 or more independent groups, one-way ANOVA could be performed if normal distribution can be assumed. Non-parametric tests can be used when normal distribution cannot be assumed due to small sample size. Since at least one of the groups had small sample size, we used Kruskal-Wallis test (non-parametric) for multiple comparison, followed by a post hoc Wilcoxon rank sum test (or, equivalently, the Mann-Whitney test) when 3 or more independent groups were compared. In case of an extremely small sample size, i.e., less than 4 in either of the groups, the Wilcoxon test was not used *(Janušonis S 2009)*. In such cases, t-test was used if the effect size is large *(de Winter JCF 2013)*.

3. Results

Previous studies on the classification of nFS interneurons were performed mainly using transgenic mouse models expressing green fluorescence protein (GFP) in SOM interneurons, which constitute 30% of the total interneuron population *(Halabisky B et al. 2006; Ma Y et al. 2006; McGarry LM et al. 2010; Rudy B et al. 2011; Xu H et al. 2013)*. However, large-scale single-cell RNA sequencing has recently revealed at least 16 different interneuron types based on the molecular markers, and they show a huge overlap between different interneuron types, with an exception of PV *(Zeisel A et al. 2015)*. This data suggests that classification based on the expression of a certain molecular marker alone might not provide complete information about a particular interneuron type.

The choice of parameters used to classify interneurons plays an important role in providing a reliable classification. Previous studies relied on morphological parameters such as the size, and shape of soma, number of axonal and dendritic nodes, branching angle, segment length, and so on, to characterise the interneuron types *(McGarry LM et al. 2010)*. Classifications based on such parameters do not provide any meaningful information regarding functional compartments the neuron will receive or transmit synaptic information. Morphological parameters such as axonal projection pattern have a critical influence on the intra- and inter-columnar processing. Therefore, in this study, we performed the quantitative classification based mainly on the axonal innervation domains of nFS interneurons with reference to cortical layers and columns.

We were able to successfully perform whole-cell patch-clamp recordings, with simultaneous biocytin filling on 80 nFS interneurons in L4 of adult rat barrel cortex. After biocytin processing, neurons were carefully selected to be able to make complete 3D reconstructions. Some neurons with incomplete filling, or high background staining were not reconstructed, resulting in 44 high quality complete 3D reconstructions of nFS interneurons **(Supplementary Fig. 1,2)**. Furthermore, another important factor in providing a complete neuronal morphology is the brain-slicing angle. Therefore, we used an additional criterion that calculates the number of axonal truncations, with careful visual inspection on the location of truncation. With this criterion, neuronal reconstructions having more than 15% truncations, and those near the cell soma were excluded from the data analysis, resulting in 38 complete 3D reconstructions.

Analysis of 3D reconstructed neurons was performed using the Neuroexplorer software (MicroBrightField, USA). We measured the total axonal and dendritic length, as well as the fraction of axonal and dendritic length in different layers and columns **(Fig. 3.1.1)**.

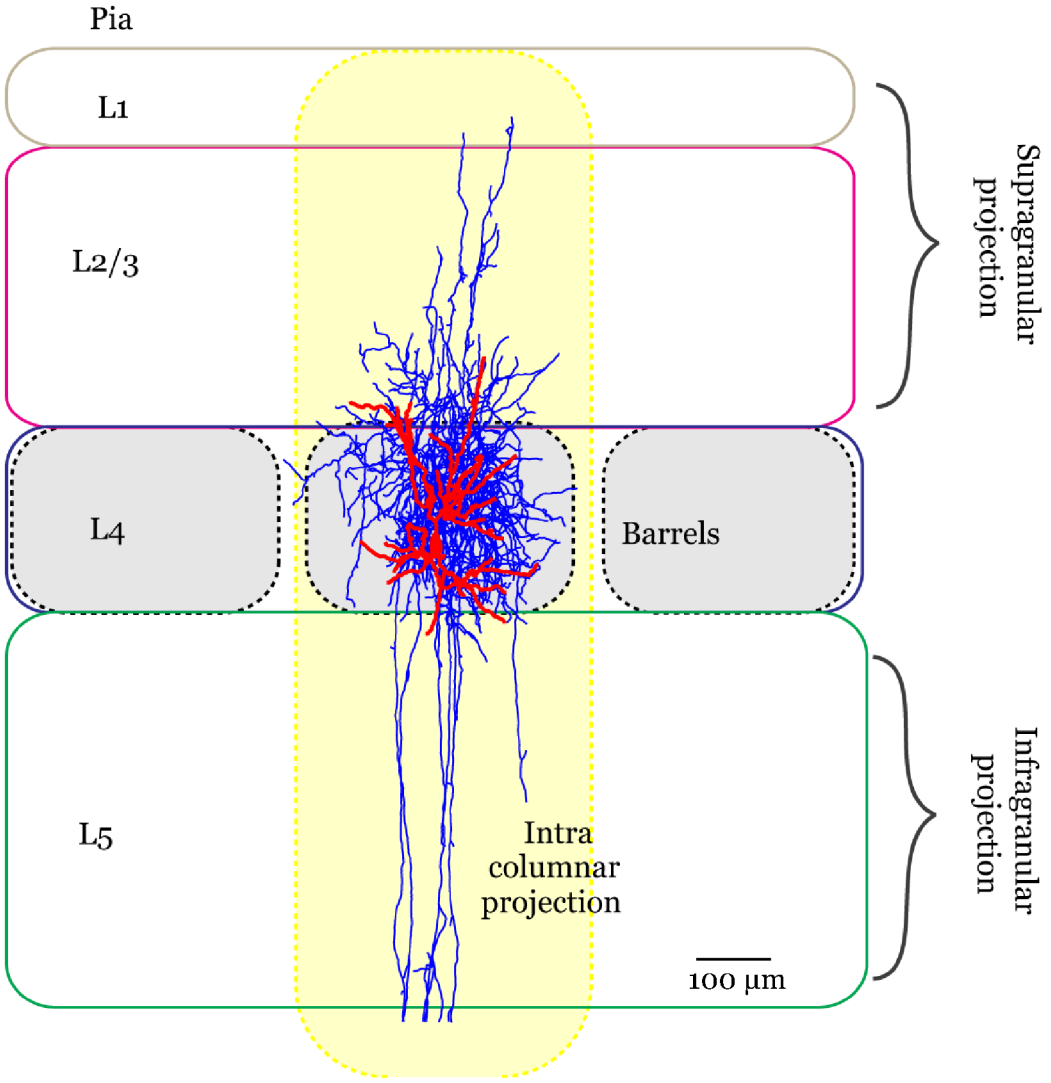

Fig. 3.1.1. Morphological 3D reconstruction of L4 nFS interneuron. *Soma and dendrites are labeled in red, and axon in blue. Layers and barrel borders were demarcated during reconstruction, to determine the fraction of axonal and dendritic lengths in different layers, barrels (grey) and in the home and neighbouring barrel columns (yellow).*

3.1. Morphological Classification of nFS interneurons

Based on the morphological parameters we obtained, we performed CA on the dataset of 38 neuronal reconstructions in PC space to classify nFS interneurons based on their axonal and dendritic projection patterns. The first three PCs with eigenvalues greater than one were retained for cluster analysis, and they show a variance of more than 80% **(Fig. 3.1.2)**. Hierarchical unsupervised CA revealed three distinct morphological clusters of L4 nFS interneurons, as shown in the dendrogram in **Fig. 3.1.3A** (labeled violet, light

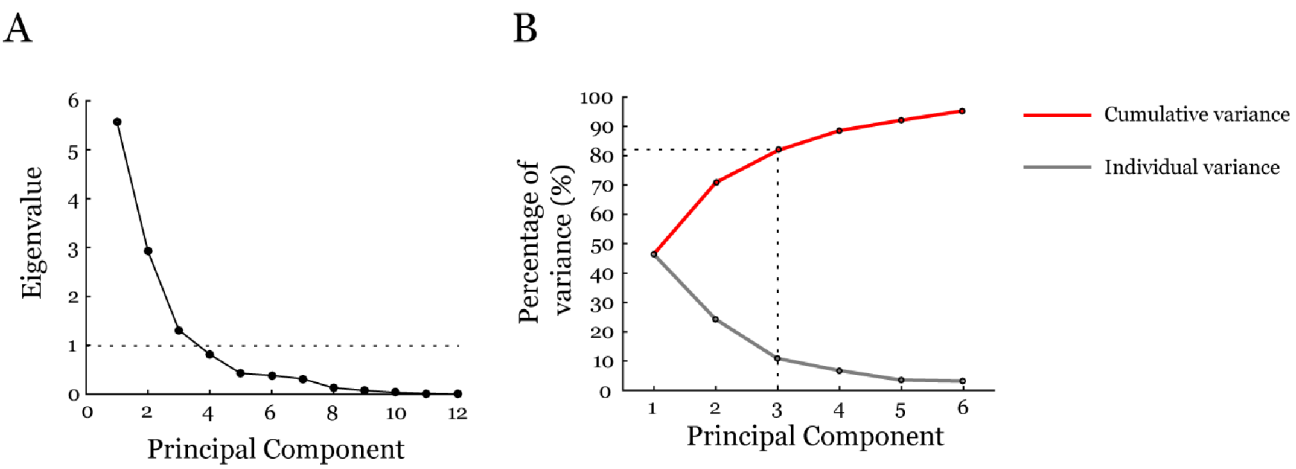

Fig 3.1.2. Principal component analysis of L4 nFS interneurons. (A) *The dataset were standardised. The numbers of principal components (PC) to be retained for cluster analysis were determined using Kaiser's rule (with eigenvalues greater than one).* ***(B)*** *Pareto plot shows the percentage of variance explained by each PC. Grey line represents the variance explained by individual PC, and red line represents the variance explained by cumulative PCs.*

blue and teal). The optimal number of clusters was determined by Thorndike method with the largest linkage distance, which is used as the cut-off **(Fig. 3.1.3B)**. The three clusters were distinct in their axonal and dendritic projections patterns. Cluster 1 (C1) neurons showed distinct axonal and dendritic projections to neighbouring barrels and was therefore designated as lateral projection neurons. Cluster 2 (C2) neurons were distinguished by their columnar confinement of axons and dendrites and thus called as intra-columnar projection neurons. Furthermore, two subcategories of C2 were found, with differences in their projection in home barrel. Cluster 3 (C3) neurons displayed a distinct axonal projection, with extensive branching in extra-granular layers, and little projection in the home layer. C3 was further divided into two sub-clusters. C3a showed massive projections in L2/3, whereas C3b showed bipolar dendritic pattern and sparse

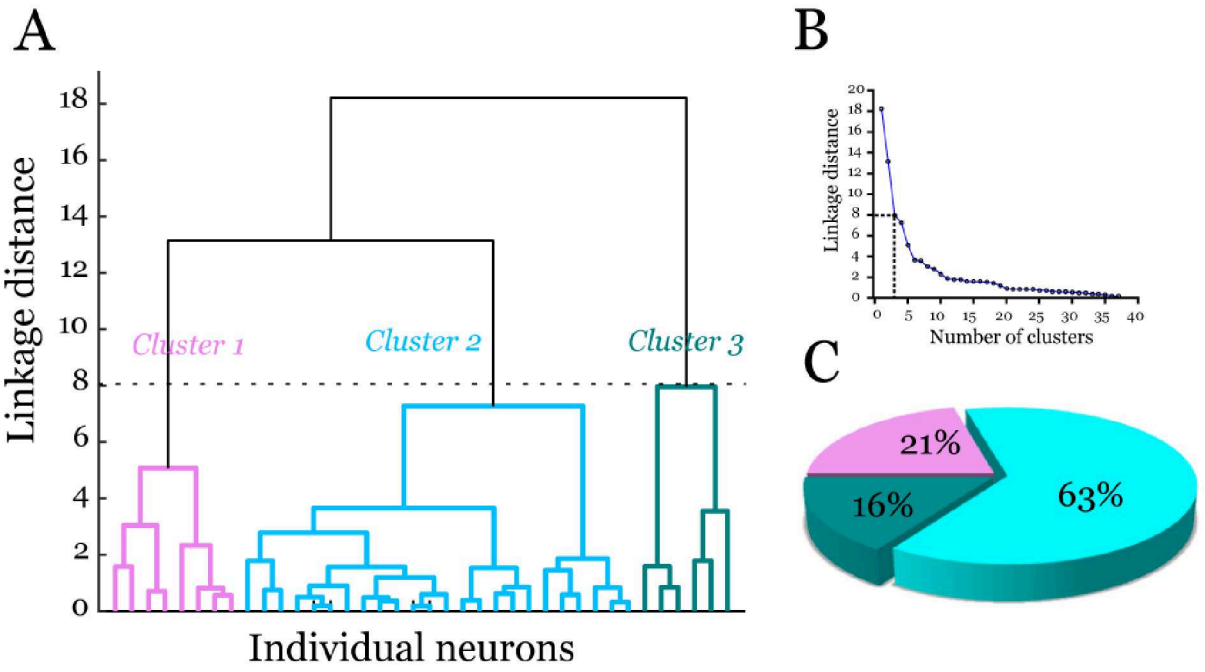

Fig 3.1.3. Morphological analysis of L4 nFS interneurons using Hierarchical clustering. ***(A)*** *Ward's method of hierarchical cluster analysis was used to identify different clusters from 38 nFS interneurons based on morphological parameters. The X-axis of dendrogram shows individual neurons, and the Y-axis corresponds to the linkage distance measured by Euclidean distance.* ***(B)*** *The cut-off for significant clusters was determined using the Thorndike method. Cluster 1 is shown in violet, cluster 2 in light blue, and cluster 3 in teal.* ***(C)*** *The pie chart projects the percentage of each cluster, with the same colour code as in dendrogram.*

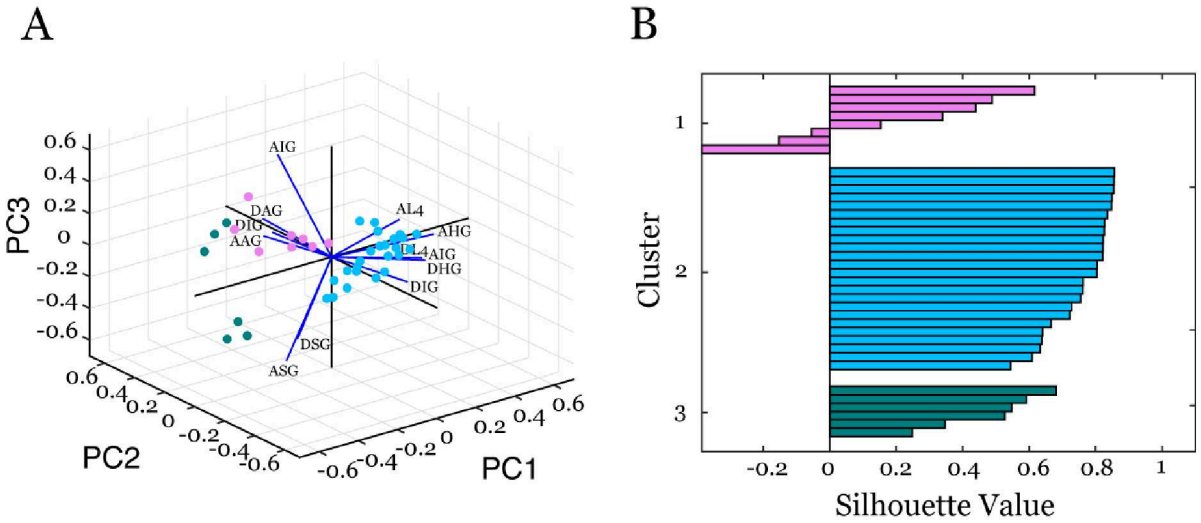

Fig 3.1.4. Validation of morphological analysis of L4 nFS interneurons. ***(A)*** *Biplot of the dataset in principal component space. The morphological parameters are labeled in blue vectors, and illustrate the contribution of each parameter in 3PC space. Each dataset is color coded as in the dendrogram.* ***(B)*** *Silhouette plot for the morphological clusters. The x-axis represents the silhouette value, and Y-axis represents the different clusters. Large values close to 1 indicate that clusters are well separated.*

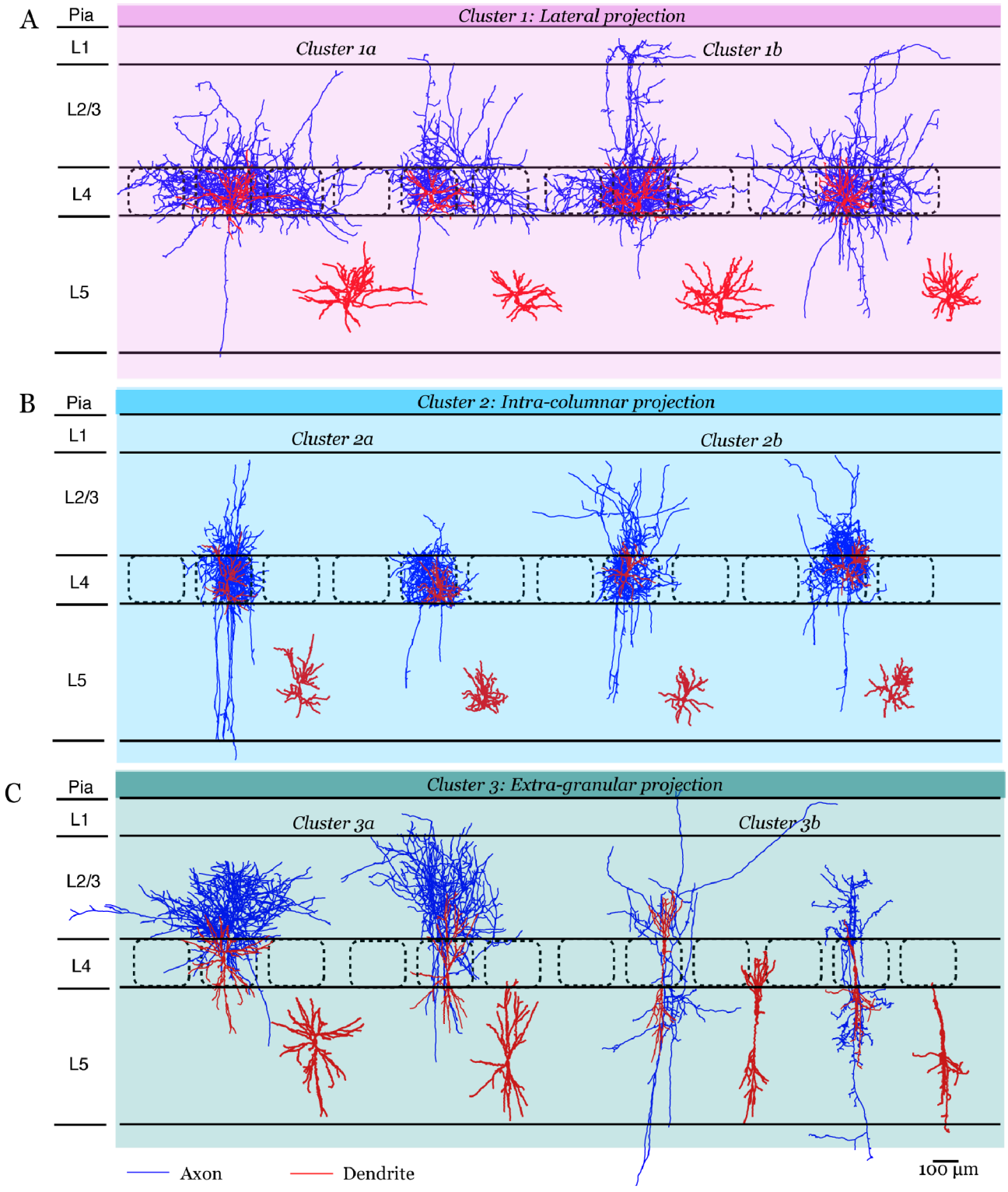

Fig. 3.1.5. Representative examples for each of the three clusters. *Neurolucida reconstructions of L4 nFS interneurons are classified into three distinct clusters, based on their axonal and dendritic projection pattern. (A) Cluster 1 shows interneurons with lateral projection pattern, (B) Subgroups of Cluster 2 showing intra-columnar projection pattern, (C) Subgroups of Cluster 3 showing extra-granular projection patterns. Axons are labeled in blue, and somatodendrites in red. Somatodendritic domains are shown again separately near each reconstruction for clarity purpose.*

projections to the supra- and infra-granular layers, much like VIP neurons. To summarise, 38 nFS interneurons in L4 were classified into three main clusters, with 8 neurons in C1 (21%), 24 neurons in C2 (63%), and 6 neurons in C3 (16%) **(Fig. 3.1.3C)**. The representative neurons for each cluster are shown in **Fig. 3.1.5**. (See Supplementary figures for individual neurons belonging to each cluster)

Parameters	Cluster 1 (8)	Cluster 2 (24)	Cluster 3 (6)	Kruskal -Wallis	1 vs 2	1 vs 3	2 vs 3
Axon Supra-granular	23.71±7.41	23.13±14.17	59.71±27.23	*	ns	**	**
Axon Layer 4	69.07±7.42	70.37±12.32	14.47±6.63	***	ns	***	****
Axon Infra-granular	8.73±5	6.77±5.42	24.41±21.44	ns	ns	ns	ns
Axon Home barrel	37.96±8.21	61±12.16	10.25±4.45	****	****	***	****
Axon Adjacent barrel	16.38±4.96	1.74±3.03	1±0.82	***	****	***	ns
Axon Intra-columnar	69.11±10.61	93.22±7.34	82.09±8.56	****	****	*	**
Dendrite Supra-granular	1.49±1.99	7.23±11.05	29.61±20.61	**	ns	**	**
Dendrite Layer 4	88.32±15.09	92.97±11.62	42.79±20.79	***	ns	**	****
Dendrite Infra-granular	5.08±6	0.6±1.21	37.82±23.76	****	**	**	****
Dendrite Home barrel	70.62±12.21	88.1±11.61	35.67±14.46	****	**	***	****
Dendrite Adjacent barrel	6.13±8.21	0.06±0.28	0.83±1.53	**	****	ns	ns
Dendrite Intra-columnar	85.27±14.96	99.5±1.25	97.23±3.17	**	***	ns	ns

Table 3.1: Statistical analysis of the morphological parameters of L4 nFS interneurons. *All data are represented as mean ± standard deviation. Statistical significance between all the clusters were performed using Kruskal-Wallis test, and Wilcoxon rank sum test was performed for the significant difference between individual clusters. Significant p-value is represented as * < 0.05, ** < 0.01, *** < 0.001, **** < 0,0001*

3D projections of the individual neurons in the PC space showed clear separation between the three clusters (labeled with the same colour code as in dendrogram) with relative contribution to each morphological parameter (blue lines) was shown in the biplot **(Fig. 3.1.4A)**. Cluster 3 showed 2 sub clusters, but they were clearly separated from the other main clusters. In order to assess the quality of the hierarchical clusters obtained by

Ward's method, we performed K-means clustering with the predefined number of clusters from hierarchical clustering. We found that the dataset in each cluster was exactly the same for both the K-means and Hierarchical clustering. We plotted the silhouette width of each clustering and found that the data points were well assigned for each cluster with most of the widths close to 1 **(Fig. 3.1.4B)**.

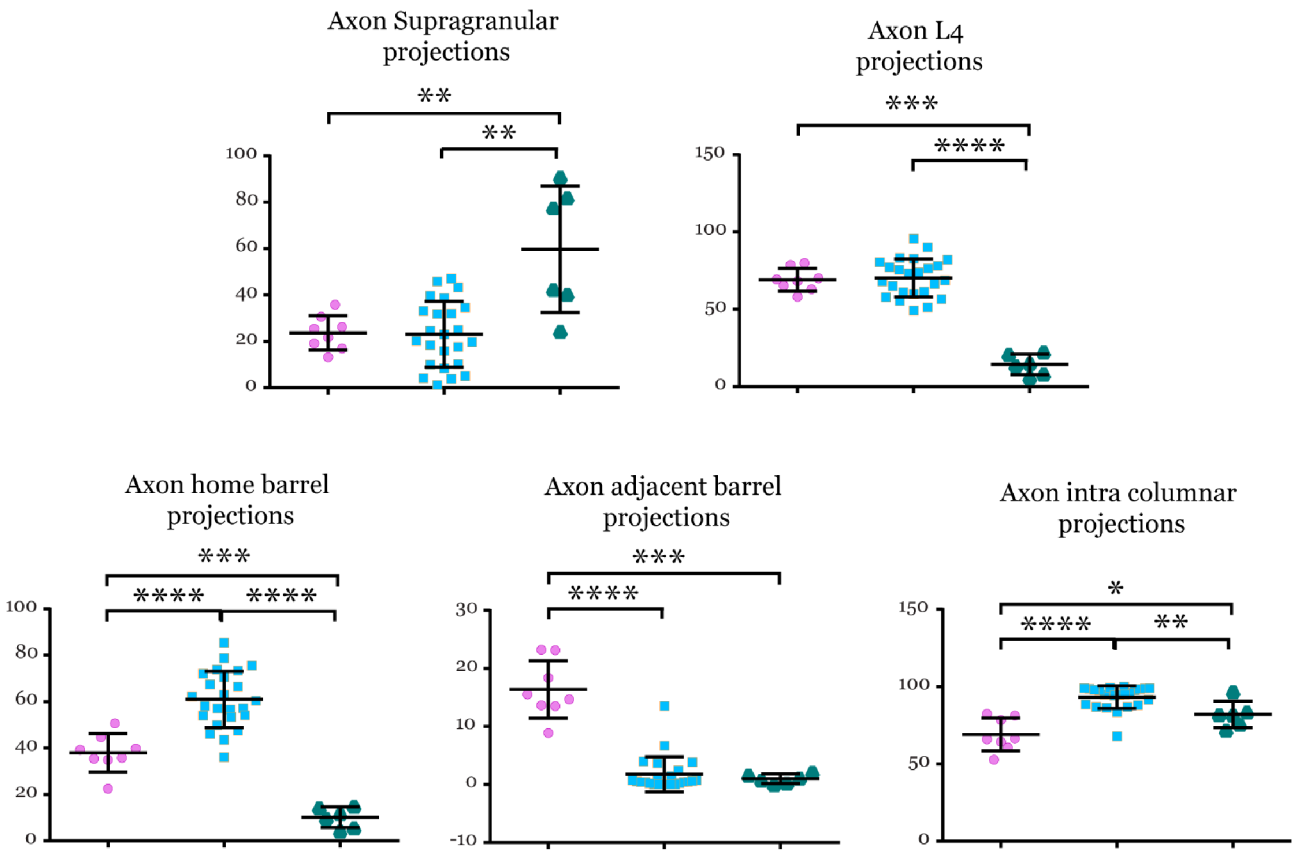

Fig 3.1.6. Comparison of axonal parameters between three clusters. *Axonal parameters are significantly different in almost all the three clusters. Significant p-value is represented as * < 0.05, ** < 0.01, *** < 0.001, **** < 0,0001*

Cluster 1: Lateral projection neurons

The first group of neurons, i.e., C1 neurons consists of 8 neurons and thus constitutes 21% of the total nFS interneurons. The distinctive feature of C1 neurons was the significant projection to adjacent barrels. This is a novel feature that has not yet been described for L4 interneurons **(Fig. 3.1.10)**; these lateral projection interneurons may form the cellular basis for lateral inhibition. C1 neurons also showed very dense and complex axonal arborisation, having an average total axonal length of around 45,000 µm. One of the lateral projection neurons displayed a massive axonal length of around 60,000 µm, which

is one of the highest recorded in L4 neocortical interneurons. Dendrites had an average total length of around 6,000 µm.

Only 69.1±10.6% of the axonal projections were within the home column, indicating that significant fraction of axonal projections were outside the column. Almost half of the lateral projections (16.4±5.0%) were targeted to the adjacent barrels **(Fig. 3.1.5 A, 3.1.10 top)**. Such a high percentage of lateral projections have been found for some L2/3 interneuron types, but never in L4 interneurons *(Helmstaedter M et al. 2009b)*. This indicates that lateral inhibition may occur already at the first site of cortical processing. In most cases, axons ascended and sent several collaterals to L2/3 and in few cases, the axons terminated in L1 with horizontal collateral branches **(Fig. 3.1.5A, 3.1.10 top)**. Axonal branches to the infra-granular layers were limited (8.7±5.0%) to L5, and no projections in L6 were found.

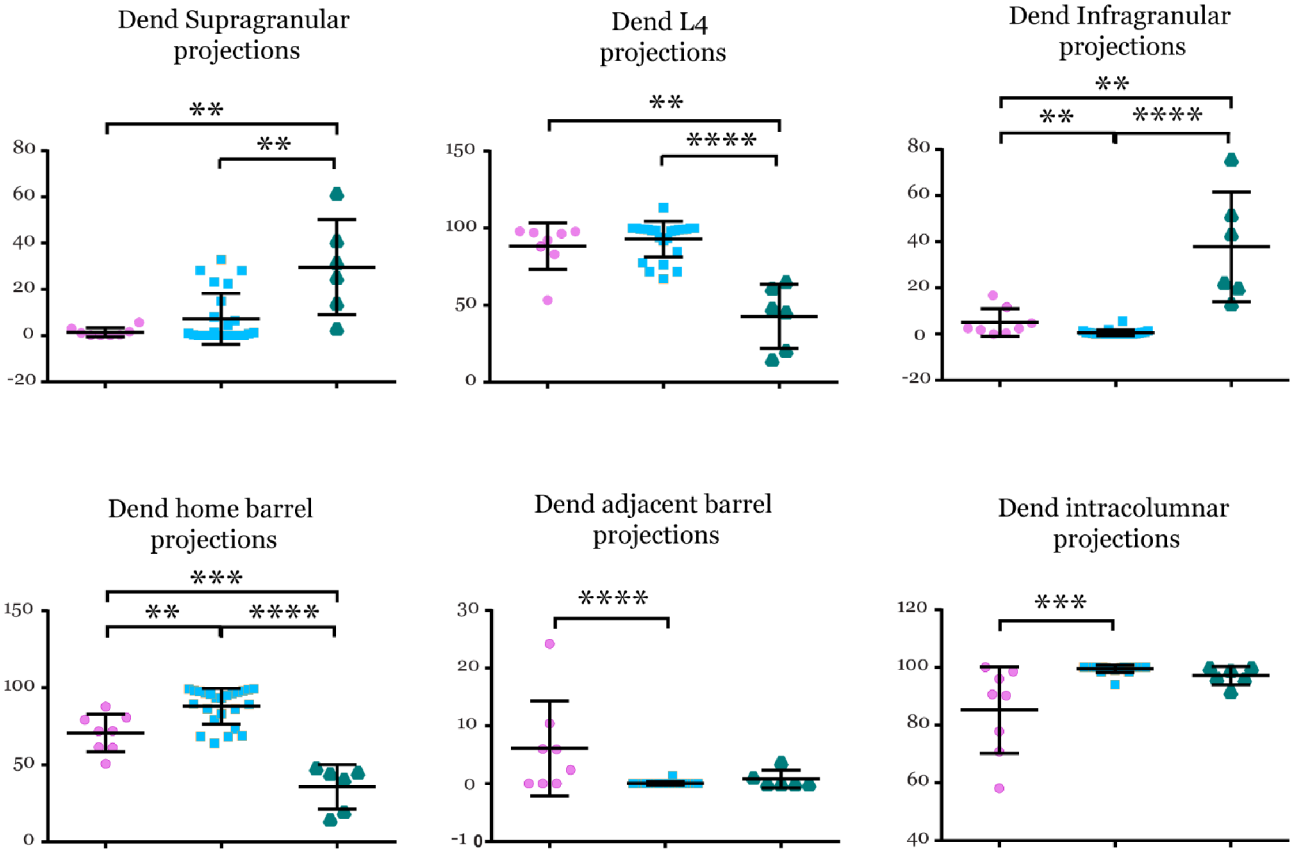

Fig 3.1.7. Comparison of dendritic parameters between three clusters. *Dendritic parameters are significantly different in almost all the three clusters. Significant p-value is represented as * < 0.05, ** < 0.01, *** < 0.001, **** < 0,0001*

Interestingly, dendritic projections followed similar projection pattern as axons, with significant projections (6.1±8.2%) to the adjacent barrels **(Fig. 3.1.7)**. However, they showed only few axonal projections to the supra- or infra-granular layers. The dendrites typically show multipolar arbors, with 4-7 primary dendrites. In most cases, the position of soma was at the middle lower end of the barrel.

Cluster 2: Intra-columnar projection neurons

The second cluster, C2 comprised of 24 neurons, which constitute 63% of the total nFS interneurons. Axonal branches were mostly confined to the home column (93.22±7.34%) **(Fig. 3.1.5B, 3.1.10 top)**. The two subgroups of C2 showed differences in the axonal projection in the home barrel **(Fig. 3.1.8)**.

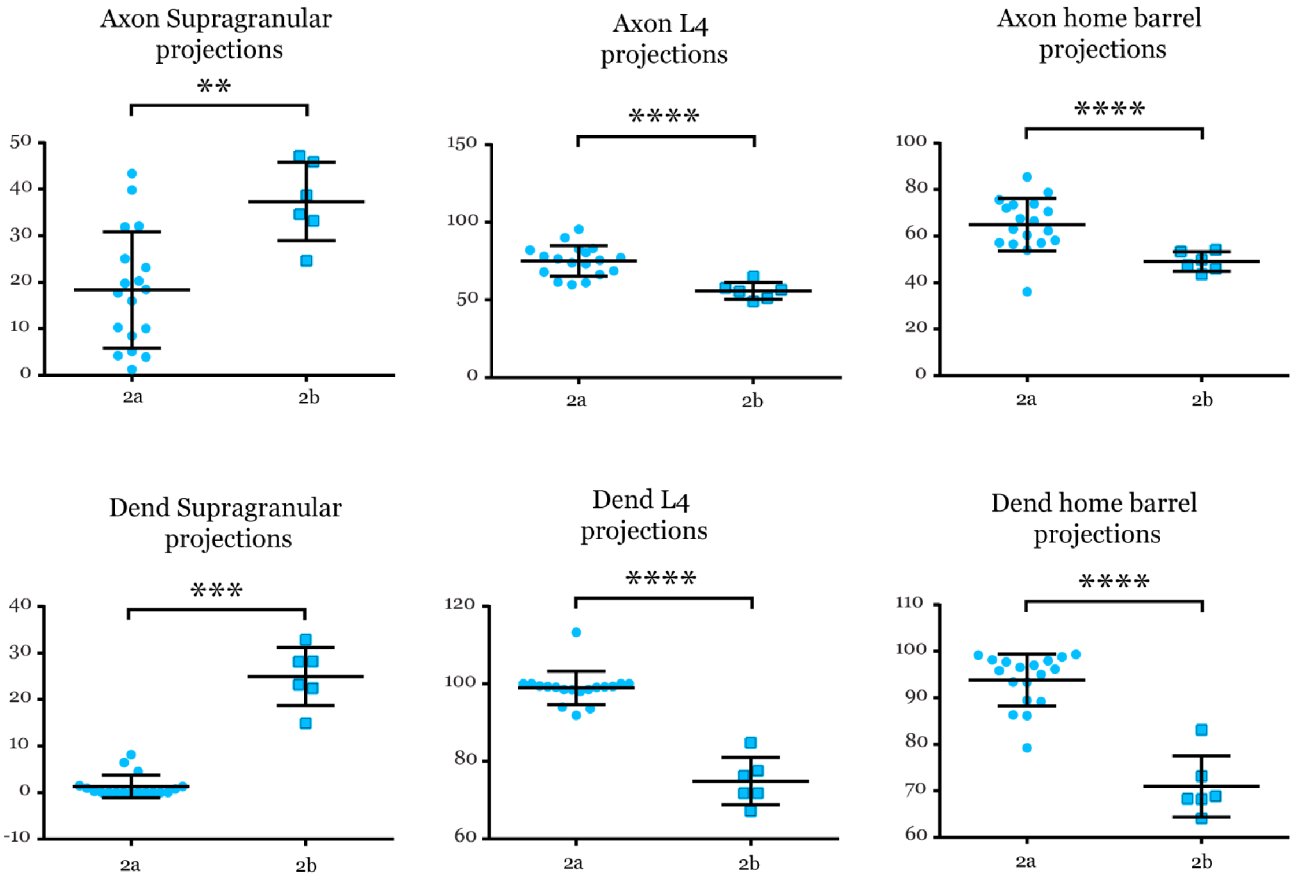

Fig 3.1.8. Comparison of Cluster 2 subtypes. *Axonal and dendritic parameters are significantly different in supra-granular, L4 and home barrel projections between C2a and C2b sub-clusters. C2a is labeled as blue circles, and C2b as blue squares. Significant p-value is represented as ** < 0.01, *** < 0.001, **** < 0,0001*

The first subgroup – C2a, comprised 18 neurons. The average total axonal length was around 36,000 µm, and the average total dendritic length was around 4,200 µm. The characteristic feature of this cluster was the dense local axonal projection that was largely confined to the home barrel, a feature characteristic of neurogliaform cells (NGFC). Such dense local axonal morphology limited to home barrel, designated as L4 barrel inhibitor interneurons has also been described for fast-spiking cells in L4 of rat barrel cortex *(Koelbl C et al. 2015)*. Most of the total axonal projections were confined to the home barrel (64.96±11.35%), with few projections to the supra- and little to infra-granular layers (18.38±12.47% and 7.15±6.02% respectively) **(Fig. 3.1.5, 3.1.8, 3.1.10 bottom)**. Dendrites displayed multi-polar arborisation and showed similar extensive projection to the home barrel at 93.98±4.3%, with little to no projection to the supra- and infra-granular layers **(Fig. 3.1.8)**.

The second subgroup – C2b, contained 6 neurons with an average axonal length of around 37,000 µm and an average dendritic length of around 4,500 µm. Confined to the home column, C2b neurons showed around only 49.14±4.17% of the axonal branches in L4 **(Fig. 3.1.5, 3.1.10 bottom)**. A significant fraction of axonal branches (37.37±8.44%) ascended and sent collaterals to L2/3 and L1, with little projections to L5 (5.65±3.13%). Unlike C2a, a significantly high percent (24.96±6.22%) of the dendritic arbors ascend to the supra-granular layers. Cell soma of all C2b neurons were positioned at the upper half of the barrel, which might contribute to the significant projection to the supra-granular layers.

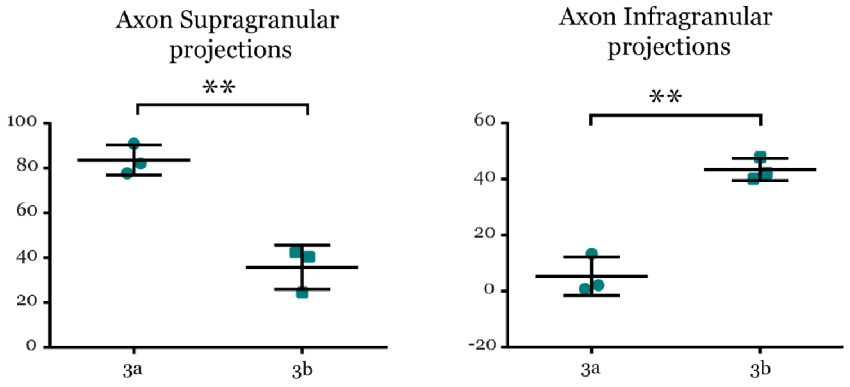

Fig 3.1.9. Comparison of Cluster 3 subtypes. *Axonal projections to the supra- and infra-granular layers are significantly different between C3a and C3b sub-clusters. C3a is labeled as teal circles, and C3b as teal squares. Significant p-value is represented as ** < 0.01*

Cluster 3: Extra-granular projection neurons

The final cluster, C3 comprised 6 neurons, and constitute 16% of the total nFS interneurons. A characteristic feature of this cluster was that axons project mainly outside the home barrel **(Fig. 3.1.5C, 3.1.10 top)**. C3 was further subdivided into two subgroups.

Axons of C3a nFS interneurons projected extensively in L2/3 and terminated in L1. C3a interneurons showed extremely dense axonal projections with a very high average total axonal length around 42,000 µm, most of which was confined to the supra-granular layers (83.59±6.75%) **(Fig. 3.1.5C, 3.1.9, 3.1.10 bottom)**. Only 8.43±5.87% of the total axon branches were within the home barrel, which was significantly different from the other clusters. C3a axons projected horizontally in L2/3, with around 20% outside the home column. The dendrites showed bipolar pattern, and displayed similar projection as axons.

The second subgroup, C3b, showed morphological feature similar to those of classical VIP-like neurons. They comprised the rarest neuron type. They showed a low number of axonal collaterals, with an average total axonal length of around 20,000 µm **(Fig. 3.1.5C, 3.1.10 bottom)**. C3b showed almost equal projections to the supra- and infra-granular layers (35.82±9.85% and 43.44±3.97% respectively) and very few projections within the home barrel (12.06±2.27%) **(Fig. 3.1.9)**. The dendrites were bipolar, and showed extra-granular projections, just like axons **(Fig. 3.1.5C)**.

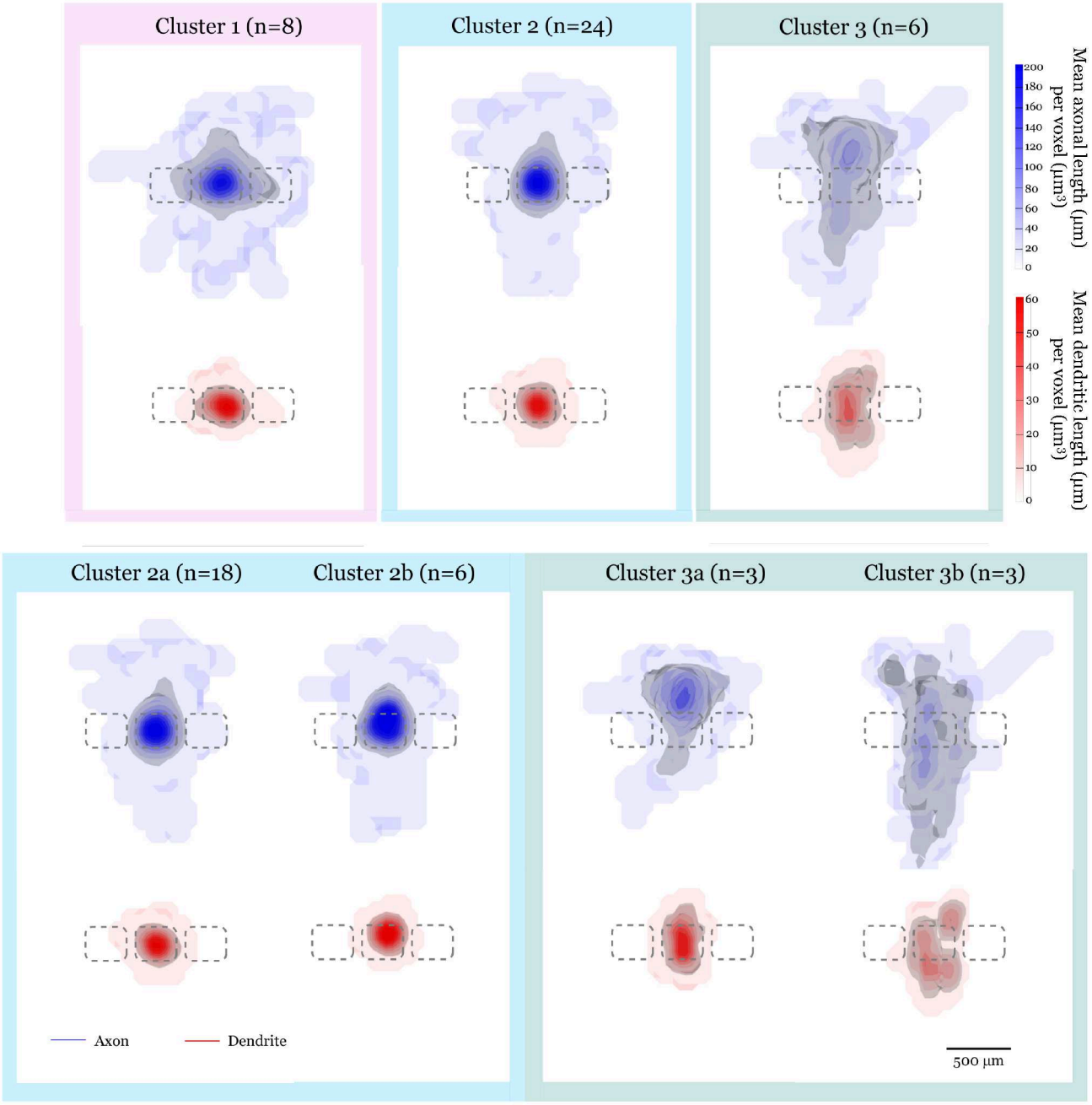

Fig. 3.1.10. Density maps of L4 nFS interneuron clusters. *(Top) The axonal (blue) and dendritic (red) maps are shown, along with 80 percentile of integrated axonal and dendritic length density, labeled in grey. The intensity of colours describes the density of axons and dendrites. The higher the colour intensity, the dense is the projection. (Bottom) Density maps of sub-clusters C2a and C2b, and C3a and C3b.*

3.2. Intrinsic electrophysiological classification

Since the firing properties of L4 nFS interneurones were heterogenous, we sought to classify the electrophysiological properties based on the passive membrane properties, action-potential properties and firing patterns. We recorded 80 nFS interneurons in L4. Only interneurons with a stable RMP that was more negative than -50 mV and a series resistance below 40 MΩ were included in the analysis, resulting in a total of 59 interneurons.

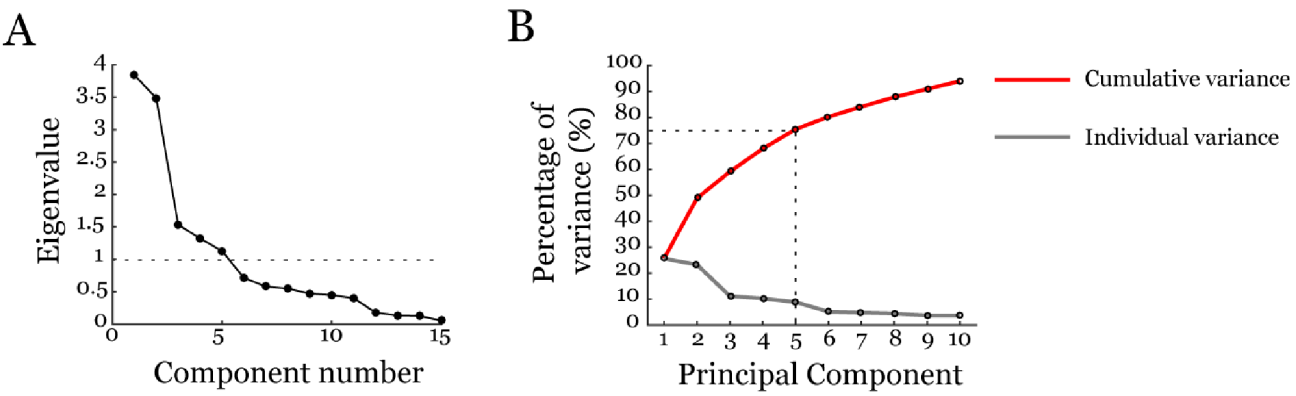

Fig. 3.2.1. Electrophysiological analysis of L4 nFS interneurons using principal component analysis. (A) *The datasets were standardised. The numbers of principal components with eigenvalues greater than one were retained for cluster analysis, leading to five PCs.* ***(B)*** *The Pareto plot shows the amount of variance explained by the PCA components. The five PCs explain around 75% of the total variance.*

For the electrophysiological classification, we included FS interneurons as a control. Parameters such as RMP, R_{in}, sag, membrane time constant, rheobase, AP threshold, AP half-width, AP amplitude, AP accommodation, AHP amplitude, AHP accommodation, ISI average, ISI standard deviation, Adaptation ratio, and firing frequency/100 pA were obtained from Igor Pro software.

Based on the above-mentioned parameters, we performed CA on the dataset of 59 single-cell recordings in PC space to classify L4 nFS interneurons. The first five PCs with eigenvalues greater than one were retained for cluster analysis **(Fig. 3.2.1A)**. The percentage of variance explained by five PCs was about 75% **(Fig. 3.2.1B)**. Using Thorndike method as a cut-off to determine the number of clusters, hierarchical unsupervised CA revealed two distinct electrophysiological clusters of nFS interneurons, with FS interneurons as a clearly separate cluster (Cluster 0/ Control). Cluster A was highly heterogenous, with many sub-groups and consisted of 42 nFS interneurons. The

second cluster was divided into two sub-clusters. Since the electrophysiological properties exhibited by the two sub-clusters were significantly different, we chose to consider them as two separate main clusters, and therefore designated as Cluster B and Cluster C respectively **(Fig. 3.2.2A)**. Cluster A neurons constituted 71% of the total population and showed strong adaptation and an irregular firing pattern; Cluster B comprised 10% of the total population, displaying characteristic early accommodation. The third cluster, Cluster C included 19% of the total population, showing regular spiking non-adapting firing pattern **(Fig. 3.2.2 C,D)**. (See Supplementary figures for firing pattern of all neurons.)

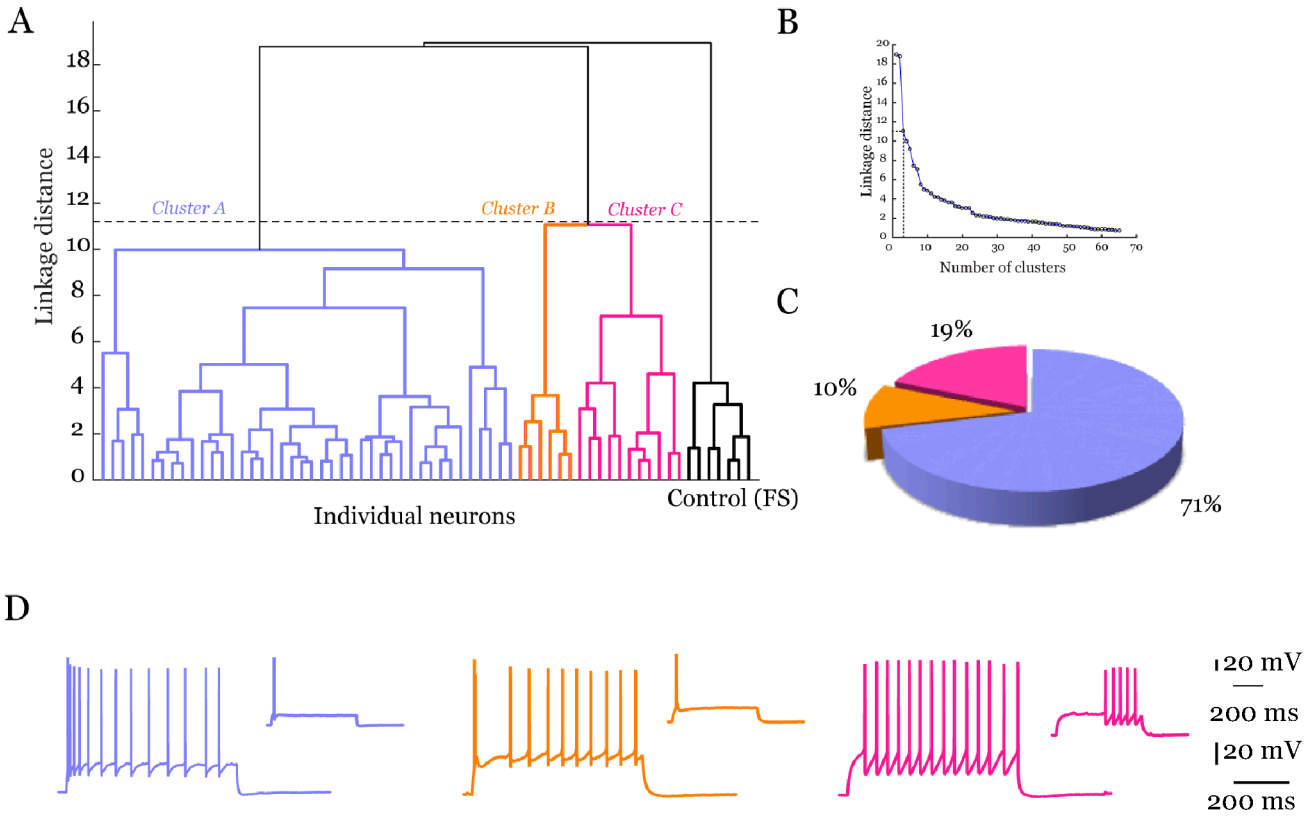

Fig 3.2.2. Electrophysiological analysis of L4 nFS interneurons using Hierarchical clustering. ***(A)*** *Ward's method of hierarchical cluster analysis was used to identify different clusters from 59 nFS interneurons based on passive, AP and firing properties. The X-axis of dendrogram shows individual neurons, and the Y-axis corresponds to the linkage distance measured by Euclidean distance. FS interneurons were used as controls and were clearly separated as one cluster (black). Cluster A is shown in violet, cluster B in orange, and cluster C in pink.* ***(B)*** *The cut-off for significant clusters was determined using the Thorndike method.* ***(C)*** *The pie chart displays the percentage of each cluster, with the same colour code as in dendrogram.* ***(D)*** *Representative firing pattern for each cluster, showing 10-spike train. The first AP is shown as inset.*

The validation of hierarchical clustering was made using K-means clustering with K equal to the number of clusters defined by the hierarchical clustering. Cluster A and the control (FS) were clearly separated, and Cluster B and C were grouped together, as in

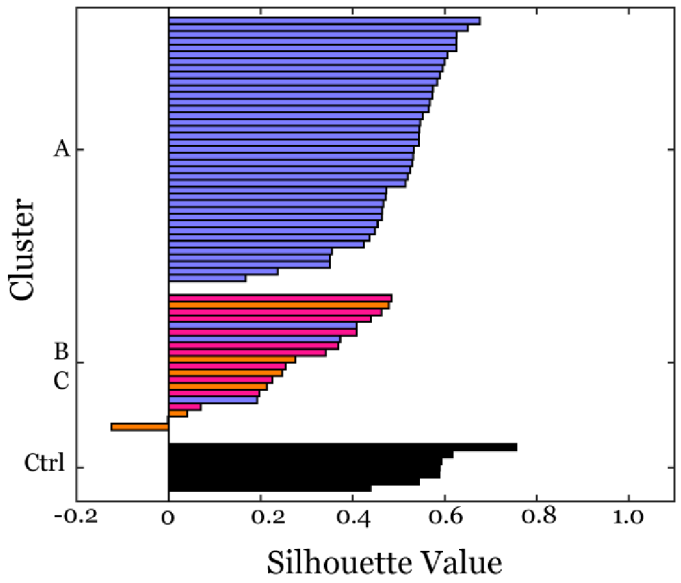

Fig 3.2.3. Electrophysiological analysis of L4 nFS interneurons using Hierarchical clustering. *Silhouette plot for the electrophysiological clusters. The x-axis represents the silhouette value, and Y-axis represents the different clusters. Large values close to 1 indicate that clusters are well separated. Cluster B shows the mixed subgroups, with few outliers from Cluster A.*

hierarchical clustering. The second group also displayed some outliers from Cluster A. The silhouette plot was used to assess the quality of clustering, which revealed that almost all the clusters showed silhouette widths close to 1, proving well assigned clustering **(Fig. 3.2.3)**.

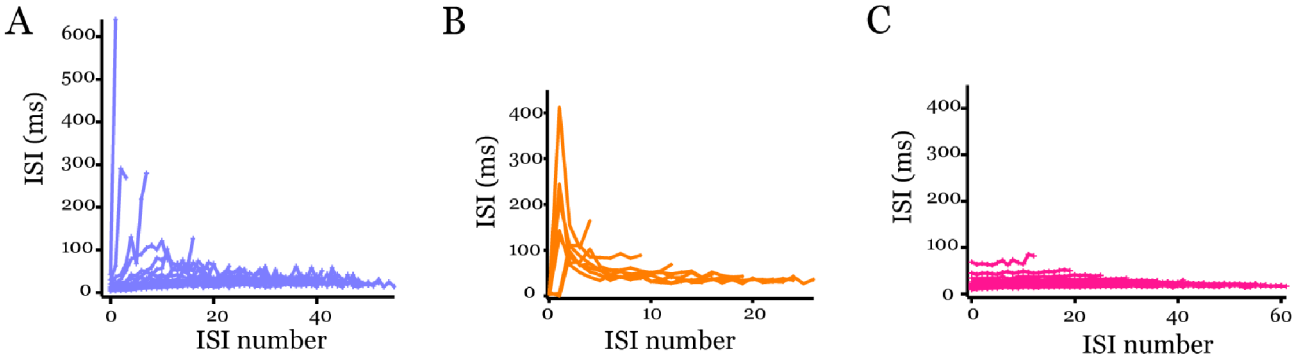

Fig. 3.2.4. Inter-spike interval of the three clusters. ***(A)*** *In Cluster A, the ISI shows a high degree of irregularity during the initial current injection.* ***(B)*** *In Cluster B, the ISI is highest at the beginning in all sweeps.* ***(C)*** *An almost constant ISI is found in Cluster C interneurons.*

Cluster A: Adapting neurons

Cluster A (CA) constitutes the largest group of nFS interneurons, comprising of 42 neurons, i.e., 71% of the total nFS interneurons. A characteristic feature of this cluster was the high frequency adaptation with irregular firing behaviour. The adaptation ratio of

Parameters	Ctrl - FS	CA	CB	CC	CA vs. CB	CA vs. CC	CB vs. CC
RMP (mV)	-58.71±3.13	-60.56±4.28	-72.37±2.19	-66.91±6.56	****	***	NS
R_{in} (MΩ)	84.94±13.86	78.69±38.31	216.78±29.07	155.21±54.64	****	****	*
Sag	9.52±3.29	12.69±6.33	2.59±1.44	4.83±3.43	***	***	NS
Tau (ms)	7.56±0.76	9.05±4.54	13.31±2.36	12.77±6.01	NS	NS	NS
Rheobase (pA)	280.00±84.46	227.26±103.60	81.67±22.29	171.82±60.47	**	NS	NS
AP threshold (mV)	-24.47±3.58	-37.22±4.47	-43.69±3.18	-33.17±5.58	**	*	****
Excitation index	0.41±0.11	0.35±0.14	0.13±0.02	0.24±0.09	NS	NS	**
AP amplitude (mV)	92.18±8.68	94.67±7.30	106.35±9.39	88.32±10.50	**	NS	***
AP half-width (ms)	0.20±0.03	0.44±0.08	0.46±0.05	0.56±0.13	NS	***	NS
AHP amplitude (mV)	23.79±3.56	11.26±3.43	9.48±3.23	21.18±2.83	NS	****	****
AHP accommodation (mV)	-1.12±0.40	-2.75±1.75	-1.21±0.67	1.05±1.57	NS	****	*
AP accommodation (mV)	5.47±3.16	6.97±2.98	0.12±3.12	3.03±1.74	****	***	NS
ISI average (ms)	31.79±7.36	78.10±12.22	79.12±17.52	77.88±13.66	NS	NS	NS
ISI std. deviation (ms)	5.74±3.21	63.86±40.52	34.90±15.06	7.48±2.98	NS	****	NS
Adaptation ratio	3.02±2.53	0.19±0.11	0.70±0.37	0.91±0.06	****	****	*
Firing frequency (Hz) / 100 pA	26.72±6.72	15.90±4.60	17.54±7.14	9.74±4.16	NS	**	**

Table 3.2: Statistical analysis of the electrophysiological parameters of L4 nFS interneurons. *All data are represented as mean ± standard deviation. Statistical significance between all the clusters were performed using one-way ANOVA, and Tukey test was performed for the significant difference between individual clusters. Significant p-value is represented as * < 0.05, ** < 0.01, *** < 0.001, **** < 0,0001*

0.2±0.1, which was calculated as the ratio of the average of first three ISI and the last three ISI in a 10-spike train, reflected extremely high adaptation. To describe the irregularity of firing pattern, we calculated the standard deviation of ISI during a 10-spike train. CA showed the maximum standard deviation of 63.9±40.5, which showed significant irregularity in the firing pattern.

To quantify the excitability of a neuron, we used the excitation index (EI) by incorporating multiple intrinsic properties such as RMP, R_{in}, and AP threshold (as described before). The higher the EI, the less excitable is the neuron, and vice versa *(Lazarus MS and ZJ Huang 2011)*. The membrane properties of CA neurons showed low

excitability with an excitability index of 0.3±0.1 **(Fig. 3.2.10)**. Although CA neurons were more depolarised at the resting state (-60.6±4.3 mV), and AP threshold (-37.2±4.5 mV), they displayed significantly lower R_{in} (78.7±36.3 MΩ) suggesting the existence of a large number of open leak channels which in turn would reduce neuronal excitability (rheobase current: 227.3± 103.6 pA) and result in a fast membrane time constant (tau: 9.1±4.5 ms) **(Table. 3.2)**. The large sag index of 12.7±6.3 indicates a high expression of HCN channels, which may also contribute to the depolarised resting state

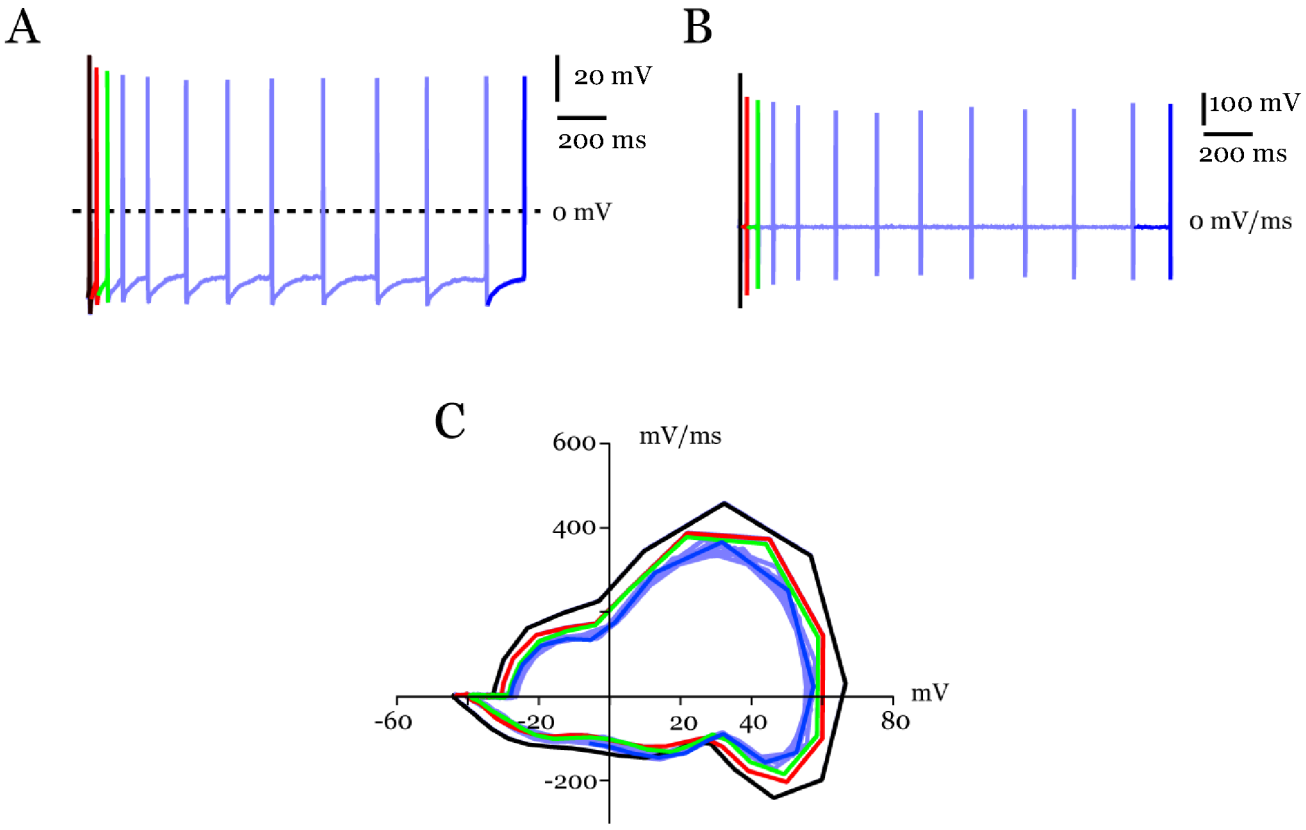

Fig 3.2.5. Representative example of Cluster-A interneurons. (A) *Firing pattern of a representative Cluster-A during 10-spike train. The first, second, third, and last spikes are labeled as black, red, green, and blue respectively.* ***(B)*** *Time derivative of membrane voltage, dV/dt of the sweep shown in A.* ***(C)*** *Phase plot of representative Cluster-A interneurons. The first, second, third, and last spikes are labeled as shown in (A). The first AP showed highest amplitude, while the others gradually showed AP adaptation in the amplitude. A rapid onset, and biphasic component during the rising phase of AP can be observed.*

The half-width of AP spikes was much longer compared to the FS interneurons (0.4±0.1 vs. 0.2±0.03 ms). To better examine the AP properties, we used phase plots in which the rate of change of membrane potential with respect to time (dV/dt) was plotted as a function of membrane potential (V) **(Fig. 3.2.5)**. In CA, the phase plot revealed a rapid spike onset and exhibits a biphasic component during the rising phase of the AP. In

Fig. 3.11, the first, second, third, and the last spikes were labeled black, red, green, and blue, respectively. The first AP displayed largest amplitude, while the others showed gradual adaptation in their amplitude. CA neurons showed highest amplitude accommodation (7.0±3.0 mV), which was calculated as the ratio of first three amplitude peaks to the last three amplitude peaks. Similarly, the amplitude of AHP also displayed significant accommodation (-2.7±1.7 mV) in a 10-spike train. The average AHP amplitude of CA neurons was 11.3±3.4 mV **(Fig. 3.2.9)**.

Cluster B: Accelerating neurons

Cluster B (CB) is the smallest cluster, consisting of only 6 neurons. One of the characteristic features of CB neurons was an initial AP doublet followed by a relatively long

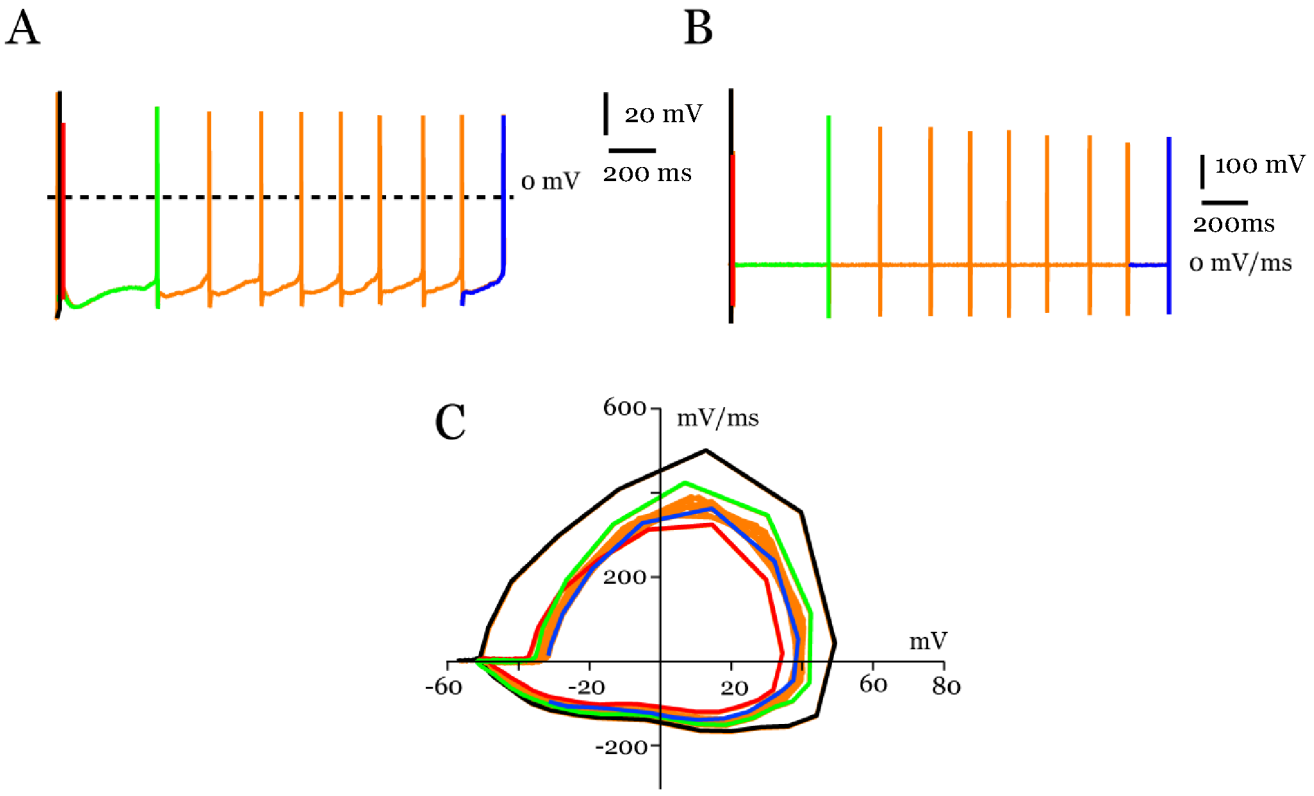

Fig 3.2.6. Representative example of Cluster-B interneurons. (A) *Firing pattern of a representative Cluster-B during 10-spike train. The first, second, third, and last spikes are labeled as black, red, green, and blue respectively.* ***(B)*** *Time derivative of membrane voltage, dV/dt of the sweep shown in A.* ***(C)*** *Phase plot of representative Cluster-B interneurons. The first, second, third, and last spikes are labeled as shown in (A). The first AP showed highest amplitude, and the second AP showed lowest amplitude. A gradual amplitude adaptation can be observed. A slow onset, and monophasic component during the rising phase of AP can be noticed.*

ISI between the second and third AP. Subsequently, the ISI became gradually shorter towards the end of the depolarisation indicating an AP acceleration **(Fig.3.2.2D)**.

The excitability index of CB neurons was 0.1±0.02. The high excitability of CB neurons was likely due to the extremely high R_{in} (216.8±29.1 MΩ) of these L4 nFS interneurons, in spite of displaying hyperpolarising RMP (-72.4±2.2 mV) and AP threshold (-43.7±3.2 mV). Therefore the rheobase current was small (81.7±22.3 pA) and membrane time constant relatively slow (13.3±2.4 ms). The small sag index was indicative of a low expression of HCN channels in CB neurons (sag: 2.6±1.4) **(Fig. 3.2.10)**.

CB neurons displayed the highest AP amplitude (106.4±9.4 mV), compared to the other clusters, whereas the AHP amplitude were relatively small (9.5±3.2 mV) **(Table. 3.2, Fig. 3.2.9)**. CB neurons exhibited a spike doublet at the onset of the AP, followed by AP amplitude adaptation. In every current injection, the initial spike exhibited the highest amplitude, whereas the second spike displayed the smallest AP amplitude, as can be seen

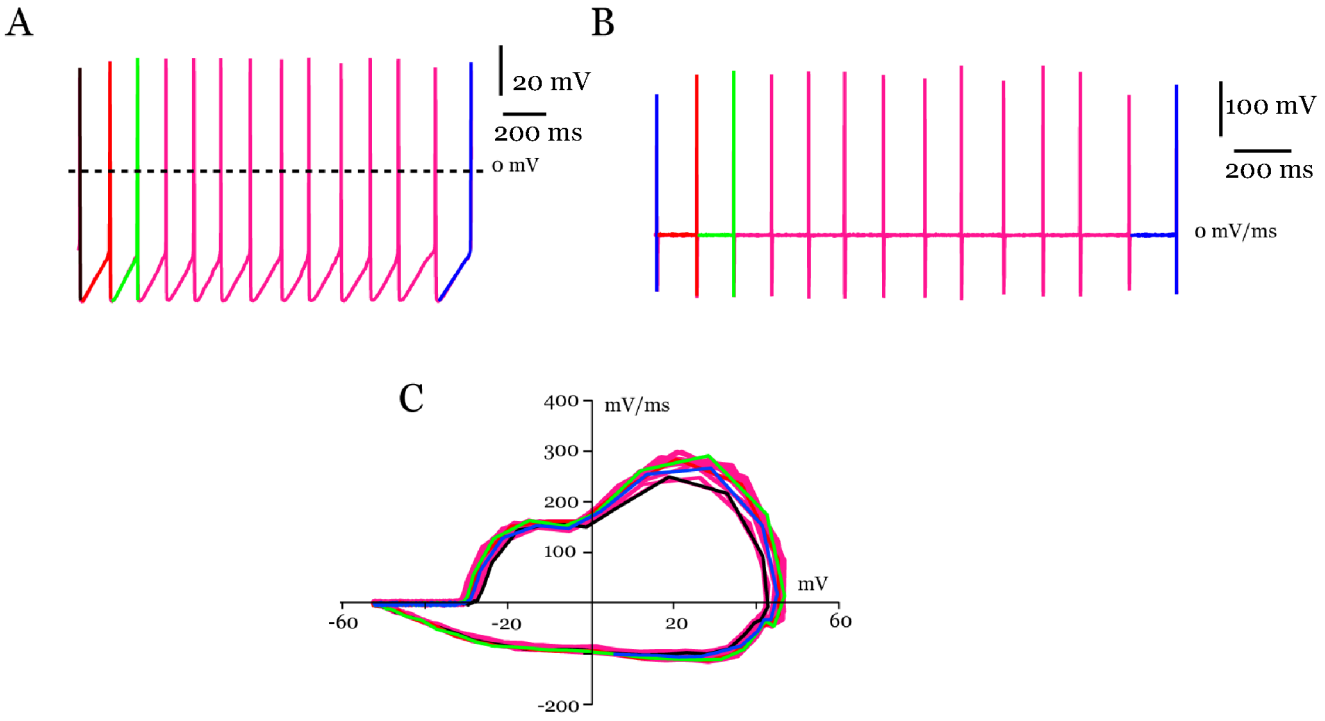

Fig 3.2.7. Representative example of Cluster-C interneurons. ***(A)*** *Firing pattern of a representative Cluster-C during 10-spike train. The first, second, third, and last spikes are labeled as black, red, green, and blue respectively.* ***(B)*** *Time derivative of membrane voltage, dV/dt of the sweep shown in A.* ***(C)*** *Phase plot of representative Cluster-C interneurons. The first, second, third, and last spikes are labeled as shown in (A). No amplitude adaptation can be observed. A rapid onset, and biphasic component during the rising phase of AP can be noticed.*

in the phase plot displaying 10-spike train (in black and red traces). The phase plot revealed monophasic component during the rising phase of the AP **(Fig. 3.2.6)**.

Cluster C: Non-adapting neurons

Cluster C (CC) represented the regular spiking non-adapting group of nFS interneurons, which constituted around 19% of the total population. Some interneuron of this cluster displayed late-spiking behaviour, which is characteristic of NGFCs *(Kawaguchi Y 1995; Tamas G et al. 2003)*. An adaptation ratio of 0.91±0.06 indicates the non-adapting firing pattern of CC neurons **(Fig. 3.2.2D)**.

CC neurons displayed an excitability index of 0.2±0.1. The RMP of CC neurons was -66.9±6.6 mV, and the AP threshold was -33.2±5.6 mV. CC neurons had a high R_{in} (155.2±54.6 MΩ), slow membrane time constant (12.8±6.0 ms) and a small sag index value (4.8±3.4). The rheobase current was 171.8±60.5 pA **(Fig. 3.2.10)**.

On average, the AP displayed significantly lower amplitude compared to CA and CB interneurons (88.3±10.5 mV). The phase plot of CC neurons revealed delayed onset of the AP and biphasic component at the rising phase of the AP **(Fig. 3.2.7)**. CC neurons displayed a low firing frequency per 100 pA current injection (9.7±4.2 Hz). Characteristic features of L4 nFS interneurons of cluster C were a broad AP width (0.6±0.1 ms) and a

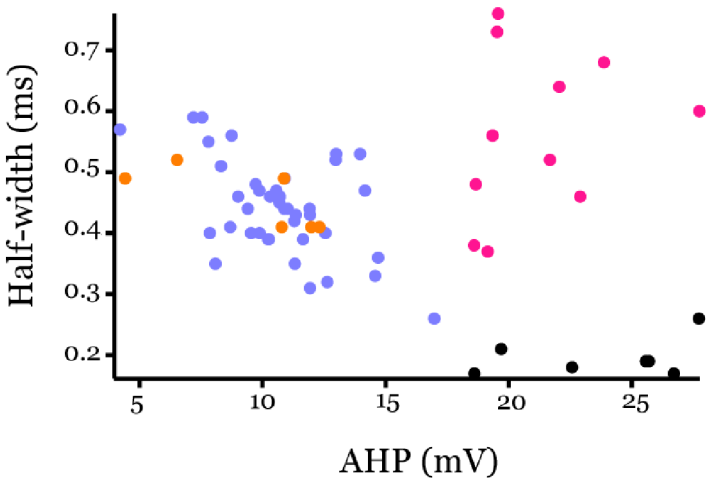

Fig. 3.2.8. Comparison of AHP amplitude and half-width among different clusters. *The clusters are displayed with the same colour code as in the dendrogram. Cluster A, B, and C of nFS interneurons in purple, orange and pink, respectively. FS interneurons in black. There is no difference between CA and CB, while CC displayed much larger AHP amplitude similar to the FS interneurons. The half-width clearly separates CC neurons and the FS interneurons.*

large AHP amplitude (21.2±2.8 mV) **(Fig. 3.2.9)**. While the AHP amplitude in CC interneurons was very similar to that of FS interneurons **(Fig. 3.2.8)** and differed significantly from that of the L4 nFS interneuron clusters A and B, the AP half-width was much longer that than of FS interneurons **(Fig. 3.2.8)**.

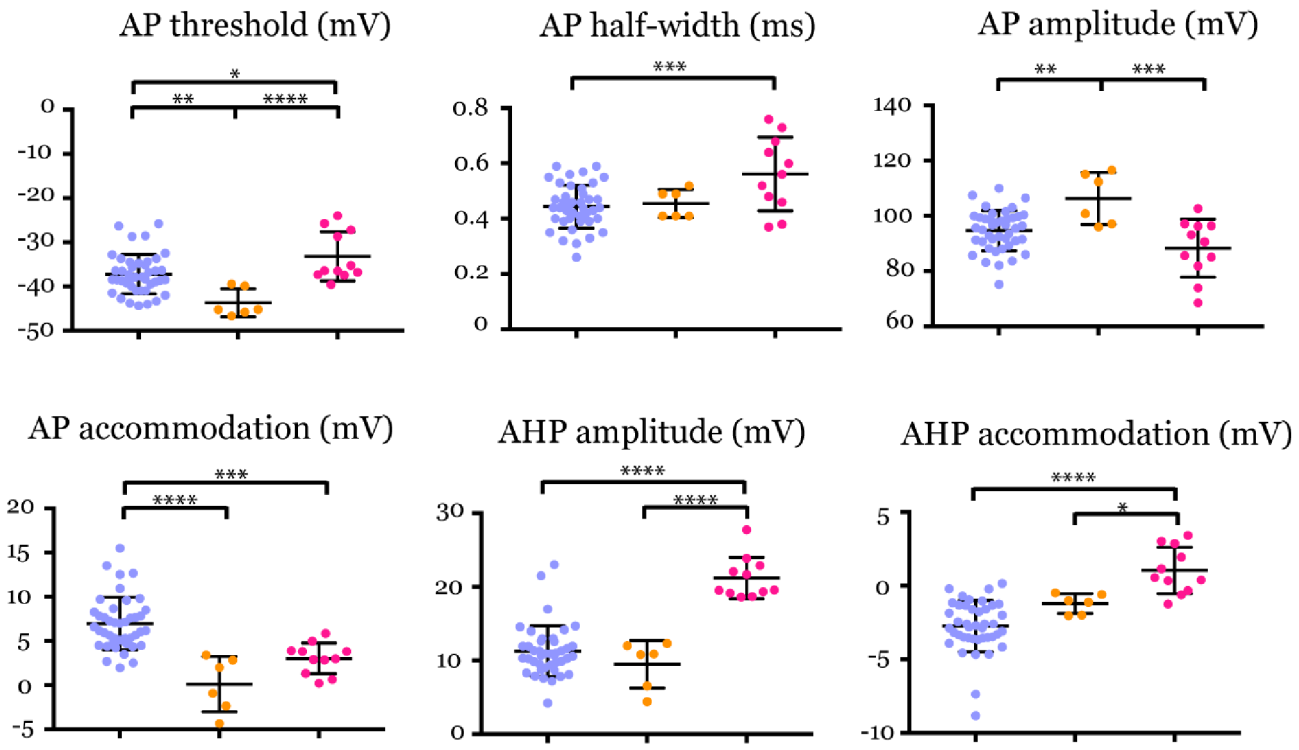

Fig 3.2.9. Comparison of action potential properties between three clusters. *The electrophysiological clusters showed differences in AP threshold, half-width, amplitude, AP accommodation, AHP amplitude and AHP accommodation. Significant p-value is represented as * < 0.05, ** < 0.01, *** < 0.001, **** < 0,0001*

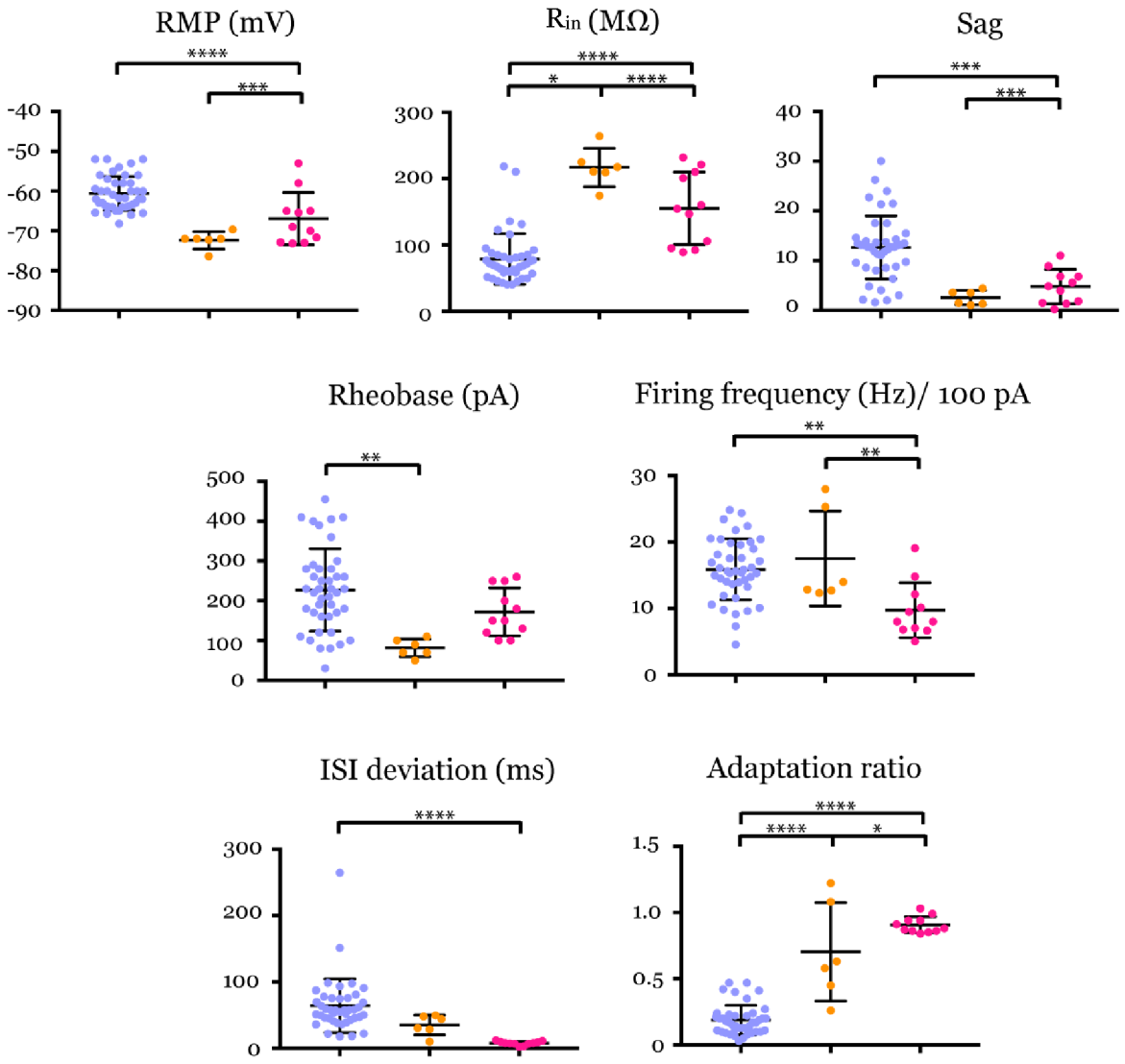

Fig 3.2.10. Comparison of passive and firing properties between three clusters. *The electrophysiological clusters showed differences in RMP, R_{in}, Sag, Rheobase, firing frequency, ISI standard deviation, and adaptation ratio. Significant p-value is represented as * < 0.05, ** < 0.01, *** < 0.001, **** < 0,0001*

3.3. Correlation between morphological and electrophysiological clusters

Three distinct morphological and electrophysiological clusters of nFS interneurons in L4 of rat barrel cortex were identified quantitatively using hierarchical unsupervised cluster analysis. We tried to determine whether a correlation exists between morphological and electrophysiological clusters, *i.e.* if a particular morphology is associated with a certain firing pattern, or vice versa. We found that the morphological and electrophysiological clusters were not tightly correlated **(Fig. 3.3.1)**.

A dataset with a high quality electrophysiological recording may not have a complete biocytin filling resulting in no morphological reconstruction. Similarly, a recording may not be included in the dataset because of poor quality, but the biocytin staining could be excellent. Such conditions may result in datasets only that are of sufficiently high quality for either a morphological or electrophysiological analysis but not for both for the same neuron. Therefore, not all the morphological reconstructions had their corresponding intrinsic data, and vice versa. Fig 3.3.1 shows the dendrogram of morphological and electrophysiological clusters with different colour codes. The vertical bars beneath each dendrogram corresponds to the colour code of the other dendrogram. For dataset without corresponding intrinsic properties or morphological reconstructions were left blank. We found that morphological and electrophysiological clusters were not tightly correlated, which is shown by the mixed colour bars for each cluster.

The difference between morphology and firing pattern could be due to several reasons. The electrophysiological characteristics are not based on the axonal projection patterns, but are linked to the presence of certain ion channels. Voltage gated ion channels can be modulated by the activity of metabotropic G-protein coupled receptors, extracellular Ca influx or intracellular Ca release and intracellular enzyme cascades. In addition, the firing patterns are subjected to change with prolonged current injection. The reliability of firing patterns can be questioned by the experimental artefacts such as changes in temperature, potential mechanical disturbances due to the movement of the recording pipette.

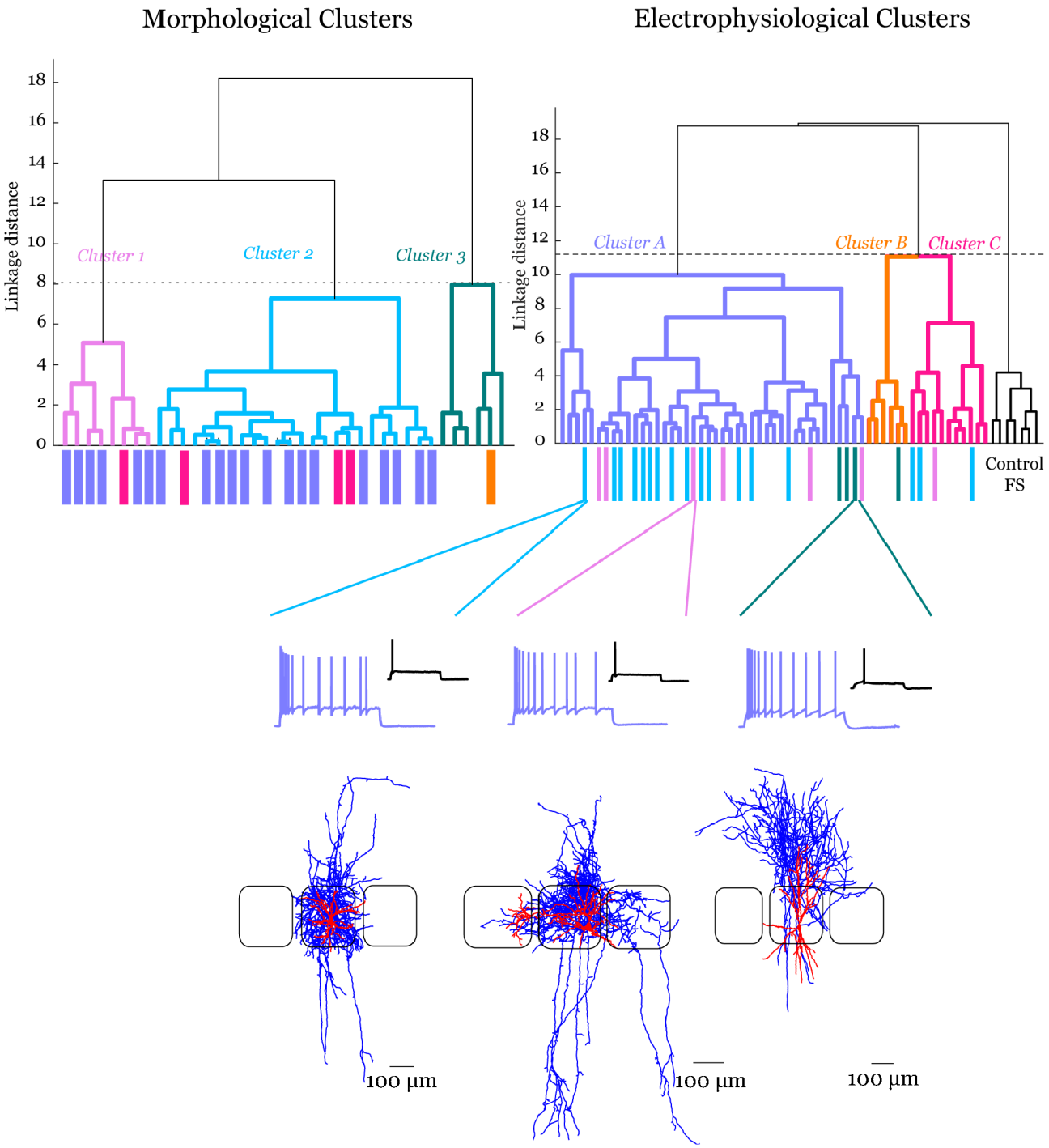

Fig. 3.3.1. Comparison of morphological and electrophysiological clusters. *Unsupervised hierarchical clustering provides three distinct morphological and electrophysiological clusters. The coloured bars beneath each dendrogram represents the colour code from the other dendrogram. In electrophysiological dendrogram, Cluster A is shown to have all the three types of morphological clusters.*

While most of the morphologies from a single cluster showed diverse firing pattern, we found that NGFCs from Cluster 2 displayed regular spiking non-accommodating firing pattern, which is Cluster C of electrophysiological classification **(Fig. 3.3.2A)**.

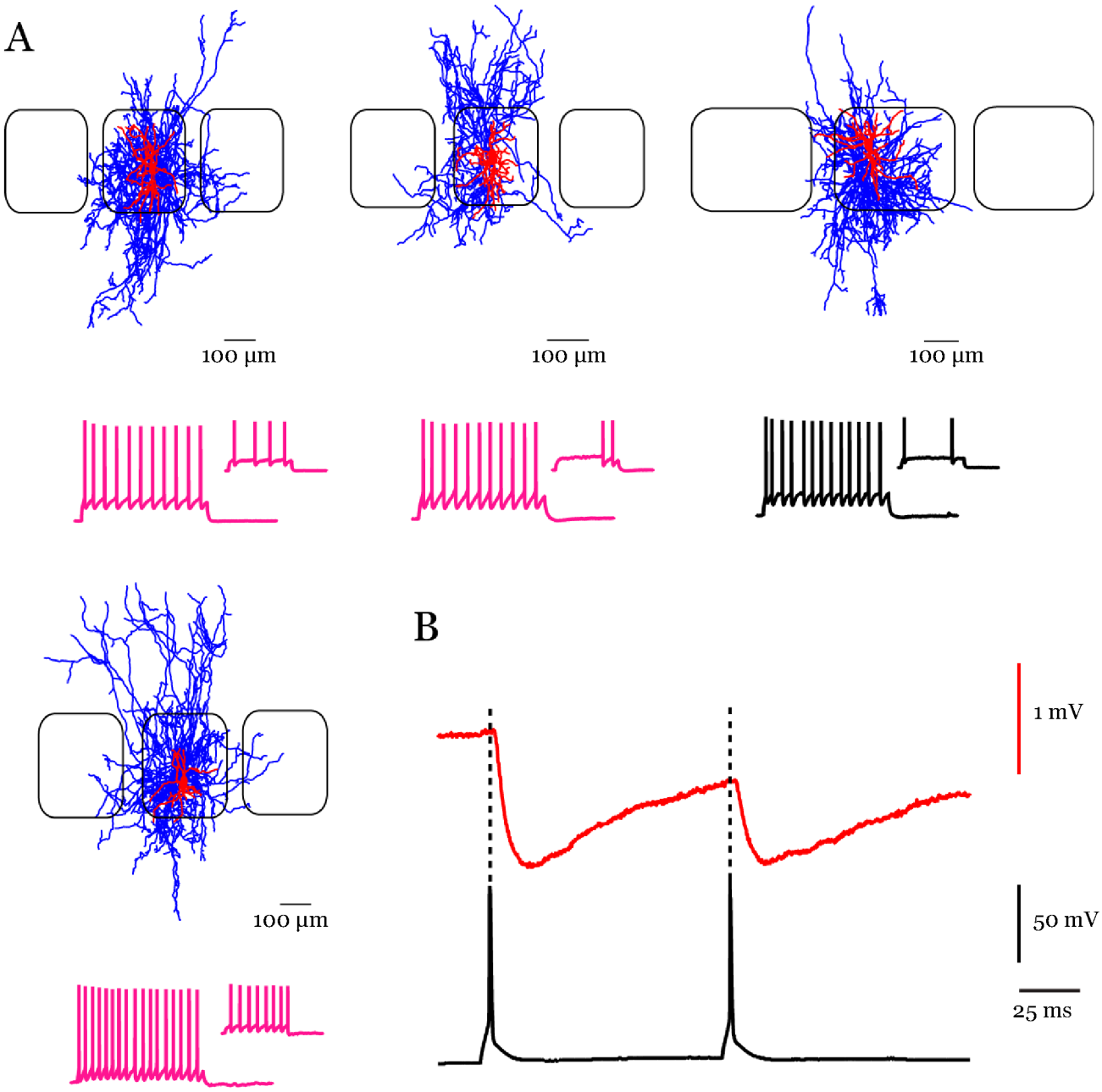

Fig. 3.3.2. NGFCs - morphological and electrophysiological correlation. (A) *Morphological Cluster 2 neurons characteristic of intra-columnar projections consists partly of NGFCs with radially projecting dense axonal plexus. All the neurons displayed here exhibit regular spiking non-accommodating firing pattern, which is Cluster C (firing pattern labelled pink) of electrophysiological classification. The firing pattern that is labelled black was not included in the classification because of its high series resistance (45.93 MΩ).* ***(B)*** *Another characteristics of NGFCs is their synaptic property of paired pulse depression.*

Morphologically, NGFCs show dense axonal plexus projecting radially, with multi-polar dendritic arborisations. Based on their intrinsic properties, NGFCs are associated with late-spiking behaviour. In this study, we found that late-onset alone cannot distinguish NGFCs from other neuron types. The shape of the AP, which is expressed by the AP half-

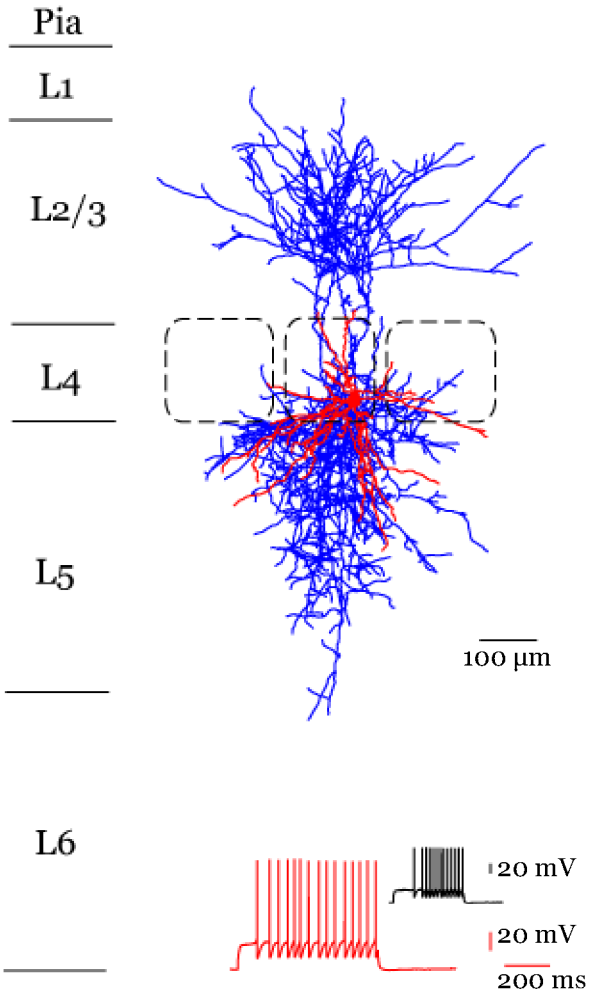

Fig. 3.3.3. Morphological reconstruction of a FS interneurons and its firing pattern. *Neuron displaying late-spiking onset and narrow AP shows bimodal axonal projection to L2 and L5.*

width is an important criteria to define NGFCs. A late onset behaviour was also found for L4 FS interneurons (see also *(Koelbl C et al. 2015)*), but these interneurons have a short AP half-width and show a completely different morphology **(Fig. 3.3.3)**. Another interesting feature of NGFCs are their synaptic properties (see also below), which exhibits short-term depression in marked contrast to all other nFS interneurons types (see also chapter 3.4 below) **(Fig. 3.3.2B)**.

3.4. Monosynaptic connections in L4 rat barrel cortex

In this study, we performed paired recordings to understand the synaptic connectivity between different cell types in L4 of rat barrel cortex. These experiments were performed in close collaboration with Dr. Guanxiao Qi. Since the connection probability of L4 interneurons was very high, we performed double-recording, using direct patching of the putative presynaptic neuron *(Koelbl C et al. 2015; Feldmeyer D and G Radnikow 2016)*, rather than the traditional search- and re-patch technique used for excitatory connections *(Feldmeyer D et al. 1999; Feldmeyer D and G Radnikow 2016)*. We were able to find 25 synaptic connections with nFS interneurons in L4 of rat barrel cortex, with high percentage of reciprocal connections (64%). Focussing on nFS interneurons, we have four possible connections with other cell types in L4: *nFS to excitatory, nFS to FS, FS to nFS, and nFS to excitatory*, which will be described below. Synaptic connections involving nFS interneurons can be characterised by the properties of post-synaptic potentials such as amplitude, amplitude variation, latency, 20-80% rise time, and decay time.

The reliability of synaptic connection is an important property and can be described by two factors: *failure rate* (the percentage of failures of a presynaptic AP to elicit an unitary post-synaptic potential (PSP)) and the *coefficient of variance* (CV - standard deviation of the unitary PSP amplitude which is normalised to the average amplitude). A synaptic connection is considered reliable if the failure rate and the coefficient of variance are low.

Short-term plasticity is an important phenomenon in synaptic physiology, that can change neural information transmission by modifying synaptic efficacy in a timescale of tens of milliseconds to few minutes. Synaptic efficacy can increase or decrease, which is referred to as *short-term facilitation*, and *short-term depression,* respectively. The short-term plasticity of synaptic connections can be characterised by the paired pulse behaviour, i.e. the change in PSP amplitude during repetitive stimulation at a fixed interval (e.g., 100 ms). If the PSPs show a decrease in amplitude over a period of continuous stimulation, this is called paired pulse depression. Similarly, paired pulse facilitation is characterised by an increase in amplitude during continuous stimulation *(Regehr WG 2012)*. The strength of a connection is mainly dependent on the synaptic release probability, which is the probability with which the release of neurotransmitter occurs in response to an AP at a

given synapse. Other factors that contribute to the strength of synaptic connections are the number of synaptic contacts, and the quantal size (the size of postsynaptic depolarisation) *(Branco T and K Staras 2009)*. The presynaptic release probability is related to the failure rate, the CV and the paired pulse behaviour: for e.g., high failure rate, large CV and paired pulse facilitation signify a low release probability.

Synaptic connectivity of NGFC

In this study two synaptic connections were found between NGFCs and excitatory neuron in L4, one of which was reciprocally connected. NGFCs were identified electrophysiologically on the basis of their broad APs, long AHPs, and non-adapting firing pattern. The firing pattern of NGFCs was also associated with a late-spiking behaviour but this was not always the case. Morphologically, NGFCs showed axonal projections mainly in the home barrel. A representative example of a synaptic connection between a NGFC and a spiny stellate (SS) neuron is shown in Fig. 3.4.1 and 3.4.2. This inhibitory pair showed a strong synaptic connection with mean IPSP amplitude of 1.17 mV. The latency between the peak of the AP and the unitary IPSP was 2.45 ms, which is significantly slower compared to the fast latencies of less than 1 ms exhibited by FS interneurons in L4. For this connection, the 20-80% IPSP rise time and decay time were also significantly longer compared to other synaptic connections. The 20-80% rise time was 4.82 ms, and the decay time was 77.05 ms. A morphological reconstruction of this connection is also shown in Fig. 3.4.1. The presynaptic NFGC displayed a dense axonal plexus within the home barrel and few projections radiating to the supra- and infra-granular layers. The postsynaptic neuron is a L4 SS neuron, showing spine-bearing dendritic branches largely confined to L4.

The short term plasticity of this inhibitory connection was demonstrated by eliciting two APs at an ISI of 100 ms, and 10 APs at an ISI of 50 ms. This pair showed a strong short-term depression with a PPR of 0.60 at an ISI of 100 ms. The small CV of 0.30 and failure rate of 0% suggests strong and reliable depression by NGFCs on L4 SS neuron. The latency for the second IPSP was longer (2.49 ms) than the first IPSP.

An excitatory connection between a SP neuron and a NGFC in L4 is illustrated in 3.4.3 and 3.4.4. This excitatory pair had a small mean EPSP amplitude of 0.51 mV, compared to the reciprocal connection showing a mean IPSP amplitude of 2.46 mV. The latency between the peak of the AP and the unitary EPSP was 1.08 ms. The 20-80% rise

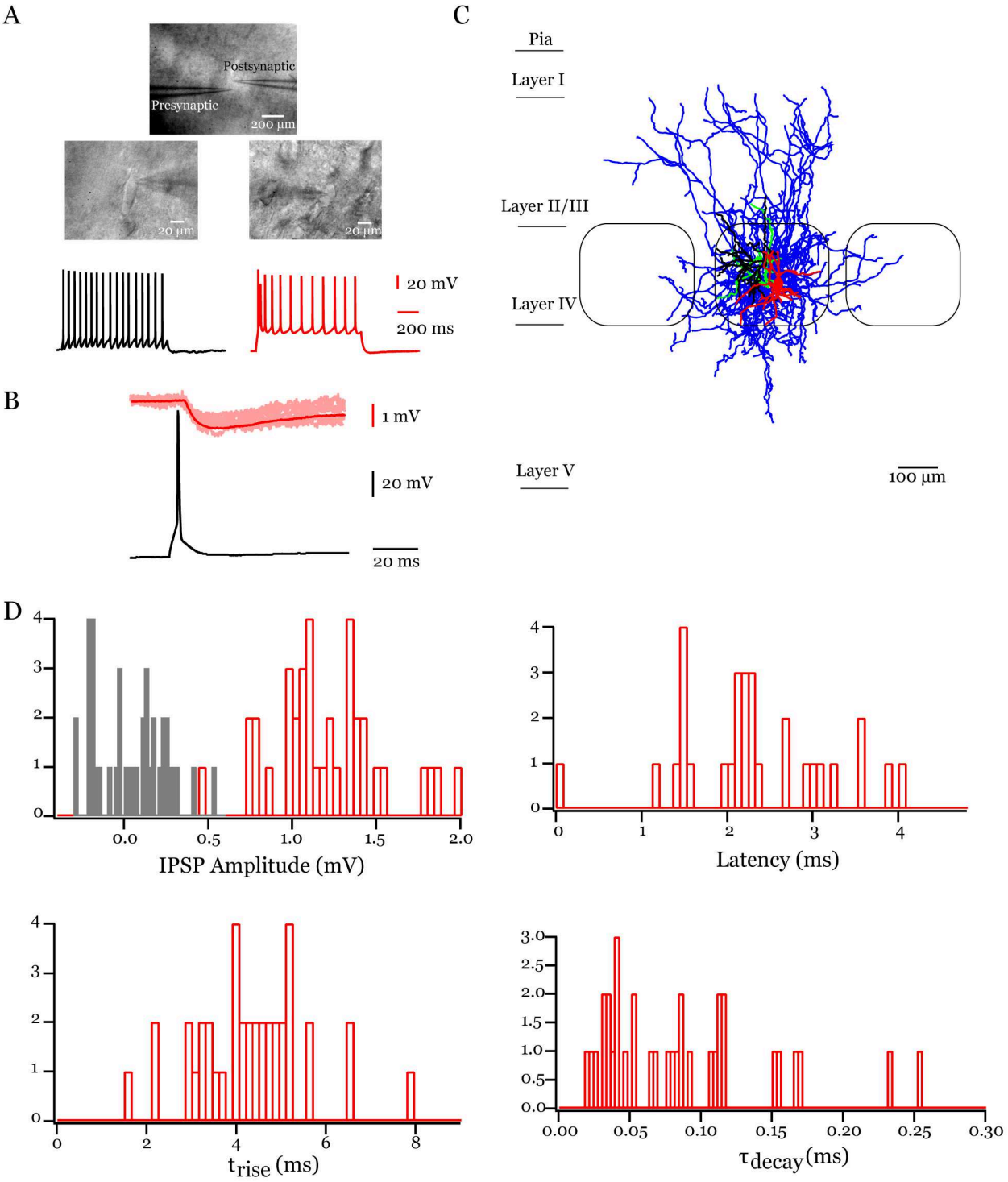

Fig. 3.4.1. NGFC-SS inhibitory connection. *(A) Top, IR-DIC image of the brain slice showing pipettes at the pre-synaptic and post-synaptic sites within a barrel. Middle, High magnification images of the pre- and post-synaptic neurons. Bottom, the corresponding firing patterns of the pre- (black) and post-synaptic (red) neurons. (B) A presynaptic AP (black trace) and 10 consecutive superimposed IPSPs (red trace) and their mean IPSP (dark red trace) are shown. (C) Morphological reconstruction of the NGFC-SS pair. NGFC axon is labeled in blue, somatodendrites in red; SS axon is labeled in black, and somatodendrites in green. (D) Histogram of IPSP amplitude, noise (grey bars, along with amplitude), latency, 20-80% rise time, and decay time are shown.*

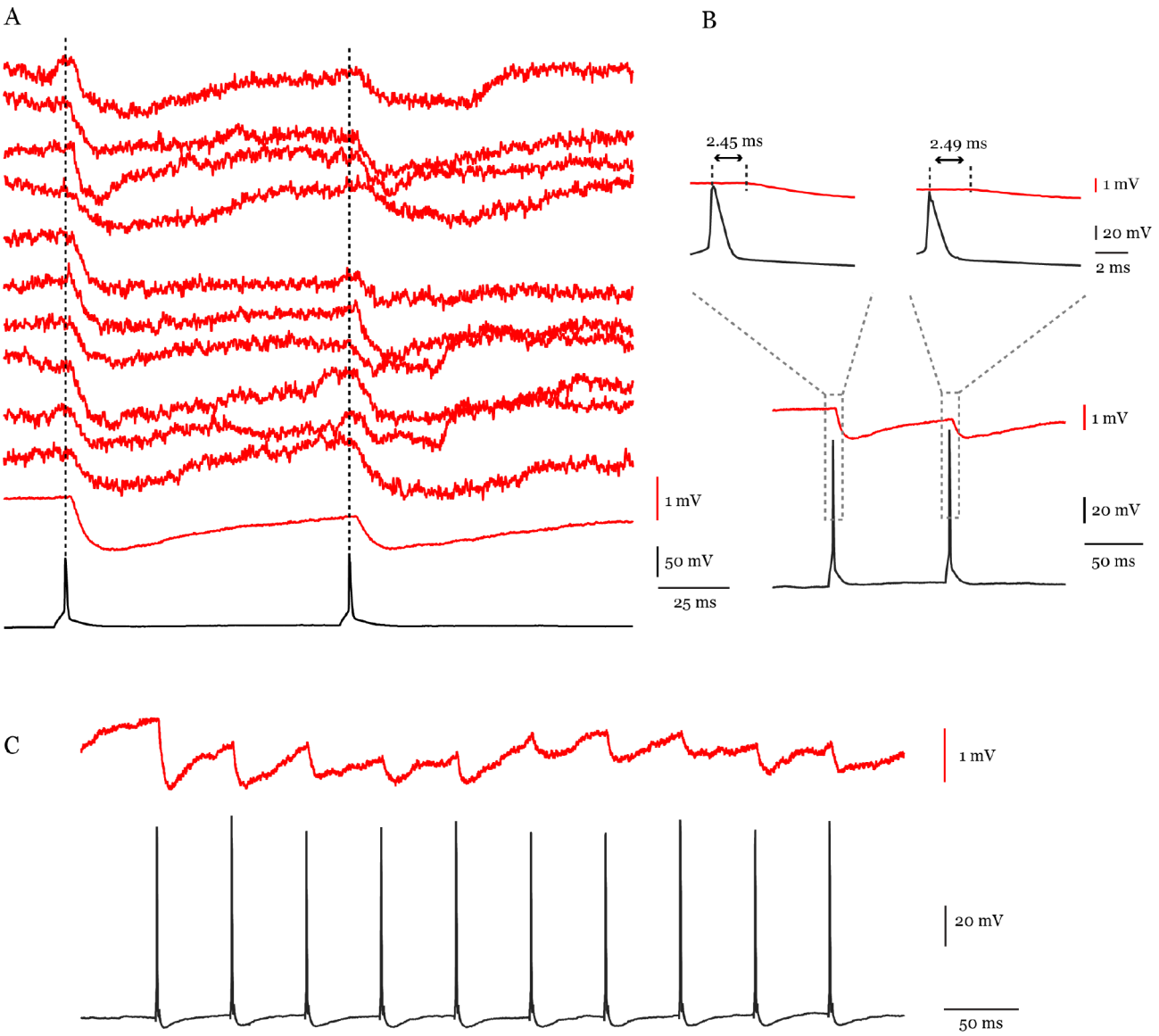

Fig. 3.4.2. Short-term plasticity of the NGFC-SS connection shown in 3.4.1. *(A) Two presynaptic APs (black trace) elicited at 100 ms interval and their corresponding 10 consecutive IPSPs (top red trace) and their mean IPSP (bottom red trace) are shown. (B) The latencies of first and second IPSPs are shown. (C) Train of ten presynaptic APs (black trace) elicited at 50 ms interval and the mean IPSP (red trace).*

time was 0.66 ms, and the decay time was 40.3 ms, similar to the reciprocal inhibitory connection with NGFC. Fig. 3.4.3 shows the morphological reconstruction of the L4 SP neuron-NGFC excitatory connection. The presynaptic SP neuron is characterised by a distinct apical dendrite extending to L2/3. The soma of the SP neuron was located in the centre of the barrel. The postsynaptic neuron is a NGFC displaying a dense axonal plexus that is mainly confined to the home barrel with few projections extended to L2/3. The short-term plasticity of this excitatory connection exhibited paired-pulse depression with a

PPR of 0.86 at an ISI of 100 ms. The failure rate and the CV were 11.7% and 0.51, respectively.

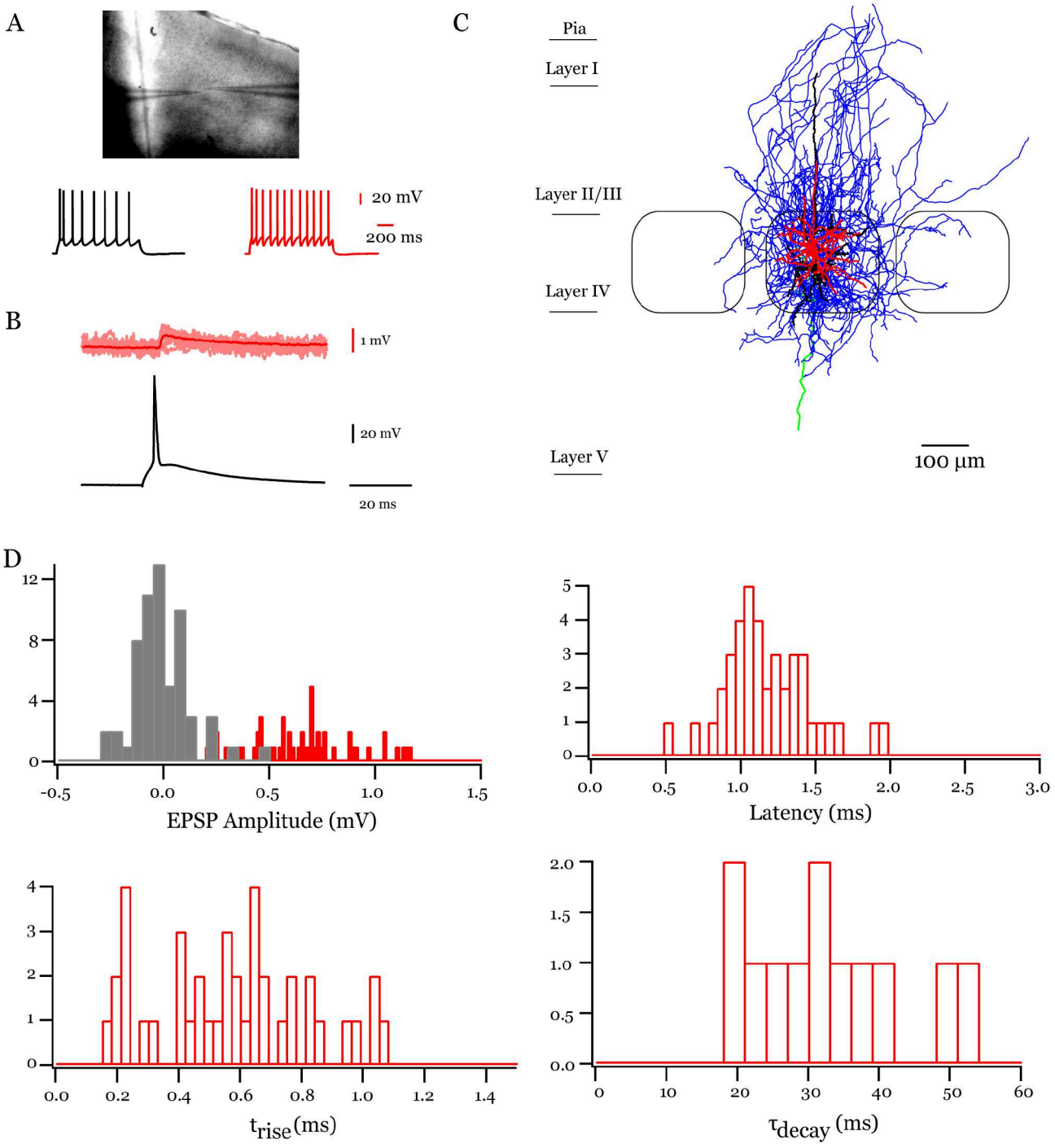

Fig. 3.4.3. SP-NGFC excitatory connection. *(A) Top, IR-DIC image of the brain slice showing pipettes at the pre-synaptic and post-synaptic sites within a barrel. Middle, High magnification images of the pre- and post-synaptic neurons. Bottom, the corresponding firing patterns of the pre- (black) and post-synaptic (red) neurons. (B) A presynaptic AP (black trace) and 10 consecutive superimposed EPSPs (red trace) and their mean EPSP (dark red trace) are shown. (C) Morphological reconstruction of the SP-NGFC pair. NGFC axon is labeled in blue, somatodendrites in red; SP axon is labeled in black, and somatodendrites in green. (D) Histogram of EPSP amplitude, noise (grey bars, along with amplitude), latency, 20-80% rise time, and decay time are shown.*

Excitatory synapse: Excitatory neuron to nFS

A representative example of a SP to lateral projecting nFS interneuron excitatory connection is shown in Figs. 3.4.5 and 3.4.6. This pair displayed EPSPs with a relatively small amplitude (0.14 mV), a rise time of 1.53 ms, decay time of 11.6 ms and latency of 1.26

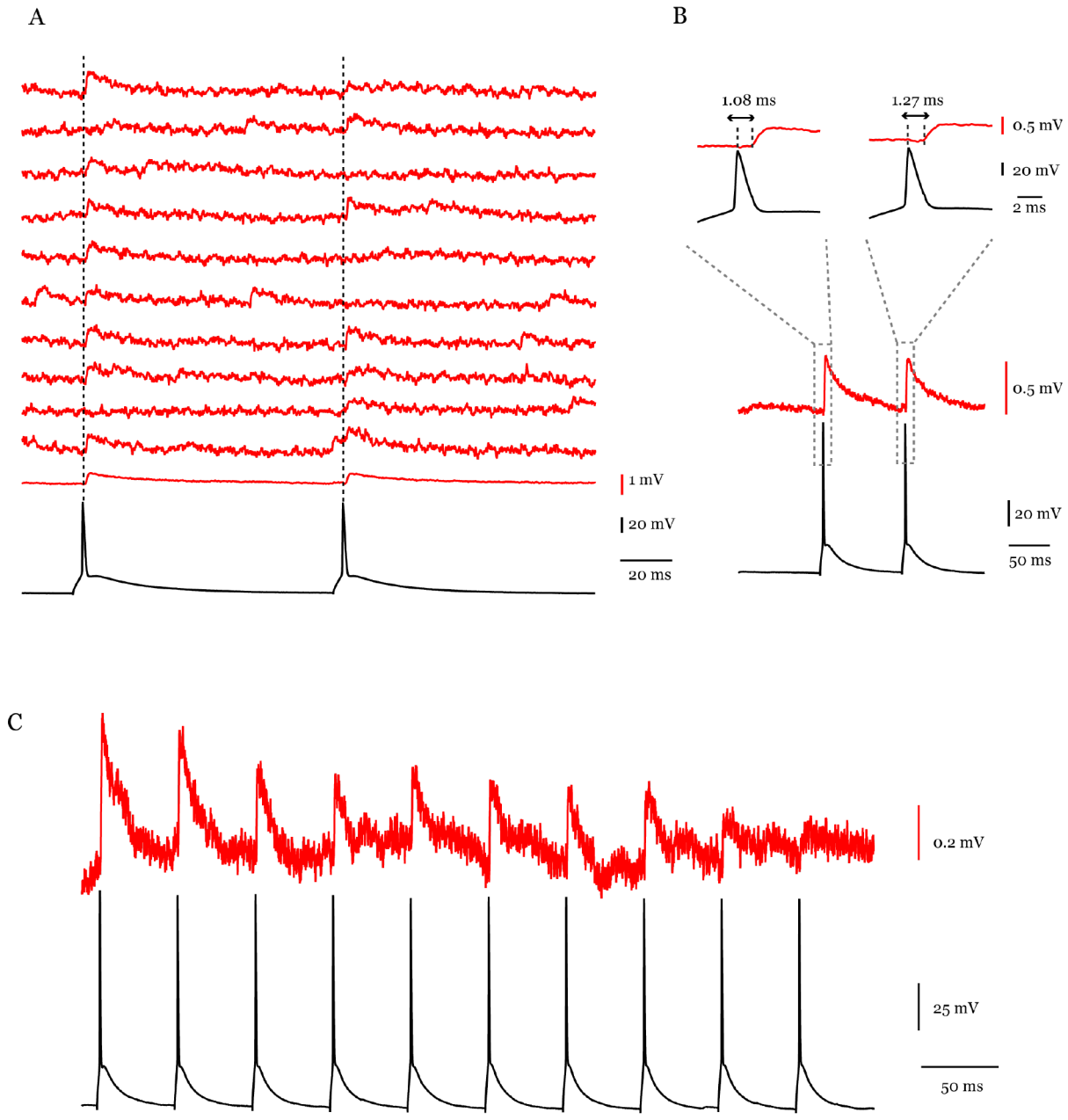

Fig. 3.4.4. Short-term plasticity of the SP-NGFC connection shown in 3.4.3. *(A) Two presynaptic APs (black trace) elicited at 100 ms interval and their corresponding 10 consecutive EPSPs (top red trace) and their mean EPSP (bottom red trace) are shown. (B) The latencies of first and second EPSPs are shown. (C) Train of ten presynaptic APs (black trace) elicited at 50 ms interval and the mean EPSP (red trace).*

ms. The morphology of presynaptic SP neuron in L4 displayed apical dendrite extending to L2/3 and axon projecting to deeper layers. The postsynaptic nFS interneurons displayed

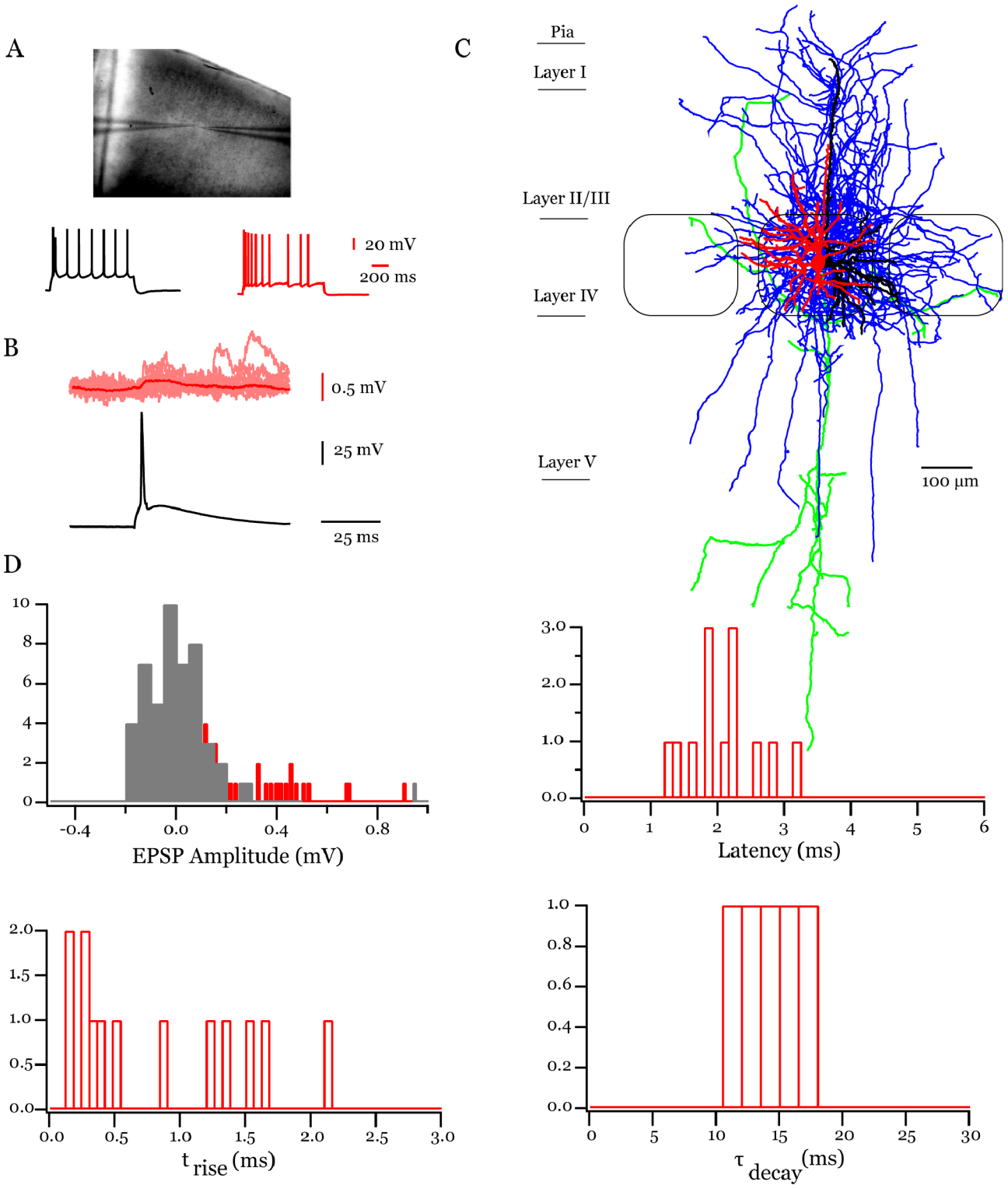

Fig. 3.4.5. SP to nFS excitatory connection. *(A)(C) The firing patterns of the pre- (black) and post-synaptic (red) neurons. (B) A presynaptic AP (black trace) and 10 consecutive superimposed EPSPs (red trace) and their mean EPSP (dark red trace) are shown. (D) Histogram of EPSP amplitude, noise (grey bars, along with amplitude), latency, 20-80% rise time, and decay time are shown.*

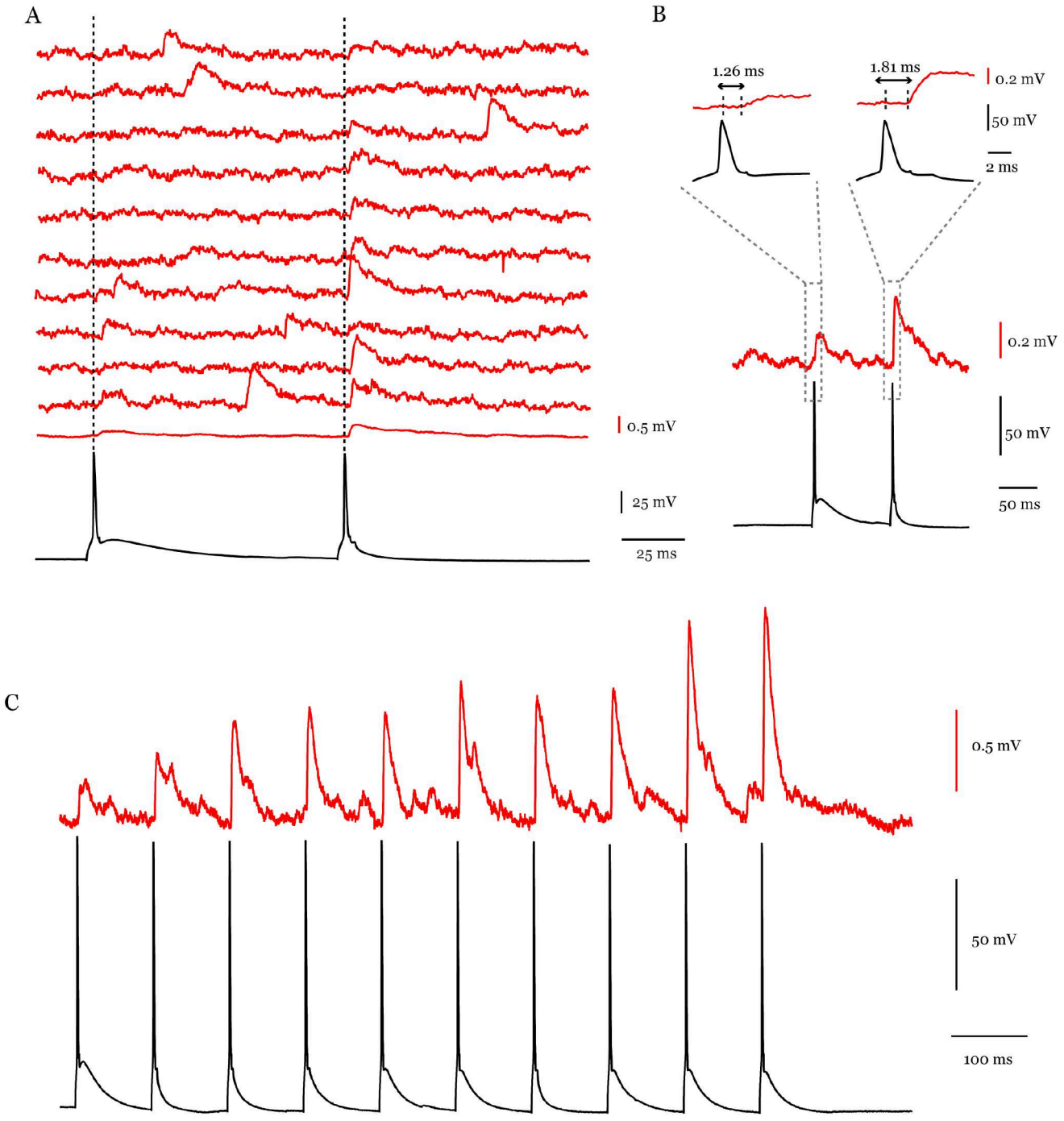

Fig. 3.4.6. Short-term plasticity of the SP to nFS connection shown in 3.4.5. *(A) Two presynaptic doublet APs (black trace) elicited at 100 ms interval and their corresponding 10 consecutive EPSPs (top red trace) and their mean EPSP (bottom red trace) are shown. (B) The latencies of first and second EPSPs are shown. (C) Train of ten presynaptic APs (black trace) elicited at 50 ms interval and the mean EPSP (red trace).*

significant axonal projections to the home barrel, supra-granular layers and also to the adjacent barrel. The soma of both pre- and postsynaptic neurons were located at the centre of the barrel, very close to each other. This weak SP-nFS connection exhibited short-term

facilitation with PPR of 2.59 at an ISI of 100 ms. A low release probability of synaptic vesicles was predicted by high failure rate (59.2%) and large CV (0.86).

Inhibitory synapse: nFS to excitatory neuron

A representative example of a synaptic connection between an intra-columnar projecting nFS interneuron and an excitatory neuron is shown in Fig. 3.4.7 and 3.4.8. Due to bad staining quality and improper embedding, the morphology of the pair could not be recovered completely. Despite the sub-standard morphology we were able to identify the intra-columnar projection pattern of the nFS interneuron. This pair is characterised by a weak synapse with mean IPSP amplitude of 0.16 mV. The other characteristics such as latency, 20-80% rise time, and decay time were measured as 0.98 ms, 1.23 ms, and 58.12

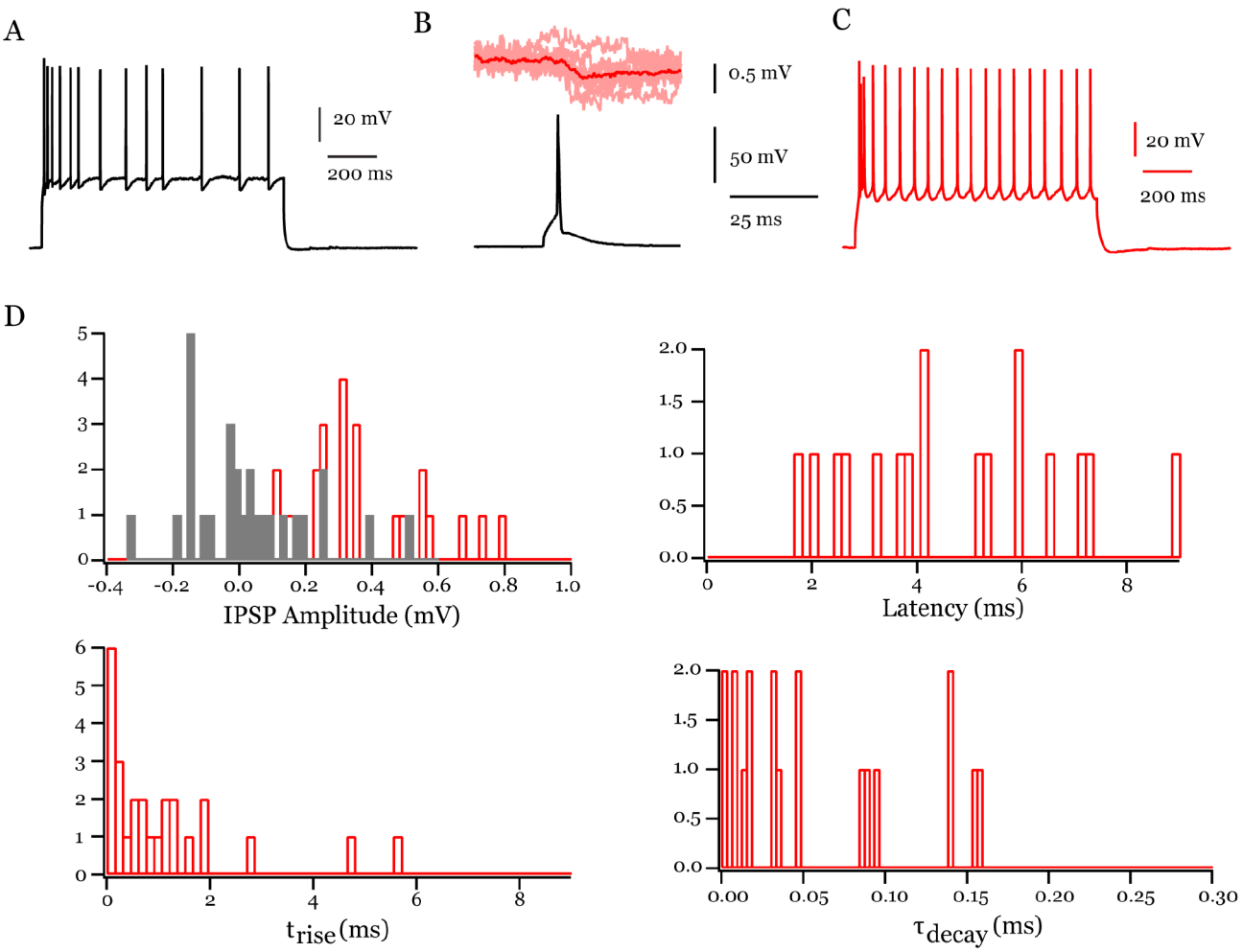

Fig. 3.4.7. nFS to SS/SP inhibitory connection. *(A)(C) The firing patterns of the pre-(black) and post-synaptic (red) neurons.(B) A presynaptic AP (black trace) and 10 consecutive superimposed IPSPs (red trace) and their mean IPSP (dark red trace) are shown.(D) Histogram of IPSP amplitude, noise (grey bars, along with amplitude), latency, 20-80% rise time, and decay time are shown.*

ms respectively. This synaptic connection between a L4 nFS interneuron and a L4 spiny neuron exhibited weak short-term depression with a PPR of 0.98 at an ISI of 100 ms. High failure rate (37%) and large CV (0.55) suggest a relatively low release probability of synaptic vesicles, therefore weak and unreliable connection. The first and second latencies of the IPSP were almost identical (0.98 and 0.99 respectively).

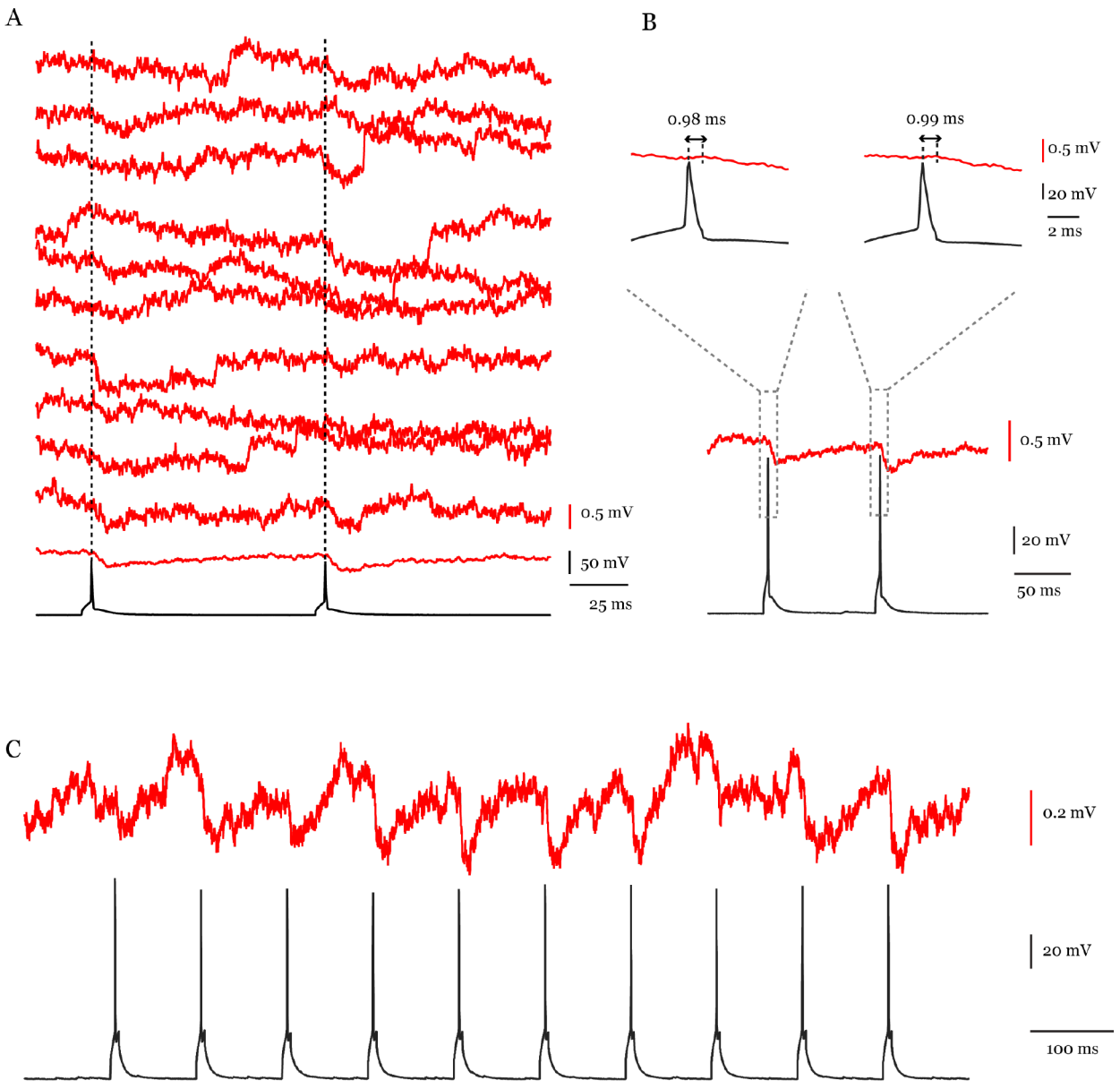

Fig. 3.4.8. Short-term plasticity of the nFS to excitatory connection shown in 3.4.7. *(A) Two presynaptic APs (black trace) elicited at 100 ms interval and their corresponding 10 consecutive IPSPs (top red trace) and their mean IPSP (bottom red trace) are shown. (B) The latencies of first and second IPSPs are shown. (C) Train of ten presynaptic APs (black trace) elicited at 50 ms interval and the mean IPSP (red trace).*

Inhibitory connection: nFS to FS

A representative example of an inhibitory synaptic connection between nFS and FS interneurons is shown in Fig. 3.4.9 and 3.4.10. From the incomplete morphology of the pairs, the morphology of nFS interneuron appears to be confined to home barrel, similar to that of the FS interneurons. As for the nFS interneuron-excitatory neuron connection, the synaptic contact was weak with mean IPSP amplitude of 0.18 mV. Furthermore, IPSPs at this connection showed a latency of 1.33 ms, 20-80% rise time was 1.12 ms, and the decay time was 7.06 ms. This pair showed weak short-term facilitation with a PPR of 1.68 at an

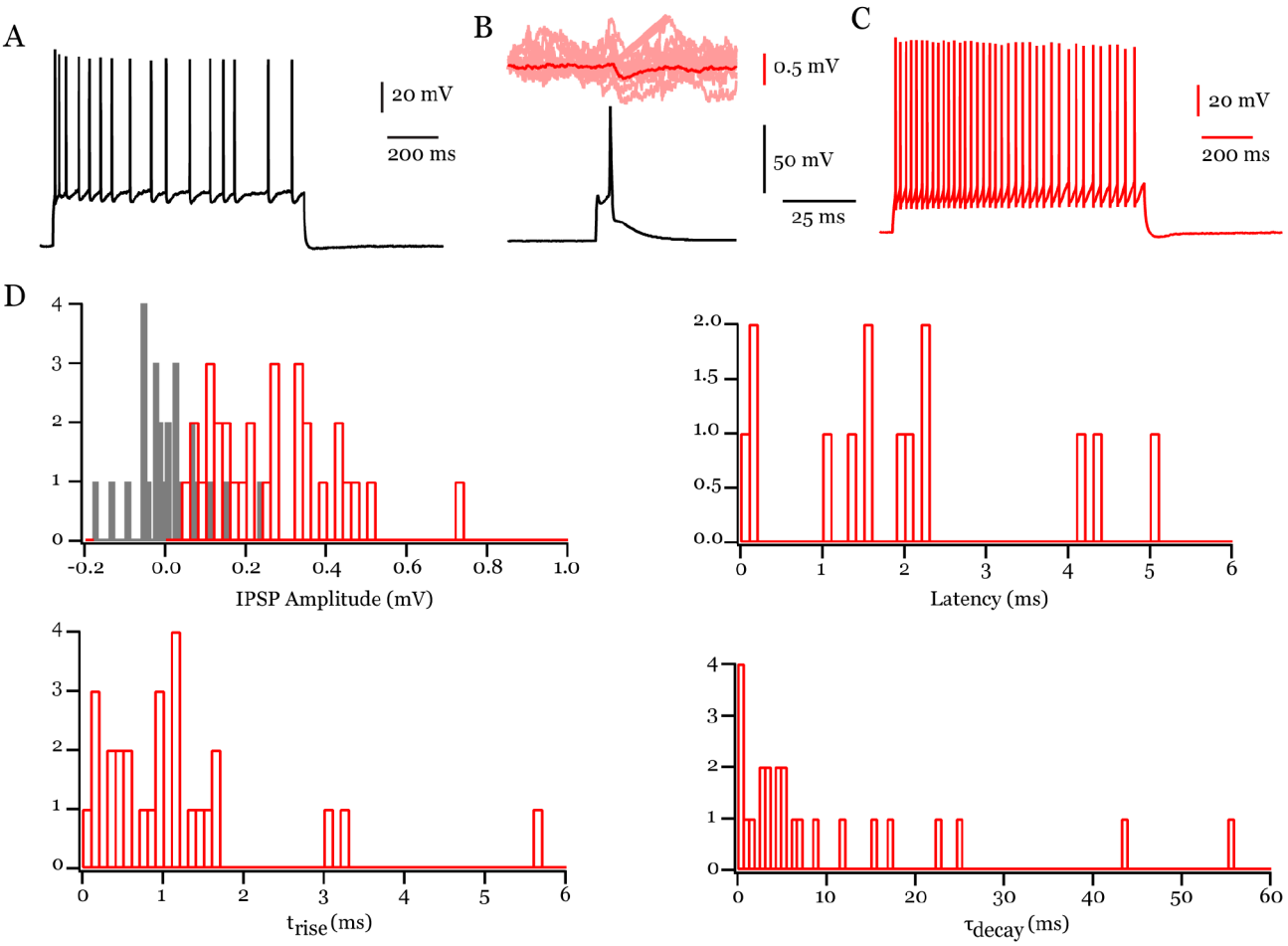

Fig. 3.4.9. nFS to FS inhibitory connection. *(A)(C) The firing patterns of the pre- (black) and post-synaptic (red) neurons. (B) A presynaptic AP (black trace) and 10 consecutive superimposed IPSPs (red trace) and their mean IPSP (dark red trace) are shown. (D) Histogram of IPSP amplitude, noise (grey bars, along with amplitude), latency, 20-80% rise time, and decay time are shown.*

ISI of 100 ms. Fig. 3.4.10 displays a clear weak inhibitory connection. During repetitive presynaptic stimulation of presynaptic AP, the facilitation became more profound. A CV

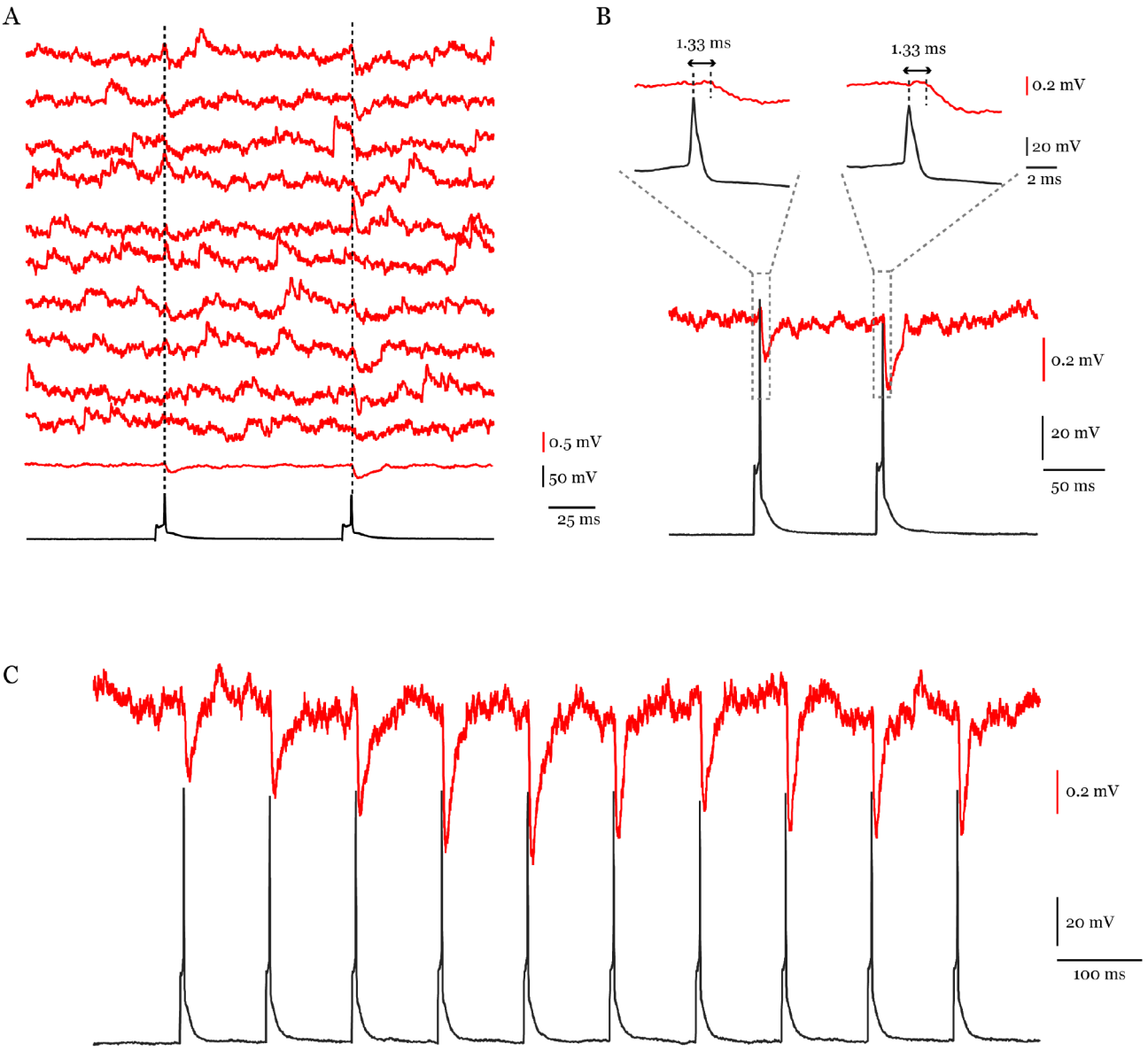

Fig. 3.4.10. Short-term plasticity of the nFS to FS connection shown in 3.4.9. *(A) Two presynaptic APs (black trace) elicited at 100 ms interval and their corresponding 10 consecutive IPSPs (top red trace) and their mean IPSP (bottom red trace) are shown. (B) The latencies of first and second IPSPs are shown. (C) Train of ten presynaptic APs (black trace) elicited at 50 ms interval and the mean IPSP (red trace).*

value of 0.61 and high failure rate at 38% is indicative of a low release probability and a highly unreliable synaptic connection between a nFS and a FS interneuron.

Inhibitory synapse: FS to nFS

Fig. 3.4.11 and 3.4.12 illustrates a representative example of a synaptic connection between a FS and a nFS interneuron. This pair displayed an inhibitory synapse with mean IPSP amplitude of 0.49 mV. The inhibitory connection is characterised by a short latency

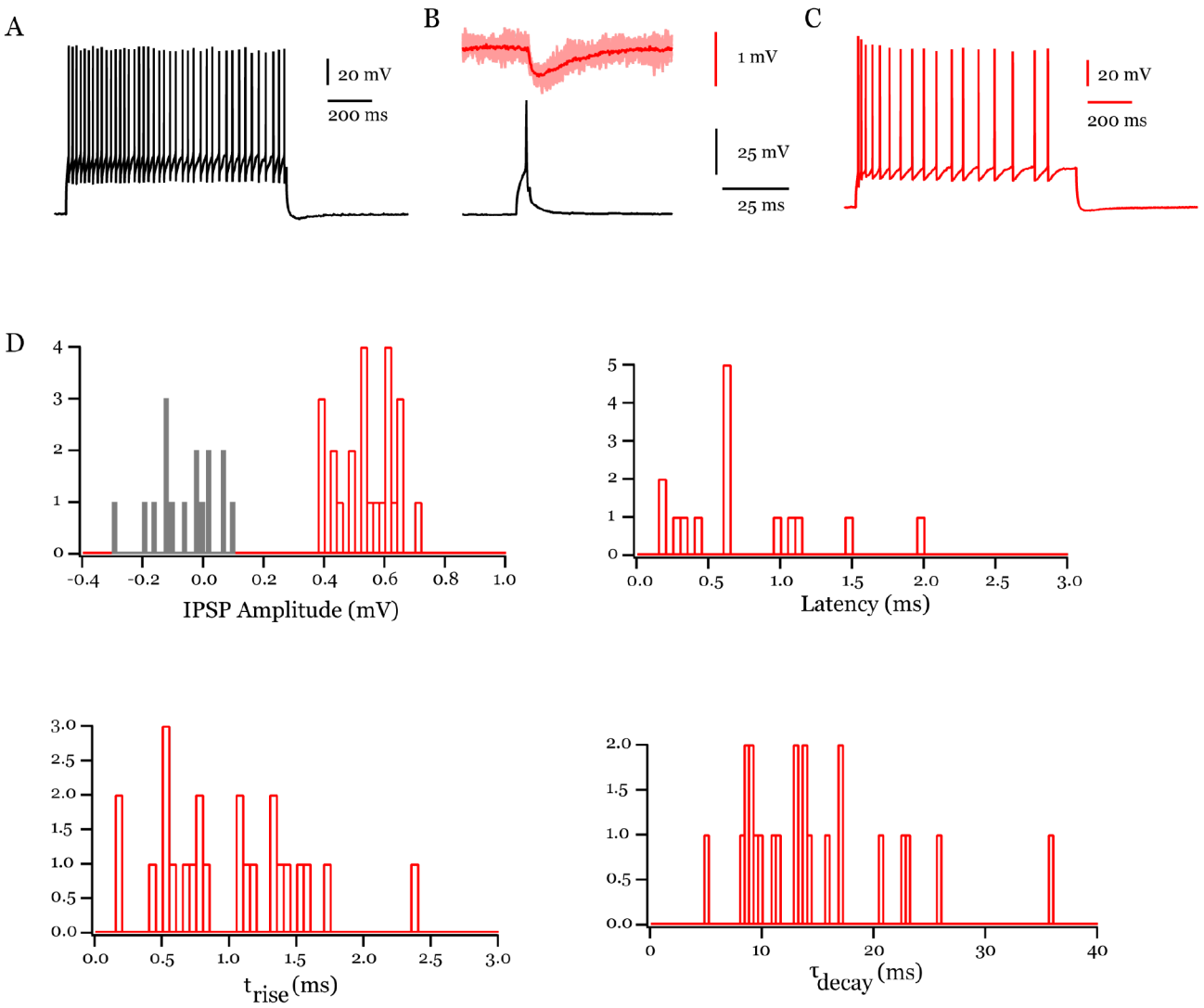

Fig. 3.4.11. FS to nFS inhibitory connection. *(A)(C) The firing patterns of the pre- (black) and post-synaptic (red) neurons. (B) A presynaptic AP (black trace) and 10 consecutive superimposed IPSPs (red trace) and their mean IPSP (dark red trace) are shown. (D) Histogram of IPSP amplitude, noise (grey bars, along with amplitude), latency, 20-80% rise time, and decay time are shown.*

of 0.64 ms, a 20-80% rise time of 1.12 ms and decay time of 14.4 ms. The strong short-term depression with a PPR of 0.58, in conjunction with a low CV and the absence of failures shows that this inhibitory connection between the FS and nFS interneuron is very reliable, i.e. has a high neurotransmitter release probability.

Excitatory synapse: Excitatory to FS

In addition to synaptic connection established by nFS interneurons, we also studied L4 neuronal microcircuits with FS interneurons. They show similar synaptic properties as reported previously *(Beierlein M et al. 2003; Koelbl C et al. 2015)*. Fig. 3.4.13 and 3.4.14

shows a representative example of a monosynaptic connection between an excitatory and an FS interneuron. EPSPs at this synapse had an average amplitude of 0.87 mV. The latency was 1.41 ms, the 20-80% rise time was 0.41 ms, and the decay time was 8.76 ms. The paired-pulse behaviour tested using two spike and ten-spike train demonstrated a strong depression with a PPR of 0.71. No failures were observed for this connection and the CV was 0.46 suggesting a highly reliable connection with FS interneuron.

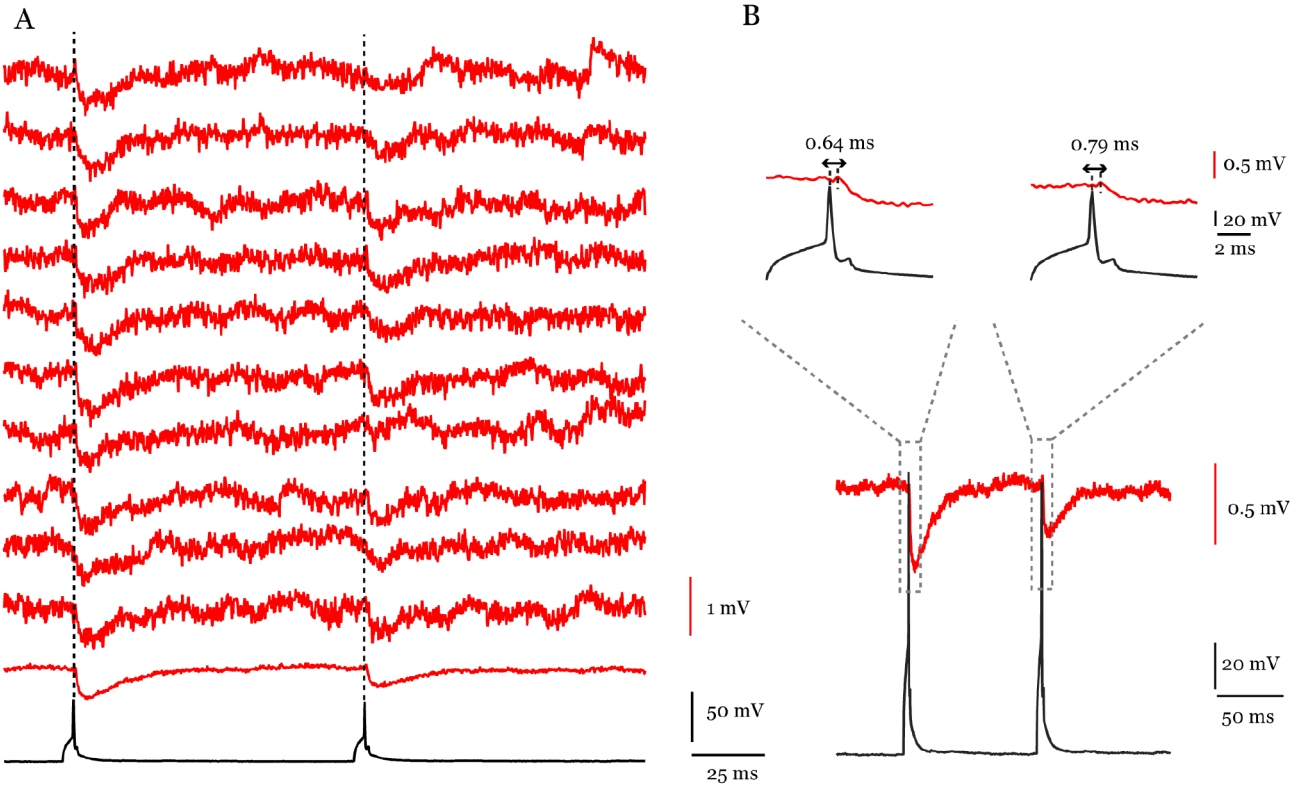

Fig. 3.4.12. Short-term plasticity of the FS to nFS connection shown in 3.4.11. *(A) Two presynaptic APs (black trace) elicited at 100 ms interval and their corresponding 10 consecutive IPSPs (top red trace) and their mean IPSP (bottom red trace) are shown. (B) The latencies of first and second IPSPs are shown.*

Inhibitory synapse: FS to excitatory neuron

A representative example of a synaptic connection between a FS interneuron and an excitatory neuron is illustrated in Fig. 3.4.15 and 3.4.16. This pair displayed an inhibitory synapse with a mean IPSP amplitude of 2.94 mV. The latency between the AP peak and the IPSP response was 0.97 ms, the 20-80% rise time was 1.24 ms, and the decay time was 37.02 ms. This synaptic connection showed a strong IPSP depression, with a PPR value of 0.79 and CV of 0.46. This pair also displayed 0% failure rate, which indicates a strong and reliable connection.

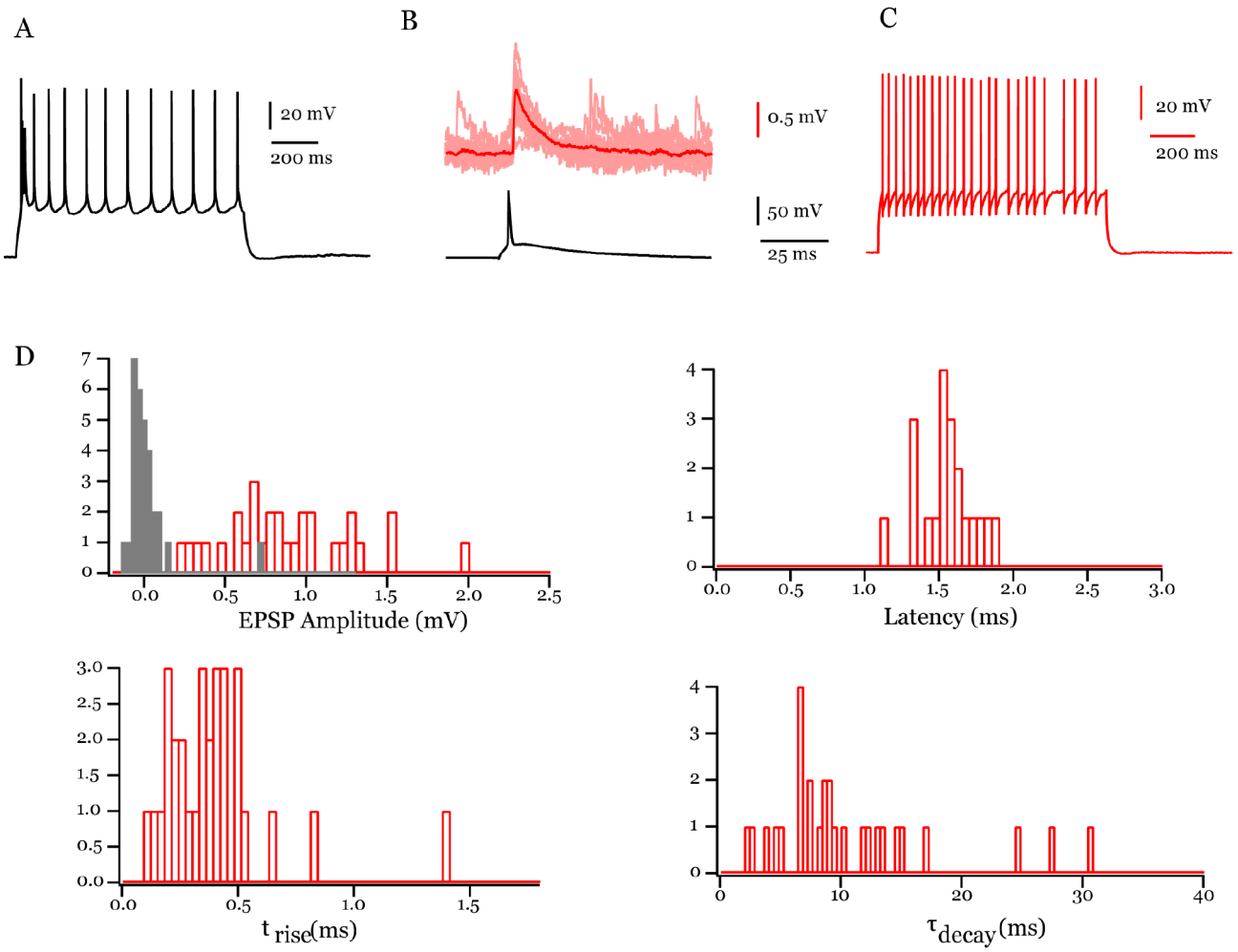

Fig. 3.4.13. Excitatory to FS excitatory connection. *(A)(C) The firing patterns of the pre- (black) and post-synaptic (red) neurons. (B) A presynaptic AP (black trace) and 10 consecutive superimposed EPSPs (red trace) and their mean EPSP (dark red trace) are shown. (D) Histogram of EPSP amplitude, noise (grey bars, along with amplitude), latency, 20-80% rise time, and decay time are shown.*

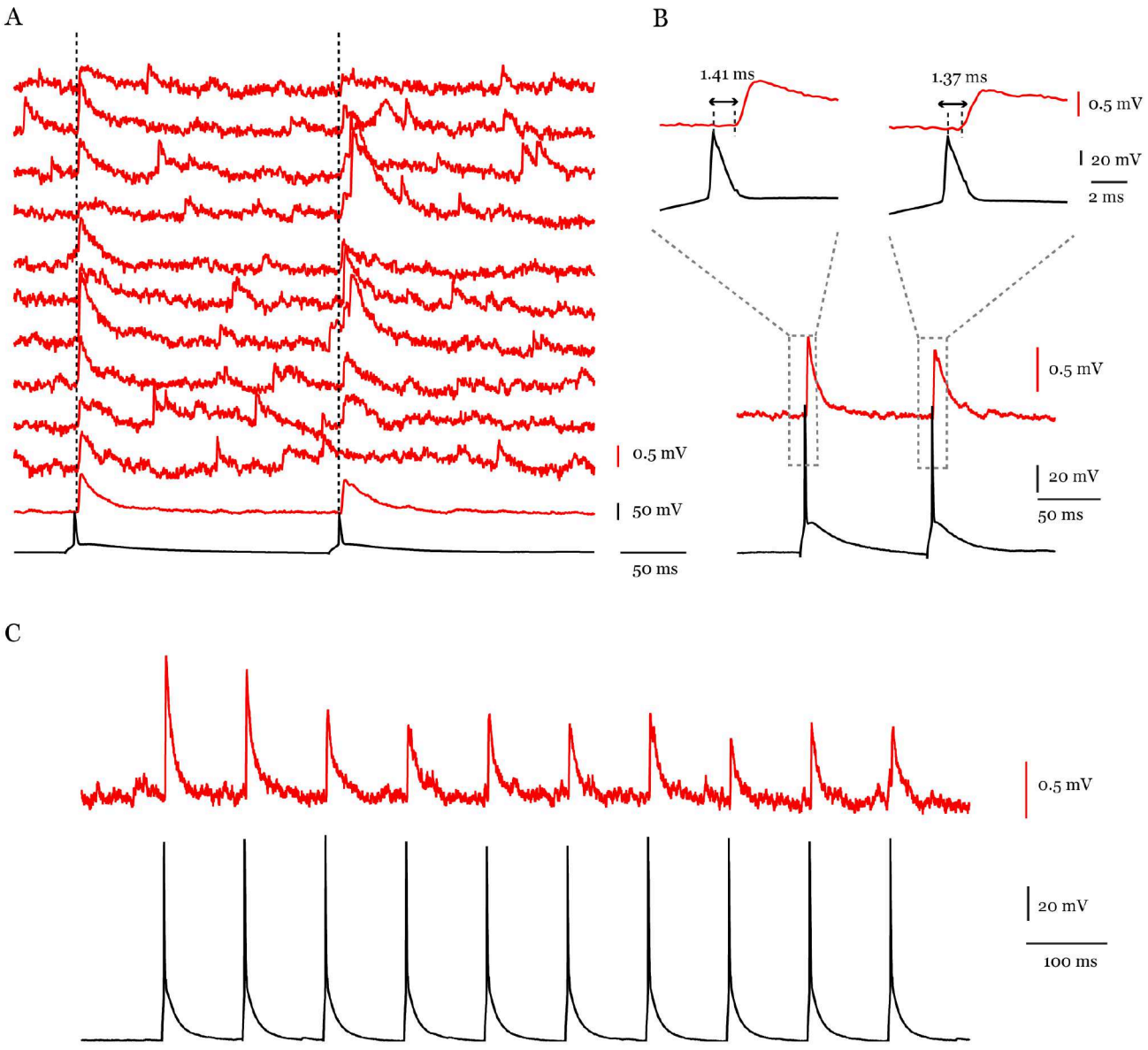

Fig. 3.4.14. Short-term plasticity of the excitatory to FS connection shown in 3.4.13. *(A) Two presynaptic APs (black trace) elicited at 100 ms interval and their corresponding 10 consecutive EPSPs (top red trace) and their mean EPSP (bottom red trace) are shown. (B) The latencies of first and second EPSPs are shown. (C) Train of ten presynaptic APs (black trace) elicited at 50 ms interval and the mean EPSP (red trace).*

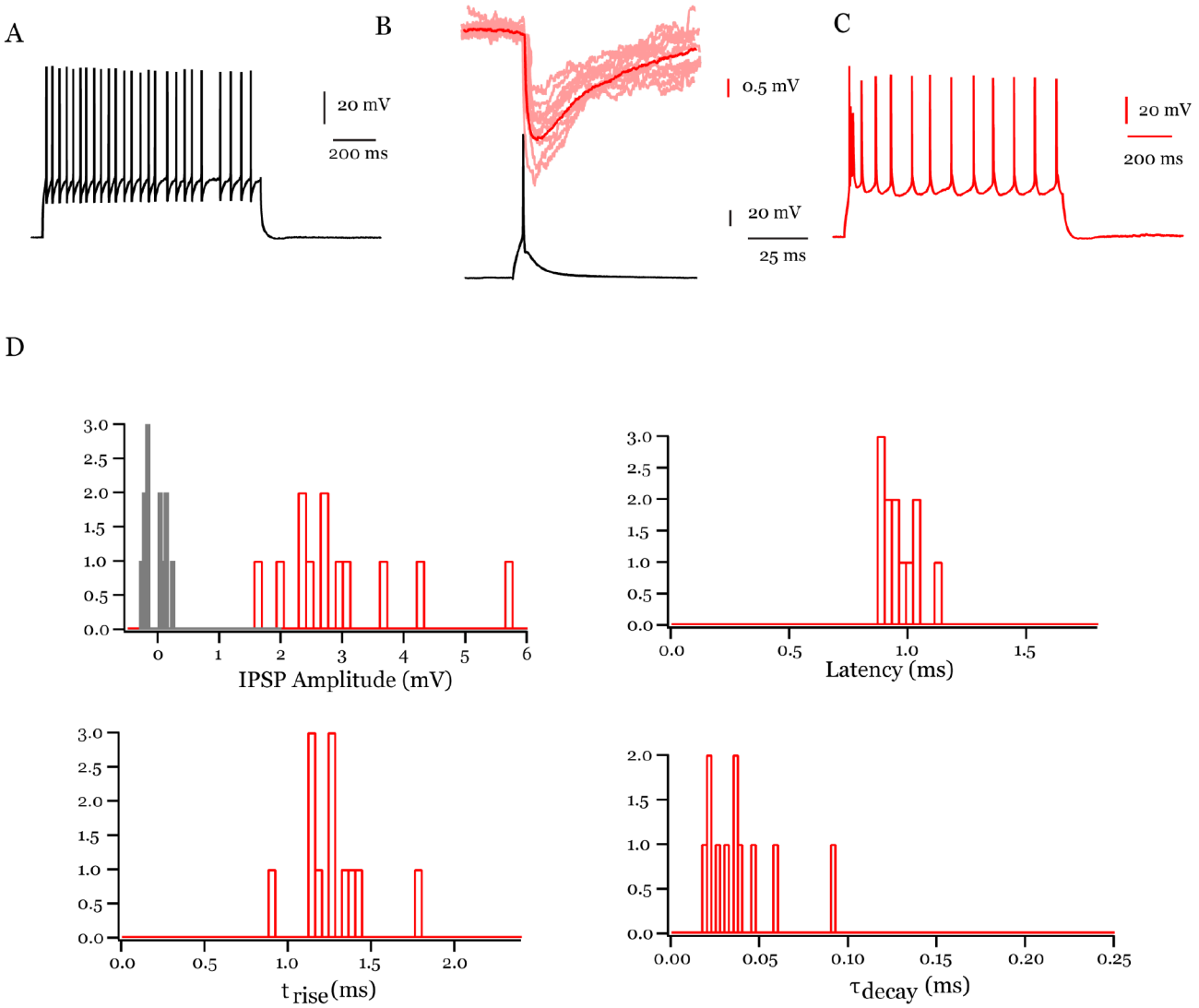

Fig. 3.4.15. FS to excitatory inhibitory connection. *(A)(C) The firing patterns of the pre- (black) and post-synaptic (red) neurons. (B) A presynaptic AP (black trace) and 10 consecutive superimposed IPSPs (red trace) and their mean IPSP (dark red trace) are shown. (D) Histogram of IPSP amplitude, noise (grey bars, along with amplitude), latency, 20-80% rise time, and decay time are shown.*

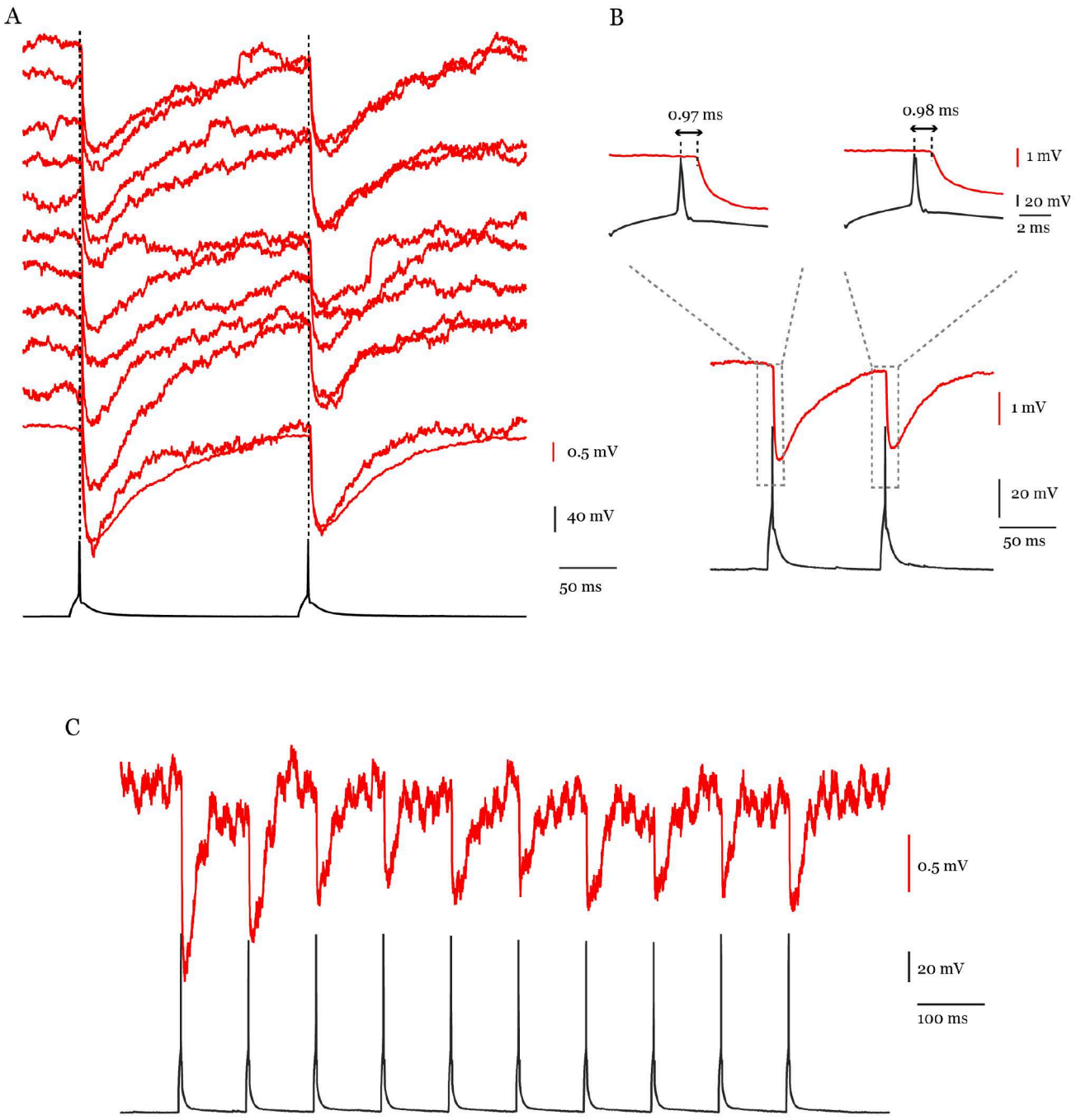

Fig. 3.4.16. Short-term plasticity of the FS to excitatory connection shown in 3.4.15. *(A) Two presynaptic APs (black trace) elicited at 100 ms interval and their corresponding 10 consecutive IPSPs (top red trace) and their mean IPSP (bottom red trace) are shown. (B) The latencies of first and second IPSPs are shown. (C) Train of ten presynaptic APs (black trace) elicited at 50 ms interval and the mean EPSP (red trace).*

Summary of L4 connections

The small PSP amplitudes, the high failure rate and the PPF observed here for synaptic connections with nFS interneurons suggests that nFS interneurons establish weak synaptic connections with a low neurotransmitter release probability. FS interneurons, on the other hand, exhibited strong and reliable synaptic depression. We also found connections with NGFC that exhibited strong short-term depression. Tables 3.4.1 - 3.4.5 summarise the properties of synaptic connections between different L4 neuron types and their EPSP/IPSP characteristics.

Table 3.4.1: IPSP characteristics of L4 NGFC-excitatory neuron connections.

NGFC-Exc (n=2)	Amplitude (mV)	Latency (ms)	20-80% rise time (ms)	Decay time	Paired-pulse ratio	Failure rate (%)	Coefficient of variation
Mean	-1.840	2.38	4.33	61.0	0.58	0	0.25
SD	0.877	0.02	0.78	26.4	0.03	0	0.04
Range	-2.46 - -1.22	2.36 - 2.39	3.78 - 4.88	42.3 - 79.7	0.56 - 0.60	0	0.23 - 0.28

Table 3.4.2: IPSP characteristics of L4 nFS-excitatory neuron connections.

nFS - Exc (n=7)	Amplitude (mV)	Latency (ms)	20-80% rise time (ms)	Decay time	Paired-pulse ratio	Failure rate (%)	Coefficient of variation
Mean	-0.59	1.26	2.55	32.3	1.15	26.3	0.58
SD	0.71	0.27	0.68	8.2	0.30	16.8	0.13
Range	-2.15 - -0.05	0.72 - 1.59	1.26 - 3.29	22.2 - 40.9	0.76 - 1.54	0 - 47.5	0.31 - 0.69

Table 3.4.3: EPSP characteristics of L4 excitatory -nFS interneuron connections.

Exc - nFS (n=8)	Amplitude (mV)	Latency (ms)	20-80% rise time (ms)	Decay time	Paired-pulse ratio	Failure rate (%)	Coefficient of variation
Mean	0.27	1.37	0.79	10.5	2.41	61.7	1.08
SD	0.54	0.79	0.49	2.6	0.75	30.2	0.51
Range	0.02 - 1.61	0.83 - 2.75	0.37 - 1.53	6.9 - 13.5	1.93 - 4.20	0 - 90	0.39 - 1.72

Table 3.4.4: IPSP characteristics of L4 nFS-FS interneuron connections.

nFS to FS (n=2)	Amplitude (mV)	Latency (ms)	20-80% rise time (ms)	Decay time	Paired-pulse ratio	Failure rate (%)	Coefficient of variation
Mean	-0.29	1.12	1.20	11.4	1.27	25.3	0.56
SD	0.06	0.32	0.63	2.5	0.42	11.4	0.06
Range	-0.34 - -0.25	0.89 - 1.34	0.75 - 1.64	9.6 - 13.2	0.97 - 1.56	17.2 - 33.3	0.52 - 0.60

Table 3.4.5: IPSP characteristics of L4 FS-nFS interneuron connections.

FS - nFS (n=5)	Amplitude (mV)	Latency (ms)	20-80% rise time (ms)	Decay time	Paired-pulse ratio	Failure rate (%)	Coefficient of variation
Mean	-0.94	0.79	1.15	15.4	0.89	7.9	0.29
SD	0.56	0.32	0.28	12.0	0.35	16.3	0.16
Range	-1.58 - -0.25	0.57 - 1.36	0.83 - 1.55	7.7 - 36.3	0.59 - 1.48	0 - 37.1	0.14 - 0.48

Fig. 3.4.17 summarises the synaptic connections of nFS interneurons showing distinct morphological properties. Four distinct morphologies of nFS interneurons, such as lateral projecting, VIP-like, Martinotti-like and NGFC-like L4 interneurons are shown here, that exhibit significantly different axonal projection patterns. nFS interneurons are labeled in blue (axon) and red (soma, dendrites), whereas the excitatory neurons are labeled in green (axon) and black (soma, dendrites). VIP-like neurons showed little to no axonal projection within the home barrel, therefore we were not able to find any inhibitory connection in L4. Almost all the nFS interneurons showed paired-pulse facilitation. The first post-synaptic amplitude was very weak showing small amplitude, which increased to more than two-fold at the second stimulus. This suggests that nFS interneurons are recruited only during continuous stimulation. NGFCs are the only group of nFS interneurons that showed paired pulse depression. The long latency and slow decay could be the result from $GABA_B$ receptor activation through volume transmission of GABA.

Fig. 3.4.18 summarises the short-term plasticity of interneurons in L4 of rat barrel cortex. The three interneuron types - FS, nFS and NGFC clearly showed distinct short-term plasticity in synaptic connections with other neuron types. Synaptic connections involving

nFS interneurons generally showed weak connections (small amplitude; -0.53±0.63 mV for inhibitory, and 0.27 mV±0.54 for excitatory connections) and short-term facilitation (PPR = 1.17±0.30 for inhibitory, and 2.41±0.75 for excitatory connections), while those involving FS interneurons tended to be strong and reliable (large amplitude; -1.54 ±1.02 mV for inhibitory, and 2.66±3.18 mV for excitatory connections) and displayed short-term depression (PPR = 0.79±0.21 for inhibitory, and 0.92±0.15 for excitatory connections). Only two synaptic connections with NGFC were found in this study, both of which showed short-term depression (PPR = 0.58±0.03 for inhibitory, and 0.86 for excitatory connection).

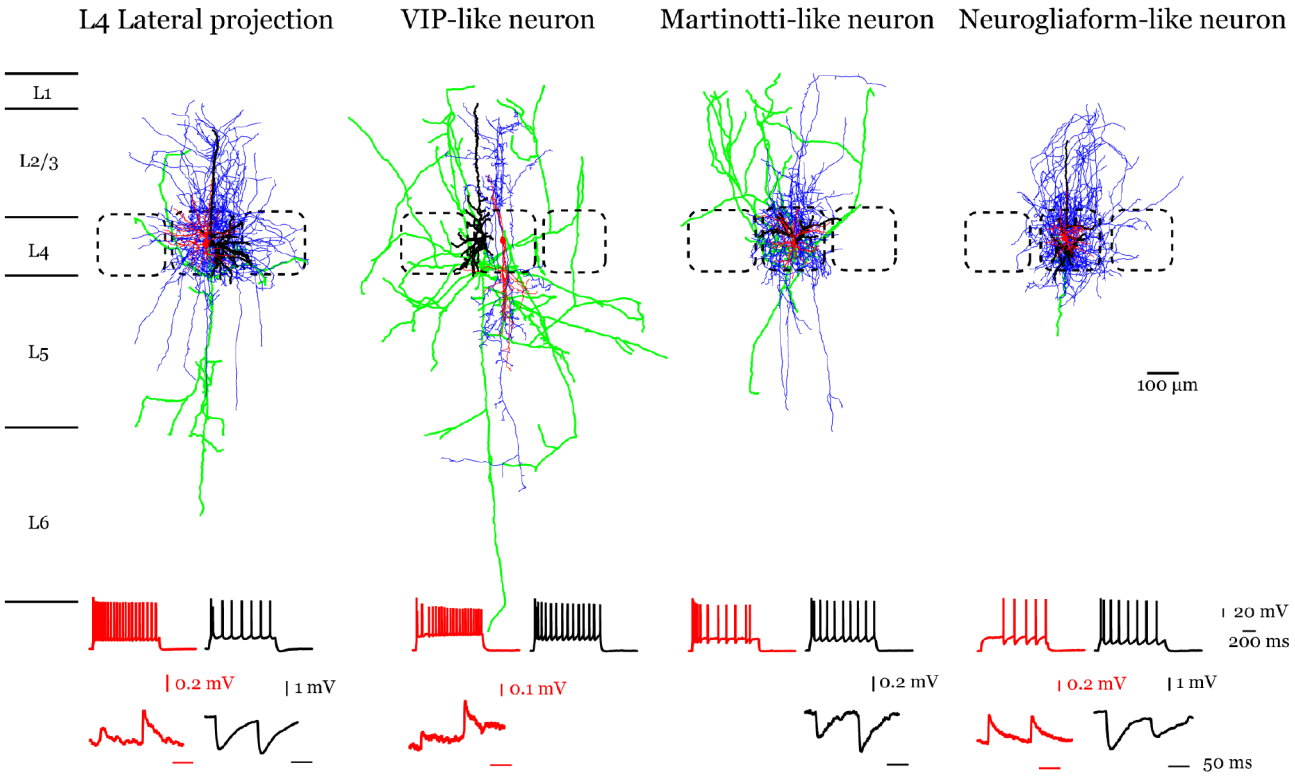

Fig. 3.4.17. Representative examples of synaptically coupled nFS interneurons showing distinct morphologies in L4 of rat barrel cortex. (Top) *Neurolucida reconstructions of a biocytin-filled synaptically coupled neurons involving L4 nFS interneurons and L4 excitatory neurons. Blue, nFS axon; red, nFS soma and dendrites; black, excitatory neuron axon; green, excitatory neuron soma and dendrites.* ***(Bottom)*** *Firing patterns of nFS interneuron (red) and excitatory neuron (black) and averaged postsynaptic potentials (PSP) during paired presynaptic firing for excitatory (red) and inhibitory (black) connections.*

An overview of the paired-pulse behaviour of different interneuron types is shown in Fig. 3.4.19. Repetitive presynaptic firing at a fixed interval of 100 ms revealed the short-term plasticity of different neuron types in L4. Most nFS interneurons exhibited weak

paired-pulse facilitation, whereas the FS interneurons showed strong paired-pulse depression **(Fig. 3.4.19B)**. NGFC was the only nFS interneuron type that showed paired-pulse depression. From this summary figure, it appears that interneurons determine the paired-pulse behaviour of synaptic connections, be it pre- or post-synaptic. Between two interneurons, it is the presynaptic interneuron that governs the short-term synaptic plasticity. An inhibitory connection from nFS to FS interneuron displayed paired-pulse facilitation, whereas the reciprocal connection showed paired-pulse depression.

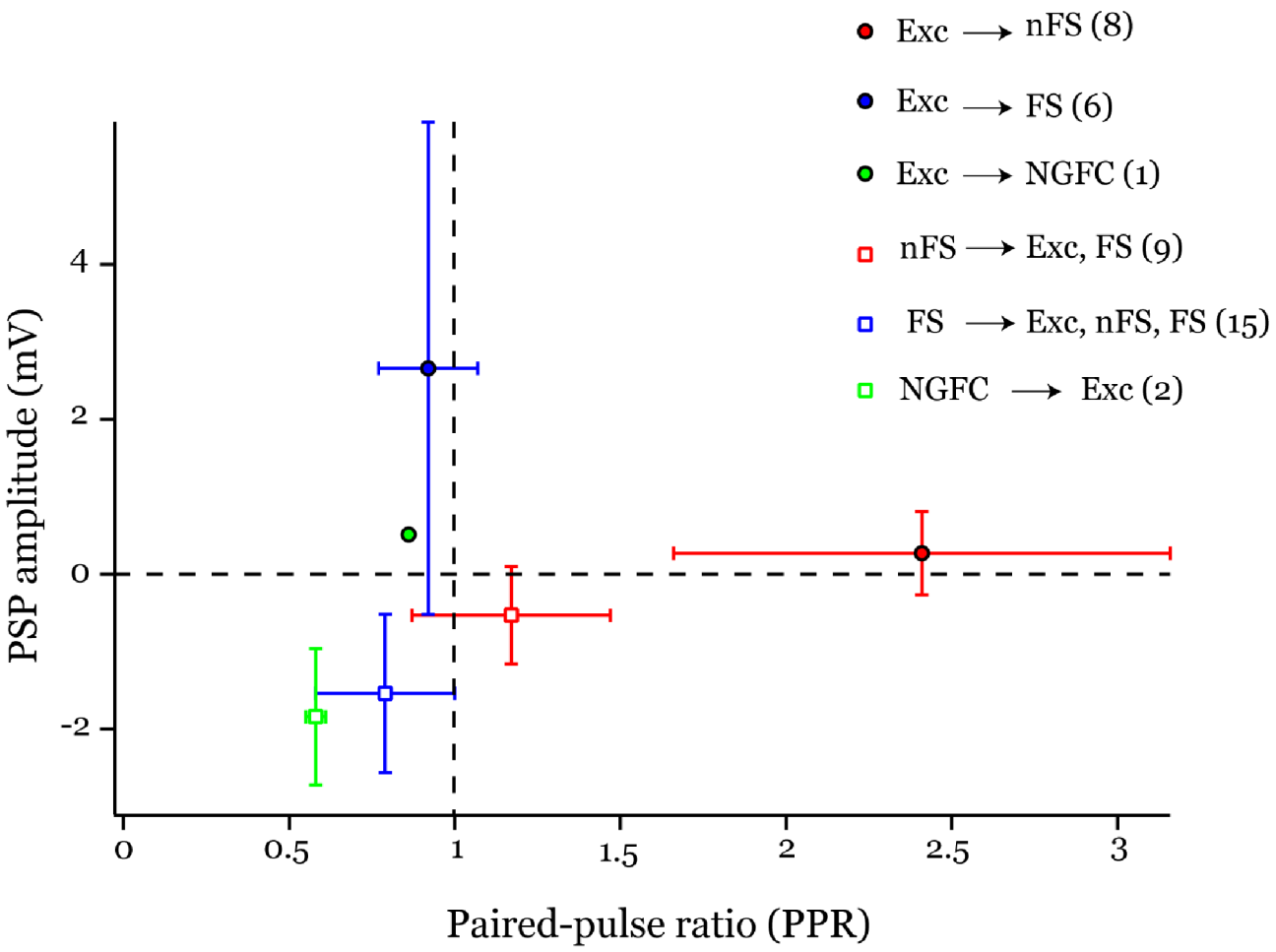

Fig. 3.4.18. Summary plot of 1st PSP amplitude versus the paired-pulse ratio (PPR) of different L4 synaptic connections. *Synaptic connections of different L4 neurons are displayed with mean (centre)and standard deviation (error bars). Red, blue, and green colours represent synaptic connections with nFS, FS, and NGFC respectively. Filled circles with black outline represent excitatory synapse, and open squares represent inhibitory synapse.*

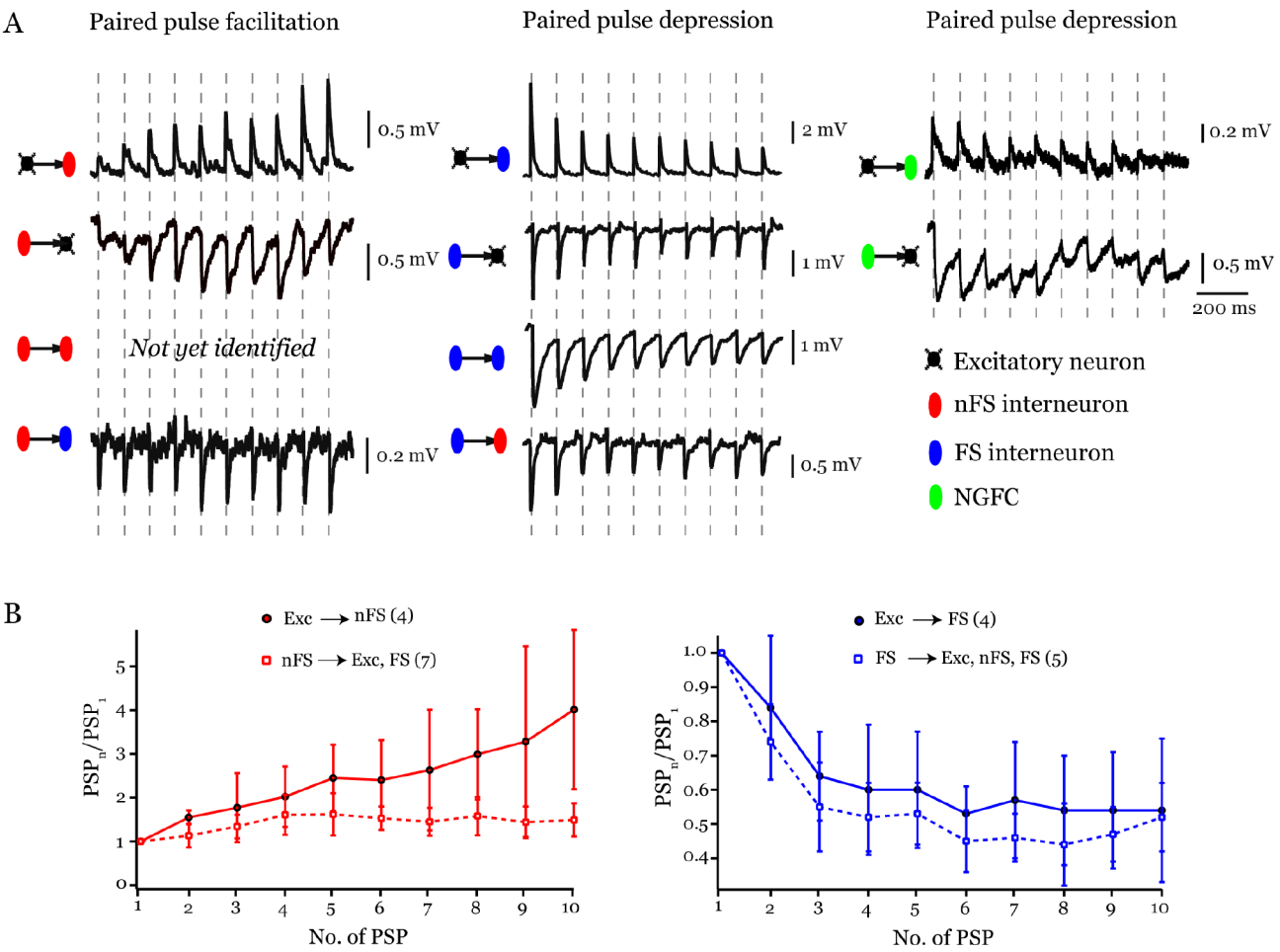

Fig. 3.4.19 Paired pulse behaviour of L4 neurons in rat barrel cortex. (A) *Comparison of averaged excitatory/inhibitory PSPs during repetitive presynaptic firing for synaptic pairs involving L4 non-fast (left), fast (middle) spiking interneurons and NGFCs (right).* ***(B)*** *Summary data of normalised PSPs during repetitive presynaptic firing for synaptic pairs involving L4 nFS, FS and excitatory neurons, shown as mean ± standard deviation (error bars). Excitatory connection is shown in black circles, filled with red colour for nFS (left) and blue colour for FS interneurons (right), which shows paired-pulse facilitation with nFS interneurons (left) and paired-pulse depression with FS interneurons (right). Inhibitory connection (open squares) displayed the paired pulse behaviour of the pre-neuron.*

3.5. Molecular markers of L4 interneurons in rat barrel cortex

Analysis of molecular expression of nFS in L4

Previous studies demonstrated that PV, SOM and 5HT3a are expressed in interneurons in rodent somatosensory cortex. PV is mostly associated with FS interneurons; SOM with Martinotti cells, and 5HT3aR with NGFC. In this study, a subset of L4 nFS interneurons in rat barrel cortex were patched to identify their molecular expression. For this purpose, we combined patch-clamp recording with simultaneous biocytin filling coupled with Alexa dye to locate the patched neuron for post hoc immunofluorescent techniques. After successful patch-clamp recording, the brain slices were processed with one of the molecular markers known to be expressed by interneurons. An epifluorescence microscope was used to visualise both the patched neuron and immunoreactivity for the molecular markers. The patched neuron was filled with Alexa Fluor® 594 and visualised with the emission and excitation filters of 591 nm and 621 nm respectively. The expression of molecular markers was visualised with 495/519 nm emission/excitation range. After collecting the fluorescence data, the slices were processed for biocytin to obtain the morphological data.

Five out of eight neurons were SOM-positive, and 5HT3aR-negative. Fig. 3.5.1 shows the expression of SOM by one of the nFS interneurons and eventual biocytin processing, which yielded the morphology of patched neuron. The percentage of SOM-positive neurons in L4 was in accordance with that found in previous studies *(Ma Y et al. 2006; Xu H et al. 2013)*. We were not able to identify any L4 interneuron expressing 5HT3aR; a reason for this could be an inefficient antibody staining. Studies showing the expression of 5HT3aR were performed using transgenic animals that express GFP under the control of 5HT3aR *(Lee S et al. 2010; Vucurovic K et al. 2010)*. There has been no study on immunofluorescent staining that labels 5HT3aR on wild type rodents. Due to the difficulties with 5HT3aR labelling, we attempted to use Prox-1, which is a homeodomain transcription factor that is expressed exclusively in post-mitotic CGE-derived interneuron precursors and is maintained into adulthood. Even though Prox-1 was expressed in brain slices, we were unable to find co-labelling of Prox-1 with any of our patched nFS interneuron **(Supplementary figures 8, 9)**.

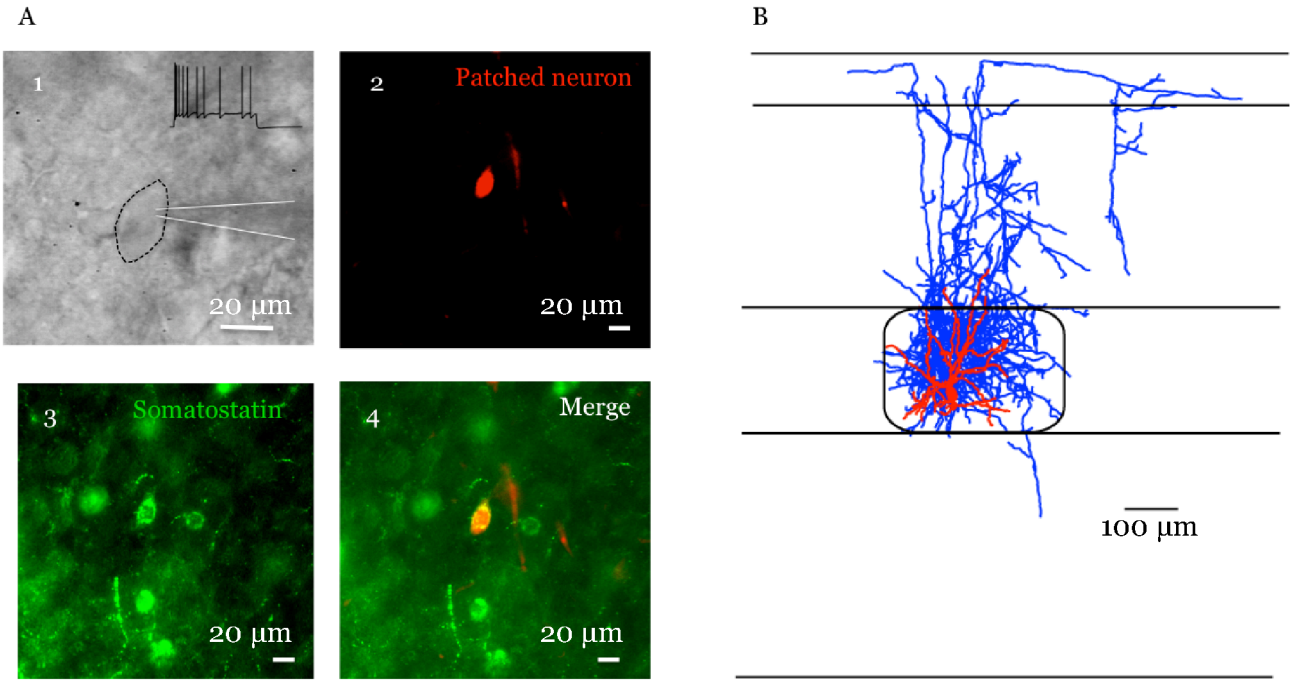

Fig. 3.5.1. Analysis of single cell patched neuron with immunofluorescence technique. (A) *Single neurons were recorded using whole-cell patch clamp technique and were filled with biocytin coupled to Alexa Fluor® 594 (1). nFS interneurons were identified using their firing pattern (1 inset). After processed with appropriate primary and secondary antibodies, the brain slices were visualised using epifluorescence microscope. The patched neuron was visualised in red (2), and the neuron was shown to express SOM (3). The merged image shows the co-localization of patched neuron in red, and SOM expression in green (4).* ***(B)*** *Later, biocytin labelling was processed using to identify the morphology of patched nFS interneuron, which was reconstructed using Neurolucida software. Axon is labeled in blue, soma and dendrites in red.*

4. Discussion

Classification of interneurons based on morphological characteristics

GABAergic interneurons play an important role in providing balanced cortical excitation, synchronised activity, and maintaining neuronal oscillatory networks *(McBain CJ and A Fisahn 2001; Markram H et al. 2004; Burkhalter A 2008; Klausberger T and P Somogyi 2008)*. Abnormalities of these functions have been associated with several neurological and psychiatric disorders including autism, epilepsy, schizophrenia, and Tourette syndrome *(Kalanithi PS et al. 2005; Tabuchi K et al. 2007; Gonzalez-Burgos G et al. 2015; Jiang X et al. 2016)*. Although GABAergic interneurons constitute only a small fraction (10-20%) of the total number of neocortical neurons, they are notorious for their heterogeneity, with respect to morphology, electrophysiology and the expression of molecular markers such as Ca-binding proteins, peptides and transcription factors *(Gupta A et al. 2000; Ascoli GA et al. 2008; DeFelipe J et al. 2013)*. In order to better understand the heterogenous population of interneurons, several parameters describing axonal and dendritic geometry, intrinsic properties and protein expression were used. Given the ample number of possible parameters to classify interneurons, it is important to consider the parameters that shows functional relevance and stability.

The electrophysiological properties of interneurons are functionally relevant, but the reliability of firing patterns can be questioned by the experimental conditions such as neuronal activity before and during the experiment, changes in temperature and potential mechanical disturbances due to the movement of the recording pipette and the modulation of ion channels by neuromodulatory transmitters (e.g. noradrenaline, acetylcholine, adenosine etc.) via G-proteins, by intracellular Ca and the degree of de- or hyper polarisation of the membrane potential *(Feldmeyer D and JHR Lübke 2010)*. The functional relevance of protein expression is not completely understood. A well known molecular marker PV is widely used to identify fast-spiking interneurons, but is associated with two morphologically distinct interneuron types, the basket and axo-axonic (chandelier) cell that show completely different morphological and synaptic properties *(Kawaguchi Y and Y Kubota 1997; Ascoli GA et al. 2008; Woodruff A et al. 2009; DeFelipe J et al. 2013; Koelbl C et al. 2015)*. In particular, basket cells target the soma and dendrites while axo-axonic interneurons innervate the axon initial segment.

The axonal and dendritic geometry can be considered rather stable parameters. However, dendritic geometry is only partly predictive of intrinsic electrical excitability *(Mainen ZF and TJ Sejnowski 1996; Helmstaedter M et al. 2009c)*. Several parameters can be extracted from a complete 3D reconstruction of an interneuron. The most meaningful and functionally relevant morphological parameters are those that define the innervation domains, as they allow a prediction of synaptic connectivity. The axonal projection pattern provides information about the potential connectivity and the density of contact formation, which cannot be obtained with other methods *(Helmstaedter M et al. 2009b; Feldmeyer D and JHR Lübke 2010; Qi G et al. 2015)*. Recent studies on neuronal classification were performed using morphological parameters such as fractal analysis, sholl analysis, fan-in analysis and so on *(McGarry LM et al. 2010; Muralidhar S et al. 2013; Santana R et al. 2013)*. To compare the morphological clusters derived from these parameters, we performed an unsupervised hierarchical cluster analysis on 38 nFS interneurons based on 64 morphological parameters extracted from Neuroexplorer, describing soma, dendrites and axon **(Supplementary table 1)**. The cluster analysis displayed a scrambled distribution of morphologies, which did not provide any meaningful information **(Supplementary figure 10)**. However, cluster analysis based on the axonal projection patterns displayed three distinct clusters, which showed functionally relevant distinct projection patterns **(Fig. 3.1.5)**.

In conclusion, it is important to consider the axonal morphology, because it is a reliable, stable and functionally relevant parameter, thus can be used as a primary classifier. Interneuron classification based on morphological parameters provides insights into the synaptic microcircuits formed by nFS interneurons and hence their functional role in intra- and inter- columnar processing of sensory signals *(Helmstaedter M et al. 2009b; Koelbl C et al. 2015)*. Electrophysiological and molecular properties can be used as additional classifiers, but not vice versa.

Different projection motifs of L4 nFS interneurons and their possible roles

C1 L4 nFS interneurons showed significant projections to neighbouring barrels; C2 interneurons showed axonal and dendritic projection confined exclusively to the home column, with predominant projections in the home barrel; and C3 interneurons showed a remarkable axonal projection largely outside the home layer, with a dense axonal plexus in

the supra granular layers (C3a), or sparse axonal projections to both supra- and infra-granular layers (C3b).

The most characteristic feature of C1 interneurons is the extensive axonal collateralisation in the adjacent barrels. The functional role of which is likely to be inhibition of excitatory neurons in the neighbouring barrels. Barrels in L4 have been described as functionally independent structures that receive little or no direct inputs from adjacent barrels *(Petersen CC and B Sakmann 2001; Laaris N and A Keller 2002)*. However, our findings suggests that L4 C1 interneurons with lateral axonal projection provide direct inhibition to the neighbouring barrels, and may form anatomical correlate to lateral inhibition in L4. In visual cortex, lateral inhibition is known to provide surround suppression thereby enhancing sensitivity to contrast edges and eliminating redundant information in the visual environment *(Jones HE et al. 2001; Smith MA 2006)*. SOM-positive interneurons have been proposed to mediate surround inhibition in L2/3 of visual cortex *(Adesnik H et al. 2012)*. Suppression of surround whiskers in the barrel system may be involved in contrast enhancement of principal whisker signalling. Previous studies have reported the existence of laterally projecting interneuron in layer 2/3 *(Helmstaedter M et al. 2009b)*, but so far such neurons have not been described for layer 4. The data presented here suggest that lateral inhibition is already happening at the very first stage of neocortical signal processing in L4 of rat barrel cortex. Apart from significant projections to the neighbouring barrels, some C1 interneurons also send ascending branches to L2/3 and terminate in L1. Few C1 neurons showed infra-granular projections descending as far down as the L5/6 border. Therefore, the main functional role of C1 neurons could be to provide early surround inhibition to the neighbouring barrels in L4, and feed-forward inhibition to other layers, thereby enhancing the signal contrast between principal vs. the surround whisker deflection in L4 microcircuitry *(Derdikman D et al. 2003; Sachdev RN et al. 2012)*. It should be noted here that some lateral projection neurons send axon collaterals even beyond two adjacent barrels.

C2 interneurons with intra-columnar axonal projections were the most common subtype of nFS interneurons in L4. Although C2 neurons showed some heterogeneity in their axonal projections, more than 90% of the axonal branches were confined within the home column, and they showed both sparse ascending and descending branches to the superficial and infragranular layers respectively. The main feature of C2 neurons is the dense local projections with an average total axonal length of more than 35,000 µm. Such

dense projection suggest a high connectivity rate to other neurons within the home barrel. This group may correspond to SOM-expressing X94 and non-X94 neurons in L4, which showed large confinement of axons to home barrel *(Ma Y et al. 2006; Xu H et al. 2013)*. C2 neurons may provide disinhibition of spiny stellate neurons by preferentially targeting L4 FS interneurons, particularly L4 barrel inhibitor interneurones (BINs) which also shows dense axonal projections within the home barrel *(Xu H et al. 2013; Koelbl C et al. 2015)*. In our study, we found that nFS and FS interneurons both displaying dense axonal innervation within the home barrel were reciprocally connected.

C3 L4 nFS interneurons showed a remarkable axonal projection motif with their extra-granular projection. Having projections outside L4, C3 neurons may form only little if any inhibitory connections within the home barrel. The two sub-clusters of C3 neurons were clearly distinct in their axonal density and projection patterns. C3a neurons preferentially innervated supra-granular layers, and may provide feed-forward inhibition to distal dendrites of L5B thick tufted pyramidal neurons, or basal dendrites of L2/3 pyramidal neurons. C3b neurons resembled the morphology of VIP neurons, with sparse axonal projections, spanning through all layers. Upon stimulation, VIP interneurons, along with nitric oxide synthase (NOS) interneurons release vasoactive intestinal peptides and nitric oxide, which in turn causes a local dilation of blood vessels in the brain *(Cauli B et al. 2004)*. During vasodilation, VIP interneurons increase the efficacy of glutamatergic synapses on excitatory neurons by modulating them *(Pellegri G et al. 1998)*. An increase in excitation throughout cortical areas was observed upon activation of VIP neurons *(Lee S et al. 2013; Fu Y et al. 2014)*.

Heterogeneity of nFS electrophysiological properties

In this study, we characterised 59 nFS interneurons in L4 of rat barrel cortex based on their intrinsic properties using unsupervised cluster analysis. We used morphological reconstructions of FS interneurons as control, and those were well separated into a distinct group. Three electrophysiological subtypes were characterised, which showed differences in various aspects, such as membrane properties, action potential properties and firing frequency adaptation.

Excitability of neurons was calculated using an index, where three factors - resting membrane potential, AP threshold, and input resistance were considered *(Lazarus MS and*

ZJ Huang 2011). The three clusters displayed variable range of excitability. Cluster A interneurons showed relatively low, Cluster B interneurons high and Cluster C interneurons intermediate excitability. Differences in firing rate adaptation clearly separated the three groups. Cluster A was characterised by an irregular spiking pattern and high frequency adaptation, similar to the firing pattern shown for non-Martinotti SOM interneurons in L4 *(Ma Y et al. 2006; Xu H et al. 2013)*. Cluster B showed an initial burst of AP followed by irregular and accelerated firing upon depolarisation, resembling the characteristic VIP neuron firing. The accelerated firing with decrease in ISI could be due to a slow inactivation of a K^+ current. It may be involved in the enhancement of synaptic gain and the synchronisation of neurons *(Porter JT et al. 1998; Miller MN et al. 2008)*. Cluster C showed little to no frequency adaptation at near threshold current injections, but displayed spike adaptation at supra-threshold current injections. A characteristic feature of Cluster C is the broad AP, large AHP, and non-adapting firing pattern. Some neurons exhibited late-spiking behaviour, much like that reported for NGFCs *(Kawaguchi Y and Y Kubota 1997; Tamas G et al. 2003; Wozny C and SR Williams 2011; Jiang X et al. 2015)*.

Correlation between morphological, electrophysiological and molecular subtypes

We tried to find a potential correlation between the morphological and electrophysiological clusters but found that there was no one-to-one correlation. The largest electrophysiological group - Cluster A exhibiting high frequency adaptation with irregular firing pattern was found for all the three morphologically distinct structures identified in our study.

The observed difference between morphology and firing pattern may be due to various reasons. Electrophysiological characteristics are not tightly correlated with the axonal projection patterns, but are rather linked to the presence of certain ion channels *(Llinas RR 1988; Connors BW and WG Regehr 1996)*. Ion channels such as K_{ir}, K_{Ca}, HCN shape the firing pattern of neurons to some degree, and their activity is subjected to change due to the modulatory effects of neurotransmitters such as acetylcholine, noradrenaline, etc., *(Dodson PD et al. 2002)*.

Three C2 interneurons showed a dense, local and radiating axonal plexus, characteristic of NGFCs and displayed regular non-adapting firing behaviour with a broad AP and a large AHP *(Chu Z et al. 2003; Oláh S et al. 2007; Jiang X et al. 2015)*. Although

there is a strong tendency to associate a late-spiking firing pattern to NGFCs, this was not found for all cells recorded.

Most of the L4 nFS interneurons were found to be SOM-positive. Given the heterogeneity of interneuron markers and the percentage of PV negative neurons in L4 (<4% of L4 neurons), it was not possible to test for all the nFS interneuron markers *(Meyer HS et al. 2011)*. Recent studies using large scale RNA sequencing shows that there are at least 14 cortical interneuron types based on the molecular markers *(Wang Z et al. 2009; Zeisel A et al. 2015; Cadwell CR et al. 2016; Fuzik J et al. 2016; Tasic B et al. 2016)*; even more subclasses may exist as the authors of this study state: in the 14 subclasses, one could clearly see that well-known markers such as SOM, the 5HT3a receptor, and reelin were expressed in many interneuron subclasses. Although PV is shown to be non-overlapping, the method used in the study failed to distinguish between two clear morphological subgroups such as the axo-axonic chandelier and the basket cells. Therefore, we believe that classification based on molecular markers alone is to a large extent ambiguous. This is also relevant for transgenic mouse lines that exhibit cell-specific labelling of neuron types based on such marker peptides or proteins.

nFS interneurons in inhibitory microcircuitry

Results from paired recordings from synaptically coupled nFS interneurons and other L4 neurons showed that nFS interneurons establish weak synaptic connections with small PSP amplitudes. This is probably due to low release probability of synaptic vesicles at these synaptic contacts. Synaptic connections with nFS interneurons showed high failure rate and large CV, and exhibited paired-pulse facilitation. The latency was significantly longer compared to the FS interneurons, which could be due to the distal location of the synaptic contacts. It should be noted that nFS interneurons displayed a much broader axonal field span, extending to both supra- and infra granular layers, unlike the barrel-confined FS interneurons. The synaptic properties of nFS interneurons are markedly different from those of FS interneurons, which form strong synaptic connections with a high release probability that exhibit invariably paired-pulse depression *(Beierlein M et al. 2003; Koelbl C et al. 2015)*. NGFCs are the only nFS interneurons that showed paired-pulse depression. The slow decay time of IPSPs formed by NGFCs has been proposed to result from $GABA_B$ receptor activation through volume transmission (i.e. not direct synaptic transmission) of GABA *(Olah S et al. 2009; Chittajallu R et al. 2013)*.

From the results of paired recording experiments from synaptic connections between nFS and FS interneurons with excitatory neurons, it is evident that FS interneurons act as a low-pass filter by triggering a strong post-synaptic response during the initial spikes following a stimulus, whereas nFS interneurons requires high frequencies to trigger a post-synaptic response. Therefore nFS interneurons constitute a synaptic high-pass filter. Excitation of L4 spiny neurons upon thalamic stimulation is limited by the early thalamocortical recruitment of FS interneurons which displays paired pulse depression. On the other hand, nFS interneurons that display paired pulse facilitation of thalamocortical EPSPs need prolonged synaptic input before inhibition is activated *(Beierlein M et al. 2003; Cruikshank SJ et al. 2007; Staiger JF et al. 2009; Cruikshank SJ et al. 2010; Hu H et al. 2011)*. Therefore, FS and nFS interneurons generate two windows of inhibition - FS shows fast recruitment and fast decay, whereas nFS shows late recruitment and slow decay. nFS interneurons could enhance the activity of excitatory neurons by disinhibiting FS interneurons in L4. SOM-positive interneurons in L4, which are similar to our C2 interneurons that show dense axonal projections within the barrel are shown to preferentially target FS interneurons, thereby providing disinhibition on excitatory neurons in L4 *(Xu H et al. 2013)*.

Short-term plasticity results from a combination of mechanisms, many of which are presynaptic in origin, including vesicle depletion and accumulation of calcium in the presynaptic terminal. On the postsynaptic site the desensitisation of neurotransmitter receptors may also play a role *(Zucker RS and WG Regehr 2002; Thomson AM 2003; Abbott LF and WG Regehr 2004; Regehr WG 2012)*. It has been shown that there is a pronounced dependence of short-term plasticity on the presynaptic interneuron type for unitary inhibitory-to-inhibitory synapses *(Ma Y et al. 2012)*. We found similar results showing that inhibitory connections with presynaptic FS interneurons showed short-term depression, whereas those with nFS interneurons displayed short-term facilitation. From previous studies on unitary excitatory synapses onto interneurons, it has been hypothesised that short-term plasticity of those excitatory synapses depend on postsynaptic neuron type *(Thomson AM 1997; Markram H et al. 1998; Reyes A et al. 1998)*. However, we found that synaptic connections involving both excitatory neurons and interneurons appears to be dependent on the type of interneuron, irrespective whether it is the pre- or post synaptic neuron. For example, excitatory neuron-nFS interneuron and nFS interneuron-excitatory neuron connections display both short-term facilitation.

Conversely, connections involving excitatory and FS interneurons show short-term depression in both excitatory and inhibitory connections. The exact mechanism behind this short-term plasticity remains unclear. We hypothesise that the interaction between pre- and post-synaptic structures may induce structural and/or functional changes that result in either short-term depression or short-term facilitation at these connections.

Advantages and limitations of current methods

Classification of interneurons is crucial to understand the functional and structural properties of neuronal microcircuits *(Gupta A et al. 2000; Ascoli GA et al. 2008; Burkhalter A 2008; DeFelipe J et al. 2013)*. By using wild-type rats, we excluded the possibility of bias resulting from a pre-selection of interneurons, which is the case when using transgenic animal models that are based on the expression of a single marker molecule (e.g. SOM or PV) to identify a population of neurons. Even though it is extremely laborious and time-consuming to patch neurons that are rare, which is the main limitations of our method, we were able to find several neuronal subtypes such as the lateral-projecting nFS interneurons that have not been described previously. Similarly, VIP interneurons are considered rare in L4, but we found that 3 of 38 nFS interneurons are VIP-like interneurons *(Pronneke A et al. 2015)*. The only explanation in finding such neurons that have so far not been identified is the unbiased neuronal patching approach. By using transgenic animals expressing neuronal markers such as VIP, SOM, several potential nFS interneuron populations that might be expressing a combination of several markers at lower levels may be left unidentified *(Lee S et al. 2010; McGarry LM et al. 2010; Pronneke A et al. 2015)*.

Future perspectives

In this study, we were able to provide a comprehensive quantitative description of the electrophysiological, morphological and molecular properties of nFS interneurons in L4 of rat barrel cortex in an *in vitro* slice preparation. A major disadvantage of the slice preparation is the reduced neuromodulatory effects of neurotransmitters such as acetyl choline, noradrenaline, dopamine, etc. As a future perspective, it would be interesting to find the neuromodulatory effects on nFS interneurons using drug application of neurotransmitters and to use their differential effects for a further functional characterisation.

As a next step to shed light on the functional aspects of nFS interneurons *in vivo,* recordings in awake behaving rodents could be performed to elucidate the activity and functional role of nFS interneurons. Due to the extremely low number of nFS interneurons in L4 of rat barrel cortex (<4% of L4 neurons), it would be advantageous to combine optogenetic and molecular tagging of nFS interneurons *(Meyer HS et al. 2011; Taniguchi H et al. 2011; Wang G et al. 2015)*. Recent advancement in RNA sequencing makes it easier to identify the molecular expression of different neuron types *(Zeisel A et al. 2015; Cadwell CR et al. 2016)*.

To expand our knowledge on nFS synaptic connectivity, it is crucial to find the target of nFS interneurons in different layers, especially L2/3. From this study, we were able to identify a cluster of nFS interneurons that project extensively to L2/3, having little or no projections to the home barrel. A functionally relevant question would be to identify the postsynaptic targets of such neurons - if the nFS interneurons provide feed-forward inhibition onto L2/3 pyramidal neurons or the distal dendrites of layer 5B, or do they have the tendency to preferably inhibit interneurons, thereby providing disinhibition on L2/3 pyramidal neurons.

5. Summary

Inhibitory GABAergic interneurons are notorious for their heterogeneity, despite constituting a low fraction of the neuronal population in neocortex (<15%). Classification of interneurons is crucial for understanding their widespread cortical functions providing a complex, and dynamic network balancing excitation and inhibition. In this study, I investigated the different subtypes of nFS interneurons and their functional properties in the L4 neuronal micro-circuitry of the rat somatosensory cortex using whole-cell patch clamp recordings, biocytin labelling, morphological 3D reconstructions and immunofluorescence techniques. A quantitative classification was performed using PCA and unsupervised cluster analysis based on morphological parameters such as laminar and columnar axonal and dendritic projections and electrophysiological parameters such as membrane properties and firing properties. Our major findings include the identification of significantly distinct morphological subtypes of nFS interneurons in L4, such as lateral projection neurons, intra-columnar projection neurons and extra-granular projection neurons. The most characteristic feature of lateral projection interneurons is the extensive axonal collateralisation in the adjacent barrels. Our finding suggests that L4 nFS interneurons with a lateral axonal projection provide direct inhibition to the neighbouring barrels, and may form an anatomical correlate to lateral inhibition in L4. Therefore, we believe that lateral inhibition is already happening at the first stage of cortical signal processing in L4 of rat barrel cortex. Intra-columnar projection neurons show a dense axonal projections within the home barrel, with few branches extending to supra- and infra-granular layers. These neurons may provide disinhibition of spiny neurons by preferentially targeting L4 FS interneurons, particularly PV-positive L4 interneurons which also shows dense axonal projections that is almost exclusively confined to the home barrel. Extra-granular projection neurons shows remarkable axonal projections outside the home barrel. The two sub-clusters of extra-granular projection neurons showed differences in axonal density and field span - one showed extensive axonal projection to L2/3 and other showed morphology similar to VIP interneuron with sparse axonal projection spanning through all layers. We also found three electrophysiological subtypes of nFS interneurons, each showing differences in passive and active intrinsic properties. When comparing the morphological and electrophysiological clusters, we did not find a one-to-one correlation between them. Molecular identification of nFS interneurons revealed that most, but not all of them were positive to SOM expression.

In addition to this, we also characterised the synaptic circuits involving nFS interneurons in L4 using paired recording technique. We were able to show that nFS interneurons establish weak synaptic connections with a low neurotransmitter release probability and small amplitude, and the connections showed paired-pulse facilitation. This is markedly different from FS interneurons, which form strong synaptic connections that exhibit invariably paired-pulse depression and thus have a high release probability. NGFCs are the only nFS interneuron group that showed strong paired pulse depression. From our study it appears that interneurons govern the short-term plasticity of synaptic connections involving excitatory and interneurons, irrespective of them being pre- or postsynaptic neuron. The paired pulse behaviour of synaptic connections between inhibitory neurons are governed only by the presynaptic interneuron type. Our findings reveal that nFS interneurons are integral elements of the L4 microcircuitry that exhibit very distinct connectivity patterns, functional roles and computational properties in the neocortical neuronal network.

Bibliography

Abbott LF, Regehr WG. 2004. Synaptic computation. Nature 431:796-803.

Adesnik H, Bruns W, Taniguchi H, Huang ZJ, Scanziani M. 2012. A neural circuit for spatial summation in visual cortex. Nature 490:226-231.

Agmon A, Connors BW. 1991. Thalamocortical responses of mouse somatosensory (barrel) cortex in vitro. Neuroscience 41:365-379.

Ahissar E, Sosnik R, Haidarliu S. 2000. Transformation from temporal to rate coding in a somatosensory thalamocortical pathway. Nature 406:302-306.

Allendoerfer KL, Shatz CJ. 1994. The subplate, a transient neocortical structure: its role in the development of connections between thalamus and cortex. Annu Rev Neurosci 17:185-218.

Angevine JB, Sidman RL. 1961. Autoradiographic study of cell migration during histogenesis of cerebral cortex in the mouse.

Ascoli GA, Alonso-Nanclares L, Anderson SA, Barrionuevo G, Benavides-Piccione R, Burkhalter A, Buzsaki G, Cauli B, Defelipe J, Fairen A, Feldmeyer D, Fishell G, Fregnac Y, Freund TF, Gardner D, Gardner EP, Goldberg JH, Helmstaedter M, Hestrin S, Karube F, Kisvarday ZF, Lambolez B, Lewis DA, Marin O, Markram H, Munoz A, Packer A, Petersen CC, Rockland KS, Rossier J, Rudy B, Somogyi P, Staiger JF, Tamas G, Thomson AM, Toledo-Rodriguez M, Wang Y, West DC, Yuste R. 2008. Petilla terminology: nomenclature of features of GABAergic interneurons of the cerebral cortex. Nat Rev Neurosci 9:557-568.

Baumgartner G. 1983. Organization and function of the neocortex. Neuro-Ophthalmology 3:1-14.

Bayer SA, Altman J. 1991. Neocortical development: Raven Press New York:.

Beierlein M, Gibson JR, Connors BW. 2003. Two dynamically distinct inhibitory networks in layer 4 of the neocortex. J Neurophysiol 90:2987-3000.

Berry M, Rogers AW. 1965. The migration of neuroblasts in the developing cerebral cortex. Journal of Anatomy 99:691.

Branco T, Staras K. 2009. The probability of neurotransmitter release: variability and feedback control at single synapses. Nat Rev Neurosci 10:373-383.

Brecht M, Preilowski B, Merzenich MM. 1997. Functional architecture of the mystacial vibrissae. Behav Brain Res 84:81-97.

Brecht M, Sakmann B. 2002. Dynamic representation of whisker deflection by synaptic potentials in spiny stellate and pyramidal cells in the barrels and septa of layer 4 rat somatosensory cortex. J Physiol 543:49-70.

Brodmann K. 1909. Vergleichende Lokalisationslehre der Grosshirnrinde : in ihren Prinzipien dargestellt auf Grund des Zellenbaues. Leipzig: J.A. Barth.

Burkhalter A. 2008. Many specialists for suppressing cortical excitation. Front Neurosci 2:155-167.

Buzsaki G. 1984. Feed-forward inhibition in the hippocampal formation. Prog Neurobiol 22:131-153.

Cadwell CR, Palasantza A, Jiang X, Berens P, Deng Q, Yilmaz M, Reimer J, Shen S, Bethge M, Tolias KF. 2016. Electrophysiological, transcriptomic and morphologic profiling of single neurons using Patch-seq. Nature biotechnology 34:199-203.

Cauli B, Audinat E, Lambolez B, Angulo MC, Ropert N, Tsuzuki K, Hestrin S, Rossier J. 1997. Molecular and physiological diversity of cortical nonpyramidal cells. J Neurosci 17:3894-3906.

Cauli B, Tong X-K, Rancillac A, Serluca N, Lambolez B, Rossier J, Hamel E. 2004. Cortical GABA interneurons in neurovascular coupling: relays for subcortical vasoactive pathways. The Journal of Neuroscience 24:8940-8949.

Caviness VS. 1982. Neocortical histogenesis in normal and reeler mice: a developmental study based upon [3 H] thymidine autoradiography. Developmental Brain Research 4:293-302.

Chittajallu R, Pelkey KA, McBain CJ. 2013. Neurogliaform cells dynamically regulate somatosensory integration via synapse-specific modulation. Nat Neurosci 16:13-15.

Chmielowska J, Carvell GE, Simons DJ. 1989. Spatial organization of thalamocortical and corticothalamic projection systems in the rat SmI barrel cortex. J Comp Neurol 285:325-338.

Chu Z, Galarreta M, Hestrin S. 2003. Synaptic Interactions of Late-Spiking Neocortical Neurons in Layer 1. The Journal of Neuroscience 23:96.

Connors BW, Regehr WG. 1996. Neuronal firing: does function follow form? Current biology : CB 6:1560-1562.

Cruikshank SJ, Lewis TJ, Connors BW. 2007. Synaptic basis for intense thalamocortical activation of feedforward inhibitory cells in neocortex. Nat Neurosci 10:462-468.

Cruikshank SJ, Urabe H, Nurmikko AV, Connors BW. 2010. Pathway-specific feedforward circuits between thalamus and neocortex revealed by selective optical stimulation of axons. Neuron 65:230-245.

Daw MI, Ashby MC, Isaac JT. 2007. Coordinated developmental recruitment of latent fast spiking interneurons in layer IV barrel cortex. Nat Neurosci 10:453-461.

de Winter JCF. 2013. Using the Student's t-test with extremely small sample sizes. Practical Assessment, Research & Evaluation 18:1-12.

DeFelipe J, Lopez-Cruz PL, Benavides-Piccione R, Bielza C, Larranaga P, Anderson S, Burkhalter A, Cauli B, Fairen A, Feldmeyer D, Fishell G, Fitzpatrick D, Freund TF, Gonzalez-Burgos G, Hestrin S, Hill S, Hof PR, Huang J, Jones EG, Kawaguchi Y, Kisvarday Z, Kubota Y, Lewis DA, Marin O, Markram H, McBain CJ, Meyer HS, Monyer H, Nelson SB, Rockland K, Rossier J, Rubenstein JL, Rudy B, Scanziani M, Shepherd GM, Sherwood CC, Staiger JF, Tamas G, Thomson A, Wang Y, Yuste R, Ascoli GA. 2013. New insights into the classification and nomenclature of cortical GABAergic interneurons. Nat Rev Neurosci 14:202-216.

Derdikman D, Hildesheim R, Ahissar E, Arieli A, Grinvald A. 2003. Imaging spatiotemporal dynamics of surround inhibition in the barrels somatosensory cortex. J Neurosci 23:3100-3105.

Diamond ME, von Heimendahl M, Knutsen PM, Kleinfeld D, Ahissar E. 2008. 'Where' and 'what' in the whisker sensorimotor system. Nat Rev Neurosci 9:601-612.

Dodson PD, Barker MC, Forsythe ID. 2002. Two heteromeric Kv1 potassium channels differentially regulate action potential firing. The Journal of neuroscience 22:6953-6961.

Dodt H-U, Zieglgänsberger W. 1990. Visualizing unstained neurons in living brain slices by infrared DIC-videomicroscopy. Brain research 537:333-336.

Ebara S, Kumamoto K, Matsuura T, Mazurkiewicz JE, Rice FL. 2002. Similarities and differences in the innervation of mystacial vibrissal follicle-sinus complexes in the rat and cat: a confocal microscopic study. J Comp Neurol 449:103-119.

Encha-Razavi Fr, Sonigo P. 2003. Features of the developing brain. Child's Nervous System 19:426-428.

Feldman DE, Brecht M. 2005. Map plasticity in somatosensory cortex. Science 310:810-815.

Feldmeyer D, Brecht M, Helmchen F, Petersen CC, Poulet JF, Staiger JF, Luhmann HJ, Schwarz C. 2013. Barrel cortex function. Prog Neurobiol 103:3-27.

Feldmeyer D, Egger V, Lubke J, Sakmann B. 1999. Reliable synaptic connections between pairs of excitatory layer 4 neurones within a single 'barrel' of developing rat somatosensory cortex. J Physiol 521 Pt 1:169-190.

Feldmeyer D, Lübke JHR. 2010. New aspects of axonal structure and function: Springer.

Feldmeyer D, Radnikow G. 2016. Paired Recordings from Synaptically Coupled Neurones in Acute Neocortical Slices. In: Korngreen A, editor. Advanced Patch-Clamp Analysis for Neuroscientists New York, NY: Springer New York p 171-191.

Fish JL, Dehay C, Kennedy H, Huttner WB. 2008. Making bigger brains - the evolution of neural-progenitor-cell division. Journal of cell science 121:2783-2793.

Fishell G. 1997. Regionalization in the mammalian telencephalon. Curr Opin Neurobiol 7:62-69.

Fu Y, Tucciarone JM, Espinosa JS, Sheng N, Darcy DP, Nicoll RA, Huang ZJ, Stryker MP. 2014. A cortical circuit for gain control by behavioral state. Cell 156:1139-1152.

Fuzik J, Zeisel A, Mate Z, Calvigioni D, Yanagawa Y, Szabo G, Linnarsson S, Harkany T. 2016. Integration of electrophysiological recordings with single-cell RNA-seq data identifies neuronal subtypes. Nat Biotech 34:175-183.

Gelman DM, Marin O. 2010. Generation of interneuron diversity in the mouse cerebral cortex. European Journal of Neuroscience 31:2136-2141.

Gelman DM, Martini FJ, Nobrega-Pereira S, Pierani A, Kessaris N, Marin O. 2009. The embryonic preoptic area is a novel source of cortical GABAergic interneurons. The Journal of Neuroscience 29:9380-9389.

Gibson JR, Beierlein M, Connors BW. 1999. Two networks of electrically coupled inhibitory neurons in neocortex. Nature 402:75-79.

Gonzalez-Burgos G, Cho RY, Lewis DA. 2015. Alterations in cortical network oscillations and parvalbumin neurons in schizophrenia. Biol Psychiatry 77:1031-1040.

Guillemot F. 2005. Cellular and molecular control of neurogenesis in the mammalian telencephalon. Current opinion in cell biology 17:639-647.

Gupta A, Wang Y, Markram H. 2000. Organizing principles for a diversity of GABAergic interneurons and synapses in the neocortex. Science 287:273-278.

Halabisky B, Shen F, Huguenard JR, Prince DA. 2006. Electrophysiological classification of somatostatin-positive interneurons in mouse sensorimotor cortex. J Neurophysiol 96:834-845.

Hamill OP, Marty A, Neher E, Sakmann B, Sigworth FJ. 1981. Improved patch-clamp techniques for high-resolution current recording from cells and cell-free membrane patches. Pflügers Archiv 391:85-100.

Hansen DV, Lui JH, Parker PRL, Kriegstein AR. 2010. Neurogenic radial glia in the outer subventricular zone of human neocortex. Nature 464:554-561.

Haubensak W, Attardo A, Denk W, Huttner WB. 2004. Neurons arise in the basal neuroepithelium of the early mammalian telencephalon: a major site of neurogenesis. Proc Natl Acad Sci U S A 101:3196-3201.

Helmstaedter M, Sakmann B, Feldmeyer D. 2009a. L2/3 interneuron groups defined by multiparameter analysis of axonal projection, dendritic geometry, and electrical excitability. Cereb Cortex 19:951-962.

Helmstaedter M, Sakmann B, Feldmeyer D. 2009b. Neuronal correlates of local, lateral, and translaminar inhibition with reference to cortical columns. Cereb Cortex 19:926-937.

Helmstaedter M, Sakmann B, Feldmeyer D. 2009c. The relation between dendritic geometry, electrical excitability, and axonal projections of L2/3 interneurons in rat barrel cortex. Cereb Cortex 19:938-950.

Henderson TA, Jacquin MF. 1995. What makes subcortical barrels. In: Jones EG, Peters A, Diamond IT, editors. Cerebral cortex, The barrel cortex of rodents New York; London: Plenum p 123-187.

Hevner RF, Daza RAM, Rubenstein JLR, Stunnenberg H, Olavarria JF, Englund C. 2003. Beyond laminar fate: toward a molecular classification of cortical projection/pyramidal neurons. Developmental neuroscience 25:139-151.

Hodgkin AL, Huxley AF. 1952. A quantitative description of membrane current and its application to conduction and excitation in nerve. J Physiol 117:500.

Horikawa K, Armstrong WE. 1988. A versatile means of intracellular labeling: injection of biocytin and its detection with avidin conjugates. Journal of neuroscience methods 25:1-11.

Horton JC, Adams DL. 2005. The cortical column: a structure without a function. Philos Trans R Soc Lond B Biol Sci 360:837-862.

Hu H, Ma Y, Agmon A. 2011. Submillisecond firing synchrony between different subtypes of cortical interneurons connected chemically but not electrically. The Journal of Neuroscience 31:3351-3361.

Inan M, Crair MC. 2007. Development of cortical maps: perspectives from the barrel cortex. The Neuroscientist 13:49-61.

Janušonis S. 2009. Comparing two small samples with an unstable, treatment-independent baseline. Journal of neuroscience methods 179:173-178.

Jiang X, Lachance M, Rossignol E. 2016. Involvement of cortical fast-spiking parvalbumin-positive basket cells in epilepsy. Progress in Brain Research.

Jiang X, Shen S, Cadwell CR, Berens P, Sinz F, Ecker AS, Patel S, Tolias AS. 2015. Principles of connectivity among morphologically defined cell types in adult neocortex. Science 350:aac9462.

Jones HE, Grieve KL, Wang W, Sillito AM. 2001. Surround suppression in primate V1. J Neurophysiol 86:2011-2028.

Kaas, Krubitzer. 1991. The organization of extrastriate visual cortex. In: Robinson BDaSR, editor. Vision and visual dysfunction London: Macmillan press p 302-323.

Kalanithi PS, Zheng W, Kataoka Y, DiFiglia M, Grantz H, Saper CB, Schwartz ML, Leckman JF, Vaccarino FM. 2005. Altered parvalbumin-positive neuron distribution in basal ganglia of individuals with Tourette syndrome. Proc Natl Acad Sci U S A 102:13307-13312.

Kandel ER. 2013. Principles of neural science. New York: McGraw-Hill.

Karagiannis A, Gallopin T, David C, Battaglia D, Geoffroy H, Rossier J, Hillman EM, Staiger JF, Cauli B. 2009. Classification of NPY-expressing neocortical interneurons. J Neurosci 29:3642-3659.

Kaufmann WE, Moser HW. 2000. Dendritic anomalies in disorders associated with mental retardation. Cereb Cortex 10:981-991.

Kawaguchi Y. 1995. Physiological subgroups of nonpyramidal cells with specific morphological characteristics in layer II/III of rat frontal cortex. J Neurosci 15:2638-2655.

Kawaguchi Y, Kondo S. 2002. Parvalbumin, somatostatin and cholecystokinin as chemical markers for specific GABAergic interneuron types in the rat frontal cortex. J Neurocytol 31:277-287.

Kawaguchi Y, Kubota Y. 1997. GABAergic cell subtypes and their synaptic connections in rat frontal cortex. Cereb Cortex 7:476-486.

Kawaguchi Y, Wilson CJ, Emson PC. 1989. Intracellular recording of identified neostriatal patch and matrix spiny cells in a slice preparation preserving cortical inputs. J Neurophysiol 62:1052-1068.

Klausberger T, Somogyi P. 2008. Neuronal diversity and temporal dynamics: the unity of hippocampal circuit operations. Science 321:53-57.

Koelbl C, Helmstaedter M, Lubke J, Feldmeyer D. 2015. A barrel-related interneuron in layer 4 of rat somatosensory cortex with a high intrabarrel connectivity. Cereb Cortex 25:713-725.

Kowalczyk T, Pontious A, Englund C, Daza RAM, Bedogni F, Hodge R, Attardo A, Bell C, Huttner WB, Hevner RF. 2009. Intermediate neuronal progenitors (basal progenitors) produce pyramidal-projection neurons for all layers of cerebral cortex. Cereb Cortex 19:2439-2450.

Kowalczyk T, Pontious A, Englund C, Daza RAM, Bedogni F, Hodge R, Attardo A, Bell C, Huttner WB, Hevner RF. 2009. Intermediate neuronal progenitors (basal progenitors) produce pyramidal,Äìprojection Neurons for all layers of cerebral cortex. Cereb Cortex 19:2439-2450.

Kriegstein AR, Noctor SC. 2004. Patterns of neuronal migration in the embryonic cortex. Trends Neurosci 27:392-399.

Laaris N, Keller A. 2002. Functional independence of layer IV barrels. J Neurophysiol 87:1028-1034.

Land PW, Erickson SL. 2005. Subbarrel domains in rat somatosensory (S1) cortex. J Comp Neurol 490:414-426.

Lazarus MS, Huang ZJ. 2011. Distinct maturation profiles of perisomatic and dendritic targeting GABAergic interneurons in the mouse primary visual cortex during the critical period of ocular dominance plasticity. J Neurophysiol 106:775-787.

Lee S, Hjerling-Leffler J, Zagha E, Fishell G, Rudy B. 2010. The largest group of superficial neocortical GABAergic interneurons expresses ionotropic serotonin receptors. J Neurosci 30:16796-16808.

Lee S, Kruglikov I, Huang ZJ, Fishell G, Rudy B. 2013. A disinhibitory circuit mediates motor integration in the somatosensory cortex. Nat Neurosci 16:1662-1670.

Lewis DA, Fish KN, Arion D, Gonzalez-Burgos G. 2011. Perisomatic inhibition and cortical circuit dysfunction in schizophrenia. Curr Opin Neurobiol 21:866-872.

Llinas RR. 1988. The intrinsic electrophysiological properties of mammalian neurons: insights into central nervous system function. Science 242:1654-1664.

Lodato S, Arlotta P. 2015. Generating neuronal diversity in the mammalian cerebral cortex. Annu Rev Cell Dev Biol 31:699-720.

Loukas M, Pennell C, Groat C, Tubbs RS, Cohen-Gadol AA. 2011. Korbinian Brodmann (1868-1918) and his contributions to mapping the cerebral cortex. Neurosurgery 68:6-11; discussion 11.

Lu S-M, Lin RCS. 1993. Thalamic Afferents of the Rat Barrel Cortex: A Light-and Electron-Microscopic Study Using Phaseolus vulgaris Leucoagglutinin as an Anterograde Tracer. Somatosensory & Motor Research 10:1-16.

Lubke J, Egger V, Sakmann B, Feldmeyer D. 2000. Columnar organization of dendrites and axons of single and synaptically coupled excitatory spiny neurons in layer 4 of the rat barrel cortex. J Neurosci 20:5300-5311.

Luna B, Minshew NJ, Garver KE, Lazar NA, Thulborn KR, Eddy WF, Sweeney JA. 2002. Neocortical system abnormalities in autism An fMRI study of spatial working memory. Neurology 59:834-840.

Ma PM, Woolsey TA. 1984. Cytoarchitectonic correlates of the vibrissae in the medullary trigeminal complex of the mouse. Brain research 306:374-379.

Ma Y, Hu H, Agmon A. 2012. Short-term plasticity of unitary inhibitory-to-inhibitory synapses depends on the presynaptic interneuron subtype. J Neurosci 32:983-988.

Ma Y, Hu H, Berrebi AS, Mathers PH, Agmon A. 2006. Distinct subtypes of somatostatin-containing neocortical interneurons revealed in transgenic mice. J Neurosci 26:5069-5082.

Mainen ZF, Sejnowski TJ. 1996. Influence of dendritic structure on firing pattern in model neocortical neurons. Nature 382:363-366.

Marin O, Rubenstein JLR. 2001. A long, remarkable journey: tangential migration in the telencephalon. Nature Reviews Neuroscience 2:780-790.

Marin O, Rubenstein JLR. 2003. Cell migration in the forebrain. Annu Rev Neurosci 26:441-483.

Marin-Padilla M. 1971. Early prenatal ontogenesis of the cerebral cortex (neocortex) of the cat (Felis domestica). A Golgi study. Zeitschrift fuer Anatomie und Entwicklungsgeschichte 134:117-145.

Marin-Padilla M. 1998. Cajal-Retzius cells and the development of the neocortex. Trends Neurosci 21:64-71.

Markram H, Toledo-Rodriguez M, Wang Y, Gupta A, Silberberg G, Wu C. 2004. Interneurons of the neocortical inhibitory system. Nat Rev Neurosci 5:793-807.

Markram H, Wang Y, Tsodyks M. 1998. Differential signaling via the same axon of neocortical pyramidal neurons. Proceedings of the National Academy of Sciences 95:5323-5328.

Marx M, Gunter RH, Hucko W, Radnikow G, Feldmeyer D. 2012. Improved biocytin labeling and neuronal 3D reconstruction. Nat Protoc 7:394-407.

McBain CJ, Fisahn A. 2001. Interneurons unbound. Nat Rev Neurosci 2:11-23.

McGarry LM, Packer AM, Fino E, Nikolenko V, Sippy T, Yuste R. 2010. Quantitative classification of somatostatin-positive neocortical interneurons identifies three interneuron subtypes. Front Neural Circuits 4:12.

Merchant H, de Lafuente V, Pena-Ortega F, Larriva-Sahd J. 2012. Functional impact of interneuronal inhibition in the cerebral cortex of behaving animals. Prog Neurobiol 99:163-178.

Meyer HS, Schwarz D, Wimmer VC, Schmitt AC, Kerr JN, Sakmann B, Helmstaedter M. 2011. Inhibitory interneurons in a cortical column form hot zones of inhibition in layers 2 and 5A. Proc Natl Acad Sci U S A 108:16807-16812.

Miller MN, Okaty BW, Nelson SB. 2008. Region-specific spike-frequency acceleration in layer 5 pyramidal neurons mediated by Kv1 subunits. J Neurosci 28:13716-13726.

Minnery BS, Simons DJ. 2003. Response properties of whisker-associated trigeminothalamic neurons in rat nucleus principalis. J Neurophysiol 89:40-56.

Mountcastle V. 1995. The evolution of ideas concerning the function of the neocortex. Cereb Cortex 5:289-295.

Mountcastle VB. 1957. Modality and topographic properties of single neurons of cat's somatic sensory cortex. J Neurophysiol 20:408-434.

Mueller SG, Laxer KD, Barakos J, Cheong I, Garcia P, Weiner MW. 2009. Widespread neocortical abnormalities in temporal lobe epilepsy with and without mesial sclerosis. Neuroimage 46:353-359.

Muralidhar S, Wang Y, Markram H. 2013. Synaptic and cellular organization of layer 1 of the developing rat somatosensory cortex. Front Neuroanat 7:52.

Nadarajah B, Parnavelas JG. 2002. Modes of neuronal migration in the developing cerebral cortex. Nature Reviews Neuroscience 3:423-432.

Neher E, Sakmann B, Steinbach JH. 1978. The extracellular patch clamp: a method for resolving currents through individual open channels in biological membranes. Pflügers Archiv 375:219-228.

Nieuwenhuys R, Donkelaar HJt, Nicholson C. 1998. The central nervous system of vertebrates. Berlin; New York: Springer.

Nissl F. 1894. Ueber eine neue Untersuchungsmethode des Centralorgans zur Feststellung der Localisation der Nervenzellen. Neurologisches Centralblatt 13:507-508.

Noctor SC, Martinez-Cerdeno V, Ivic L, Kriegstein AR. 2004. Cortical neurons arise in symmetric and asymmetric division zones and migrate through specific phases. Nat Neurosci 7:136-144.

Northcutt RG, Kaas JH. 1995. The emergence and evolution of mammalian neocortex. Trends Neurosci 18:373-379.

Oberlaender M, Boudewijns ZS, Kleele T, Mansvelder HD, Sakmann B, de Kock CP. 2011. Three-dimensional axon morphologies of individual layer 5 neurons indicate cell type-specific intracortical pathways for whisker motion and touch. Proc Natl Acad Sci U S A 108:4188-4193.

Ohno S, Kuramoto E, Furuta T, Hioki H, Tanaka YR, Fujiyama F, Sonomura T, Uemura M, Sugiyama K, Kaneko T. 2012. A morphological analysis of thalamocortical axon fibers of rat posterior thalamic nuclei: a single neuron tracing study with viral vectors. Cereb Cortex 22:2840-2857.

Olah S, Fule M, Komlosi G, Varga C, Baldi R, Barzo P, Tamas G. 2009. Regulation of cortical microcircuits by unitary GABA-mediated volume transmission. Nature 461:1278-1281.

Oláh S, Komlósi G, Szabadics J, Varga C, Tóth É, Barzó P, Tamás G. 2007. Output of neurogliaform cells to various neuron types in the human and rat cerebral cortex. Front Neural Circuits 1:4.

Parnavelas JG. 2000. The origin and migration of cortical neurones: new vistas. Trends Neurosci 23:126-131.

Pellegri G, Magistretti PJ, Martin JL. 1998. VIP and PACAP potentiate the action of glutamate on BDNF expression in mouse cortical neurones. European Journal of Neuroscience 10:272-280.

Perrenoud Q, Rossier J, Geoffroy H, Vitalis T, Gallopin T. 2013. Diversity of GABAergic interneurons in layer VIa and VIb of mouse barrel cortex. Cereb Cortex 23:423-441.

Peters A, Kaiserman-Abramof IR. 1970. The small pyramidal neuron of the rat cerebral cortex. The perikaryon, dendrites and spines. American Journal of Anatomy 127:321-355.

Petersen CC, Sakmann B. 2001. Functionally independent columns of rat somatosensory barrel cortex revealed with voltage-sensitive dye imaging. J Neurosci 21:8435-8446.

Petersen CCH. 2007. The functional organization of the barrel cortex. Neuron 56:339-355.

Pierret T, Lavallee P, Deschenes M. 2000. Parallel streams for the relay of vibrissal information through thalamic barreloids. J Neurosci 20:7455-7462.

Porter JT, Cauli B, Staiger JF, Lambolez B, Rossier J, Audinat E. 1998. Properties of bipolar VIPergic interneurons and their excitation by pyramidal neurons in the rat neocortex. The European journal of neuroscience 10:3617-3628.

Porter JT, Johnson CK, Agmon A. 2001. Diverse types of interneurons generate thalamus-evoked feedforward inhibition in the mouse barrel cortex. J Neurosci 21:2699-2710.

Pronneke A, Scheuer B, Wagener RJ, Mock M, Witte M, Staiger JF. 2015. Characterizing VIP Neurons in the Barrel Cortex of VIPcre/tdTomato Mice Reveals Layer-Specific Differences. Cereb Cortex 25:4854-4868.

Qi G, Radnikow G, Feldmeyer D. 2015. Electrophysiological and morphological characterization of neuronal microcircuits in acute brain slices using paired patch-clamp recordings. JoVE (Journal of Visualized Experiments):e52358-e52358.

Qiu S, Luo S, Evgrafov O, Li R, Schroth GP, Levitt P, Knowles JA, Wang K. 2012. Single-neuron RNA-Seq: technical feasibility and reproducibility. Frontiers in genetics 3:124.

Rakic P. 1974. Neurons in rhesus monkey visual cortex: systematic relation between time of origin and eventual disposition. Science 183:425-427.

Rakic P. 1990. Principles of neural cell migration. Experientia 46:882-891.

Regehr WG. 2012. Short-Term Presynaptic Plasticity. Cold Spring Harbor Perspectives in Biology 4:a005702-a005702.

Regehr WG. 2012. Short-term presynaptic plasticity. Cold Spring Harbor perspectives in biology 4:a005702.

Reyes A, Lujan R, Rozov A, Burnashev N, Somogyi P, Sakmann B. 1998. Target-cell-specific facilitation and depression in neocortical circuits. Nat Neurosci 1:279-285.

Rousseeuw PJ. 1987. Silhouettes: A graphical aid to the interpretation and validation of cluster analysis. Journal of Computational and Applied Mathematics 20:53-65.

Rudy B, Fishell G, Lee S, Hjerling-Leffler J. 2011. Three groups of interneurons account for nearly 100% of neocortical GABAergic neurons. Dev Neurobiol 71:45-61.

Sachdev RN, Krause MR, Mazer JA. 2012. Surround suppression and sparse coding in visual and barrel cortices. Front Neural Circuits 6:43.

Sakmann B, Neher E. 1984. Patch clamp techniques for studying ionic channels in excitable membranes. Annual review of physiology 46:455-472.

Santana R, McGarry L, Bielza C, Larrañaga P, Yuste R. 2013. Classification of neocortical interneurons using affinity propagation. Front Neural Circuits 7:185.

Simons DJ, Woolsey TA. 1984. Morphology of Golgi-Cox-impregnated barrel neurons in rat SmI cortex. Journal of Comparative Neurology 230:119-132.

Smart IH. 2008. Evolution, development, and initial function of the mammalian neocortex: response of the germinal zones to endothermy. Anat Rec (Hoboken) 291:28-48.

Smith MA. 2006. Surround suppression in the early visual system. The Journal of neuroscience 26:3624-3625.

Staiger JF, Zuschratter W, Luhmann HJ, Schubert D. 2009. Local circuits targeting parvalbumin-containing interneurons in layer IV of rat barrel cortex. Brain Structure and Function 214:1.

Stuart GJ, Dodt HU, Sakmann B. 1993. Patch-clamp recordings from the soma and dendrites of neurons in brain slices using infrared video microscopy. Pflügers Archiv 423:511-518.

Sultan KT, Brown KN, Shi S-H. 2013. Production and organization of neocortical interneurons. Front Cell Neurosci 7:221.

Sun QQ, Huguenard JR, Prince DA. 2006. Barrel cortex microcircuits: thalamocortical feedforward inhibition in spiny stellate cells is mediated by a small number of fast-spiking interneurons. J Neurosci 26:1219-1230.

Tabuchi K, Blundell J, Etherton MR, Hammer RE, Liu X, Powell CM, Sudhof TC. 2007. A neuroligin-3 mutation implicated in autism increases inhibitory synaptic transmission in mice. Science 318:71-76.

Tamas G, Lorincz A, Simon A, Szabadics J. 2003. Identified sources and targets of slow inhibition in the neocortex. Science 299:1902-1905.

Taniguchi H, He M, Wu P, Kim S, Paik R, Sugino K, Kvitsiani D, Fu Y, Lu J, Lin Y, Miyoshi G, Shima Y, Fishell G, Nelson SB, Huang ZJ. 2011. A resource of Cre driver lines for genetic targeting of GABAergic neurons in cerebral cortex. Neuron 71:995-1013.

Tasic B, Menon V, Nguyen TN, Kim TK, Jarsky T, Yao Z, Levi B, Gray LT, Sorensen SA, Dolbeare T, Bertagnolli D, Goldy J, Shapovalova N, Parry S, Lee C, Smith K, Bernard A, Madisen L, Sunkin SM, Hawrylycz M, Koch C, Zeng H. 2016. Adult mouse cortical cell taxonomy revealed by single cell transcriptomics. Nat Neurosci 19:335-346.

Taverna E, Goetz M, Huttner WB. 2014. The cell biology of neurogenesis: toward an understanding of the development and evolution of the neocortex. Annual review of cell and developmental biology 30:465-502.

Thomson AM. 1997. Activity-dependent properties of synaptic transmission at two classes of connections made by rat neocortical pyramidal axons in vitro. J Physiol 502:131-147.
Thomson AM. 2003. Presynaptic frequency-and pattern-dependent filtering. Journal of computational neuroscience 15:159-202.
Thorndike RL. 1953. Who belongs in the family? Psychometrika 18:267-276.
Urbain N, Deschenes M. 2007. Motor cortex gates vibrissal responses in a thalamocortical projection pathway. Neuron 56:714-725.
van der Loos H. 1976. Barreloids in mouse somatosensory thalamus. Neuroscience letters:1-6.
Vasistha NA, Garcia-Moreno F, Arora S, Cheung AFP, Arnold SJ, Robertson EJ, Molnar Z. 2014. Cortical and clonal contribution of Tbr2 expressing progenitors in the developing mouse brain. Cereb Cortex:bhu125.
Veinante P, Deschenes M. 1999. Single- and multi-whisker channels in the ascending projections from the principal trigeminal nucleus in the rat. J Neurosci 19:5085-5095.
Veinante P, Jacquin MF, Deschenes M. 2000. Thalamic projections from the whisker-sensitive regions of the spinal trigeminal complex in the rat. Journal of Comparative Neurology 420:233-243.
Vucurovic K, Gallopin T, Ferezou I, Rancillac A, Chameau P, van Hooft JA, Geoffroy H, Monyer H, Rossier J, Vitalis T. 2010. Serotonin 3A receptor subtype as an early and protracted marker of cortical interneuron subpopulations. Cereb Cortex 20:2333-2347.
Wang G, Wyskiel DR, Yang W, Wang Y, Milbern LC, Lalanne T, Jiang X, Shen Y, Sun Q-Q, Zhu JJ. 2015. An optogenetics- and imaging-assisted simultaneous multiple patch-clamp recording system for decoding complex neural circuits. Nat Protocols 10:397-412.
Wang Z, Gerstein M, Snyder M. 2009. RNA-Seq: a revolutionary tool for transcriptomics. Nature reviews genetics 10:57-63.
Ward Jr JH. 1963. Hierarchical grouping to optimize an objective function. Journal of the American statistical association 58:236-244.
Weigert C. 1885. Eine vergesserung der Haematoxylin Blutlaugen-salzmethod fur das Centranlnervensystem. Fortschr Deutsch Med 3:236-239.
Welker C. 1976. Receptive fields of barrels in the somatosensory neocortex of the rat. J Comp Neurol 166:173-189.
Wimmer VC, Bruno RM, de Kock CP, Kuner T, Sakmann B. 2010. Dimensions of a projection column and architecture of VPM and POm axons in rat vibrissal cortex. Cereb Cortex 20:2265-2276.
Wonders CP, Anderson SA. 2006. The origin and specification of cortical interneurons. Nature Reviews Neuroscience 7:687-696.
Woodruff A, Xu Q, Anderson SA, Yuste R. 2009. Depolarizing effect of neocortical chandelier neurons. Front Neural Circuits 3:15.

Woolsey TA, van der Loos H. 1970. The structural organization of layer IV in the somatosensory region (S1) of mouse cerebral cortex. Brain research:205-242.

Wozny C, Williams SR. 2011. Specificity of synaptic connectivity between layer 1 inhibitory interneurons and layer 2/3 pyramidal neurons in the rat neocortex. Cereb Cortex 21:1818-1826.

Xu H, Jeong HY, Tremblay R, Rudy B. 2013. Neocortical somatostatin-expressing GABAergic interneurons disinhibit the thalamorecipient layer 4. Neuron 77:155-167.

Yu C, Derdikman D, Haidarliu S, Ahissar E. 2006. Parallel thalamic pathways for whisking and touch signals in the rat. PLoS Biol 4:e124.

Zeisel A, Munoz-Manchado AB, Codeluppi S, Lonnerberg P, La Manno G, Jureus A, Marques S, Munguba H, He L, Betsholtz C, Rolny C, Castelo-Branco G, Hjerling-Leffler J, Linnarsson S. 2015. Brain structure. Cell types in the mouse cortex and hippocampus revealed by single-cell RNA-seq. Science 347:1138-1142.

Zucker RS, Regehr WG. 2002. Short-term synaptic plasticity. Annual review of physiology 64:355-405.

Supplementary data

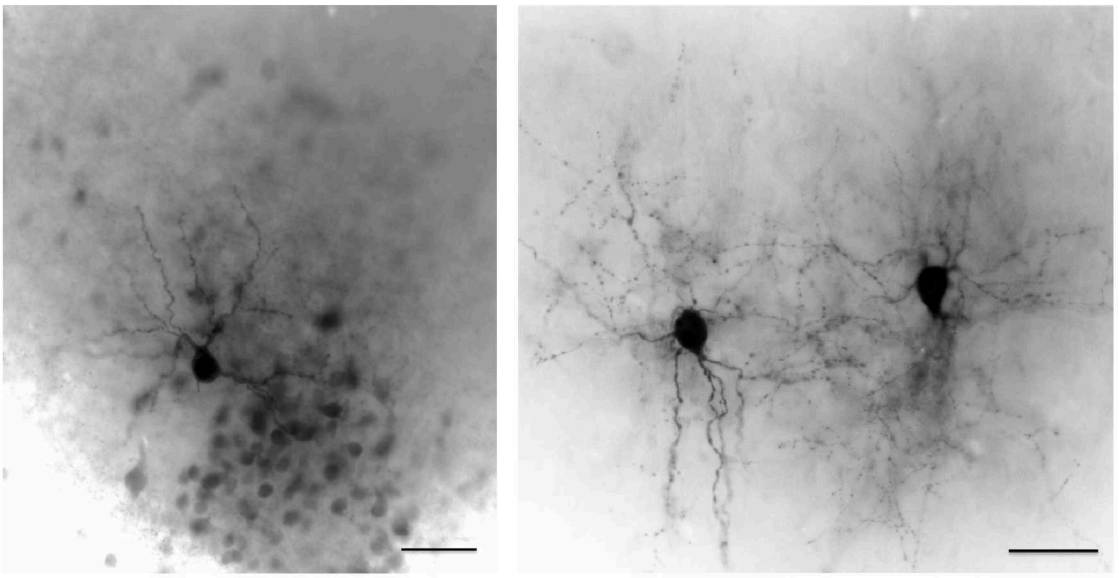

S.Fig.1. Examples of biocytin processed slices. *In order to have high quality reconstructions, we used only those slices with low background staining and clear labelling. Because of such stringent criteria, these two slices were not used for reconstruction. Scale bar - 50 μm.*

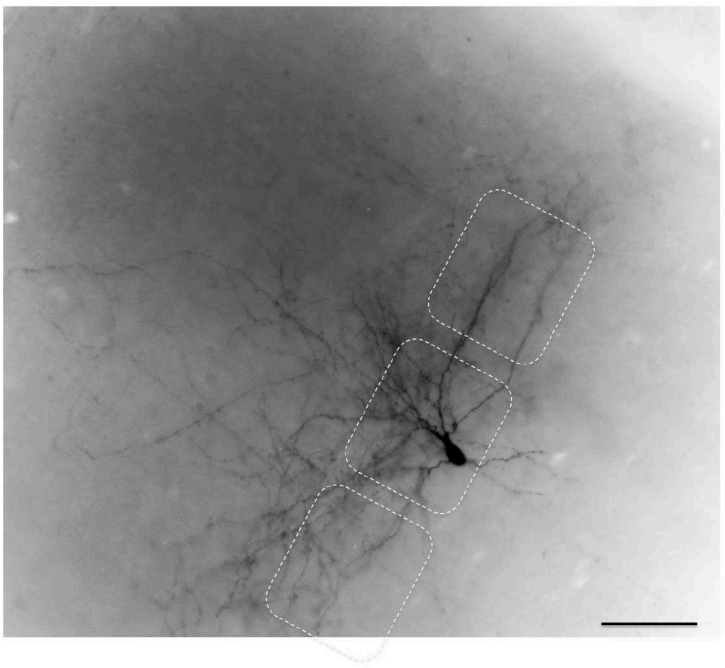

S.Fig.2. Example of high quality biocytin staining. *3D morphological reconstructions were performed on slices with high quality biocytin staining. Barrel borders were demarcated by overlapping the DIC image taken during patch-clamp recording. Note the axonal (thin lines) and dendritic (thick lines) projections to the neighbouring barrels. Scale bar - 100 μm.*

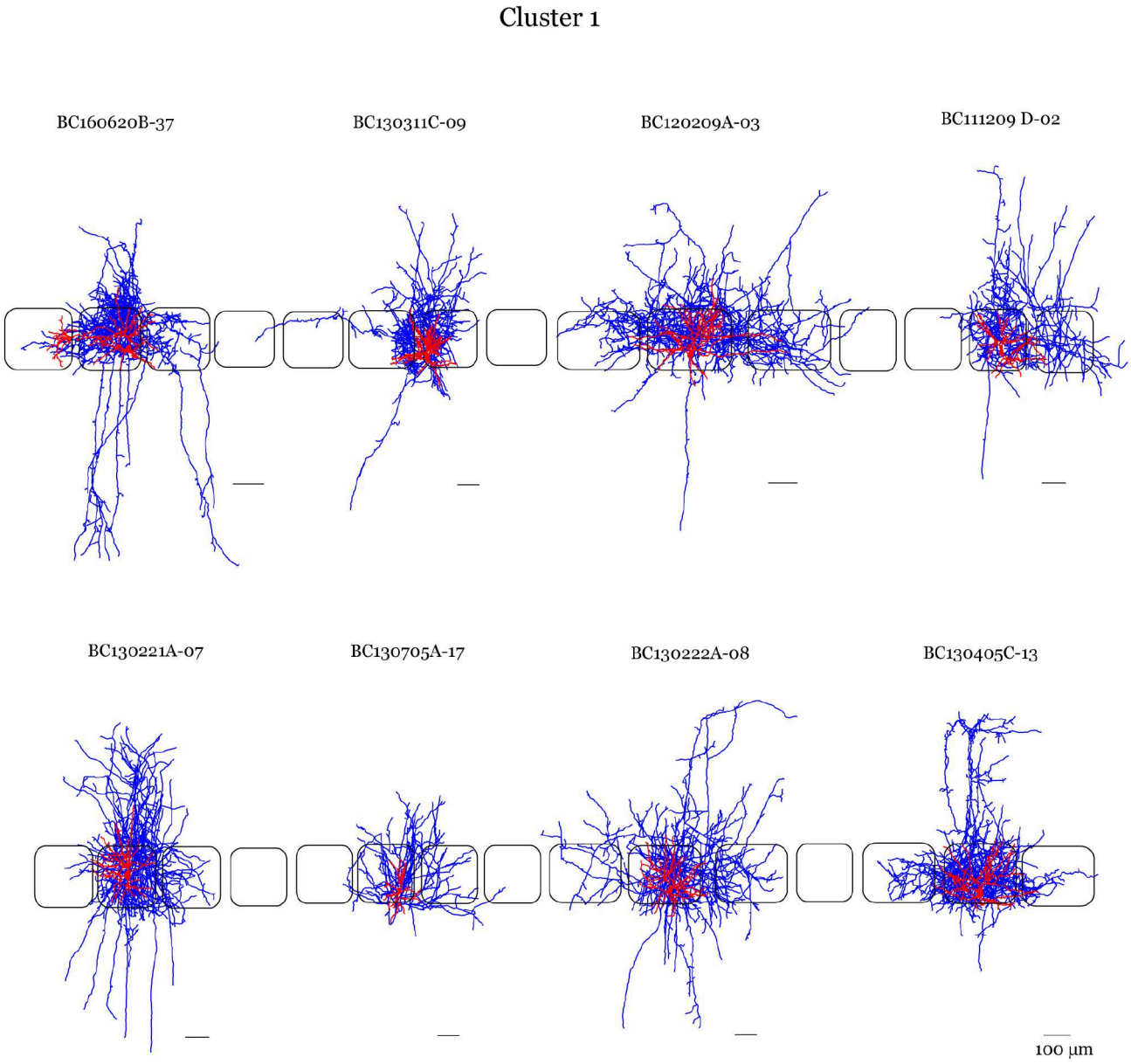

S.Fig.3. Morphological cluster 1 nFS interneurons. *Using hierarchical unsupervised cluster analysis based on morphological parameters, nFS interneurons in L4 of rat barrel cortex were classified into 3 distinct subtypes. Cluster 1 neurons with two sub-clusters - 1a (top) and 1b (bottom) are displayed here,. There were no significant difference between the two sub-clusters.*

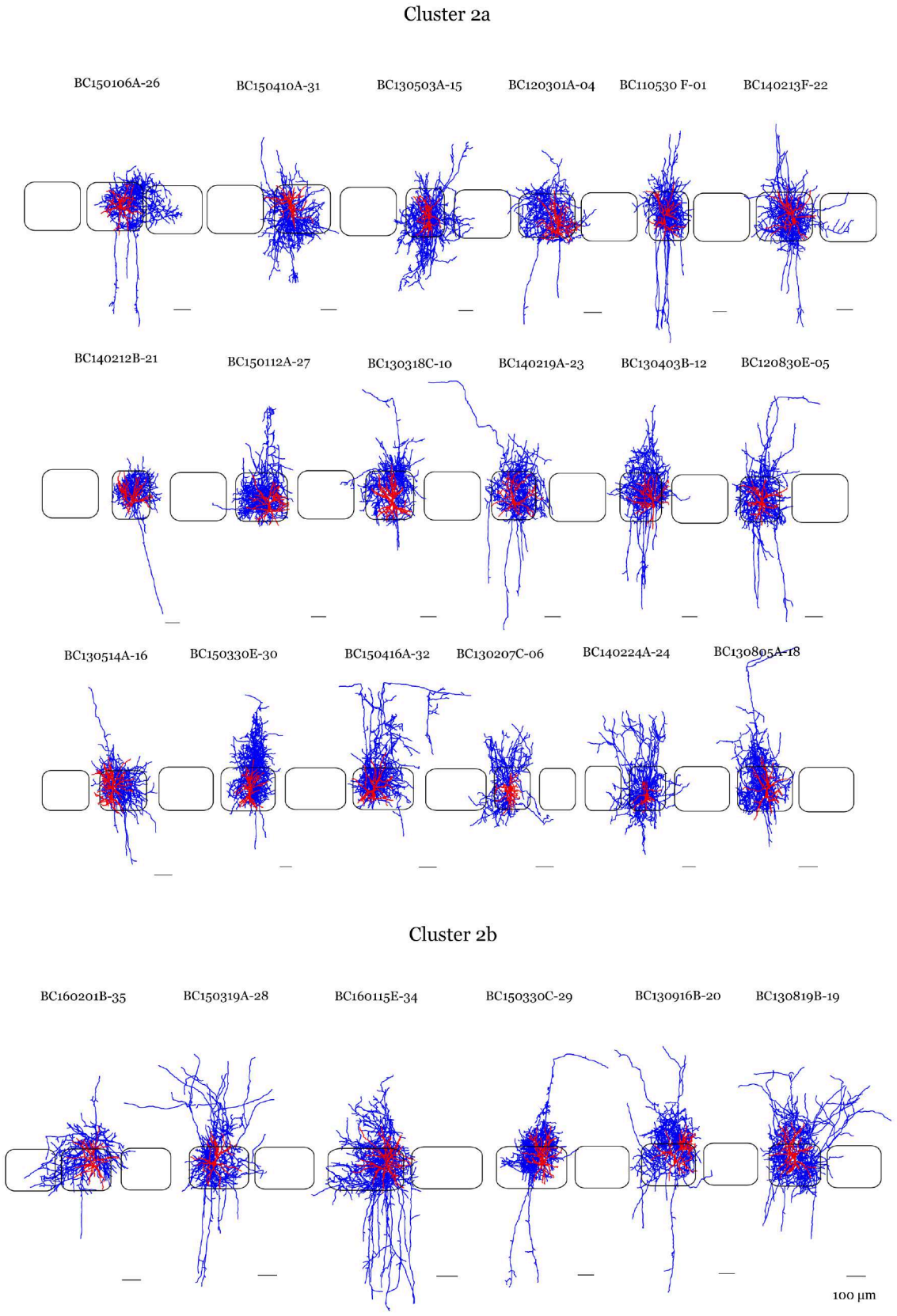

S.Fig.4. Morphological cluster 2 nFS interneurons. *Cluster 2 constitute the largest population with 24 interneurons, and was sub-divided into two clusters - 2a and 2b.*

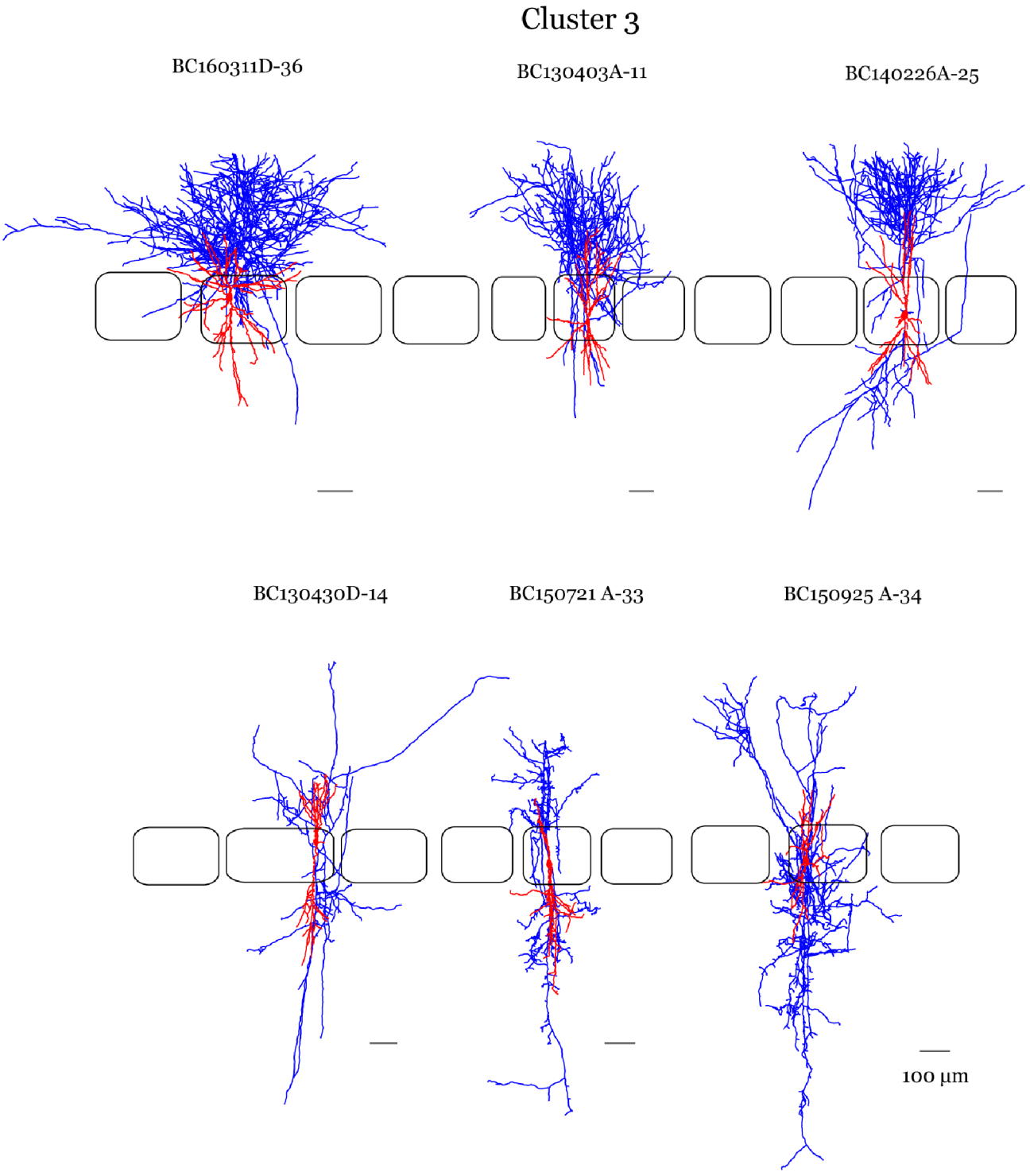

S.Fig.5. Morphological cluster 3 nFS interneurons. *Cluster 3 constitute the smallest population with 6 interneurons, and is sub-divided into two clusters - 3a and 3b. Cluster 3a showed dense supra-granular projections, whereas C3b showed sparse projections to the supra- and infra-granular layers.*

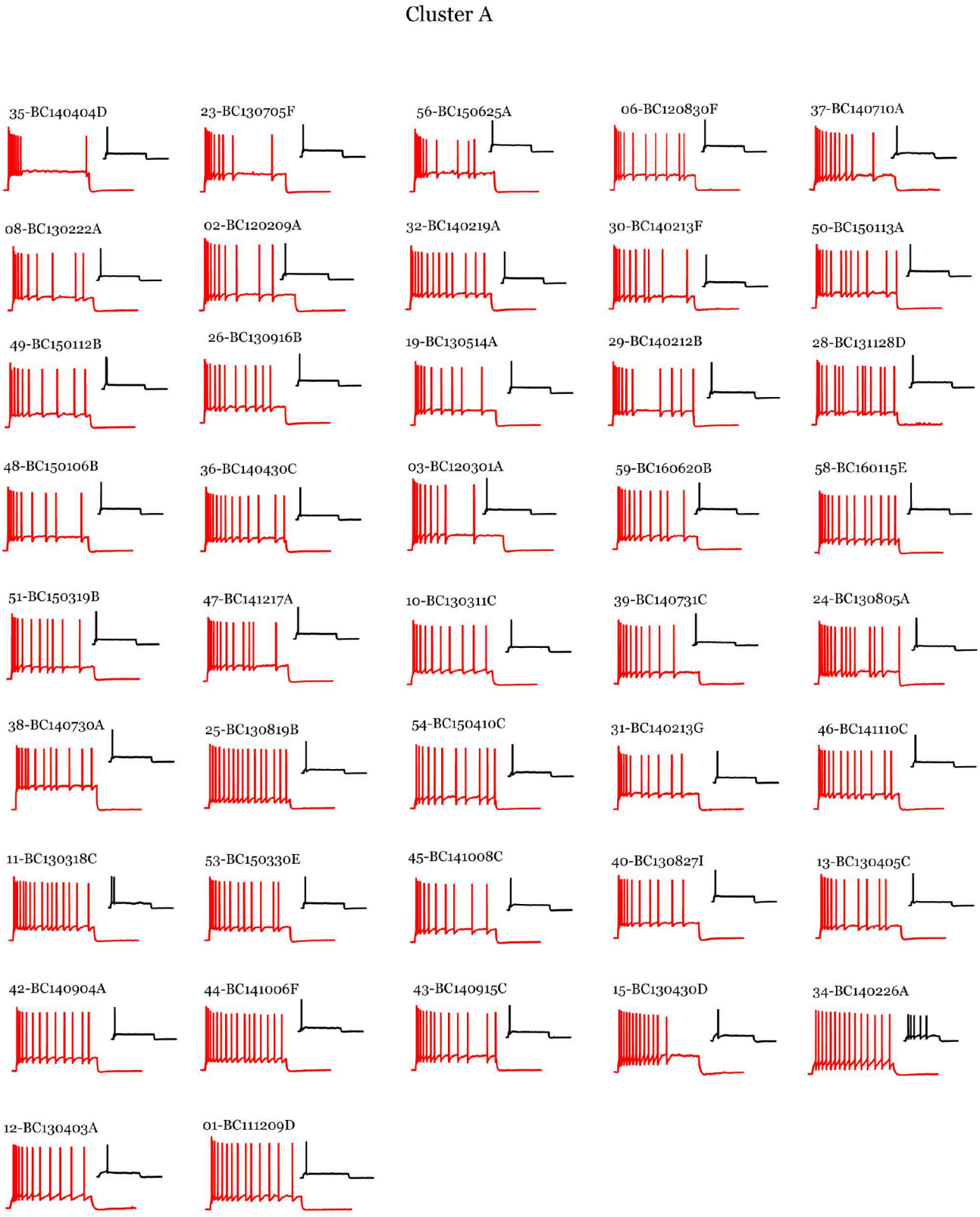

S.Fig.6. Electrophysiological classification of nFS interneurons. *Using hierarchical unsupervised cluster analysis based on electrophysiological parameters, nFS interneurons in L4 of rat barrel cortex were classified into 3 distinct subtypes. Cluster A neurons showed adapting irregular firing pattern.*

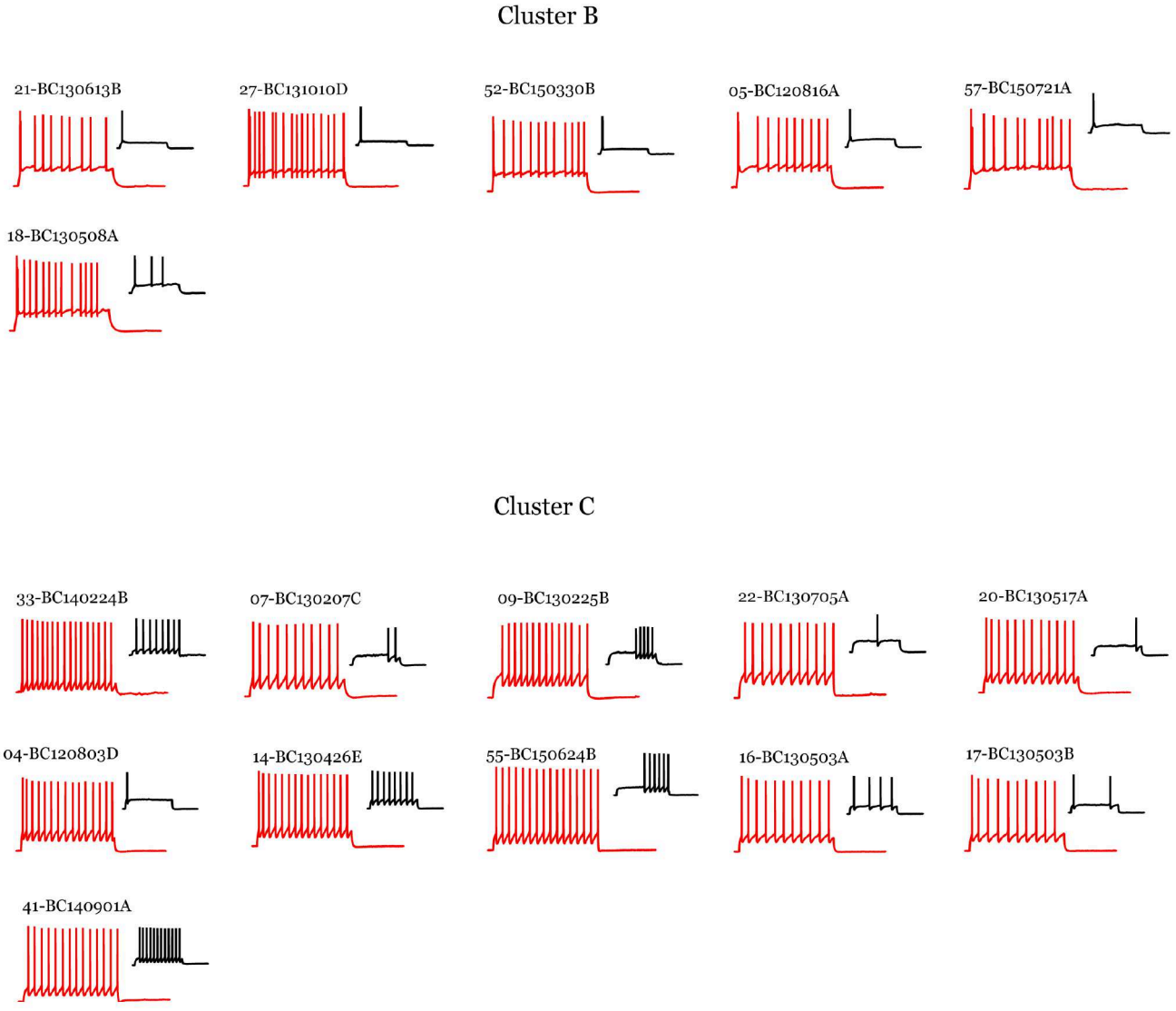

S.Fig.7. Electrophysiological classification of nFS interneurons. *Cluster B neurons displayed accelerating firing with irregular spiking pattern. Cluster C exhibited non-adapting regular spiking behaviour.*

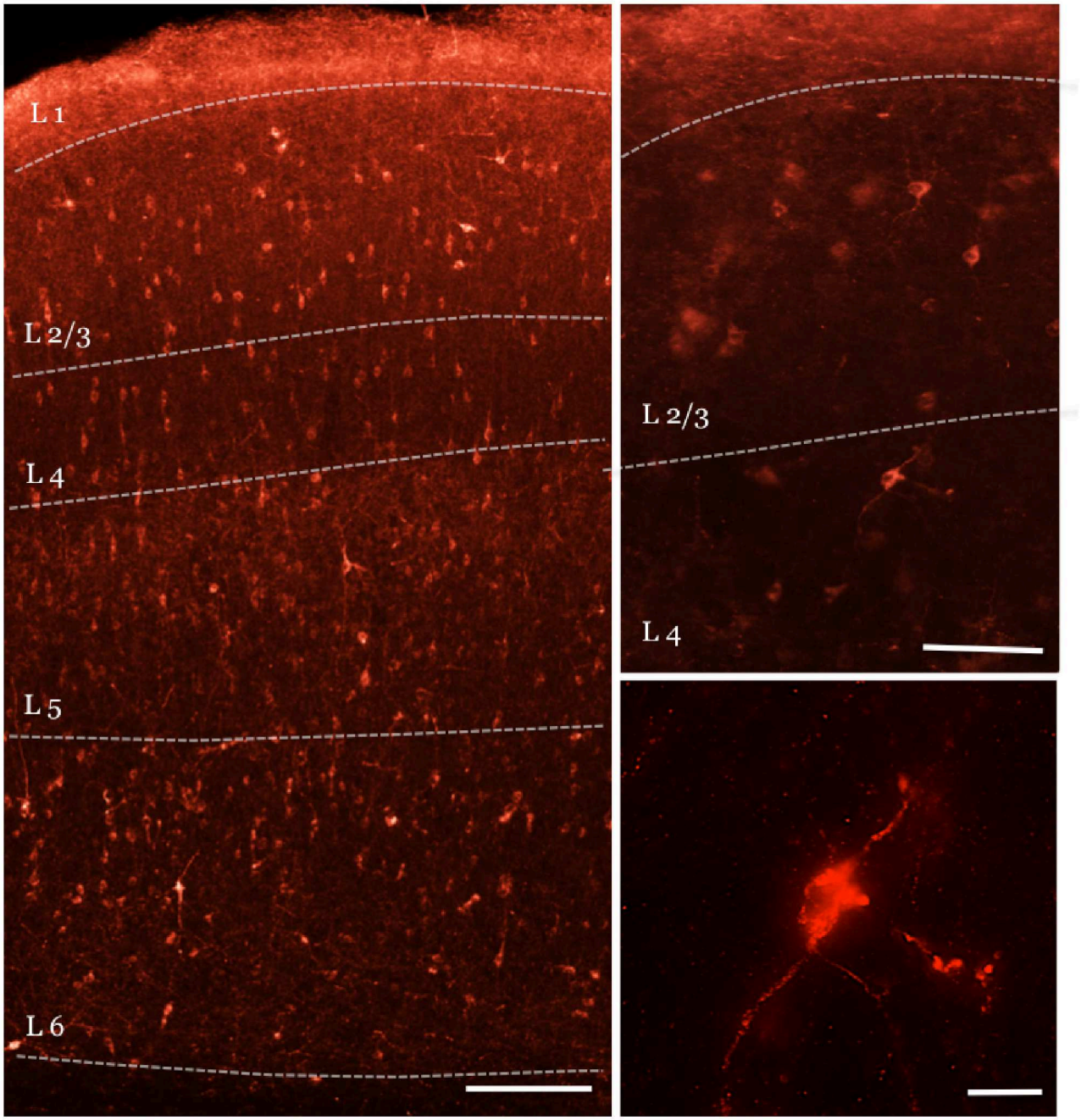

S.Fig.8. Distribution of SOM across different layers in rat barrel cortex. *Fluorescence images of SOM conjugated to Alexa Fluor® 594 acquired at different magnifications.* ***(Left)*** *An overview of SOM distributed through different layers at 40-fold magnification. Scale bar: 200 µm.* ***(Right, top)*** *100-fold magnification of the superficial layers showing differential distribution. Scale bar: 100 µm.* ***(Right, bottom)*** *A close view of L4 SOM positive neuron with dendritic processes Scale bar: 25 µm.*

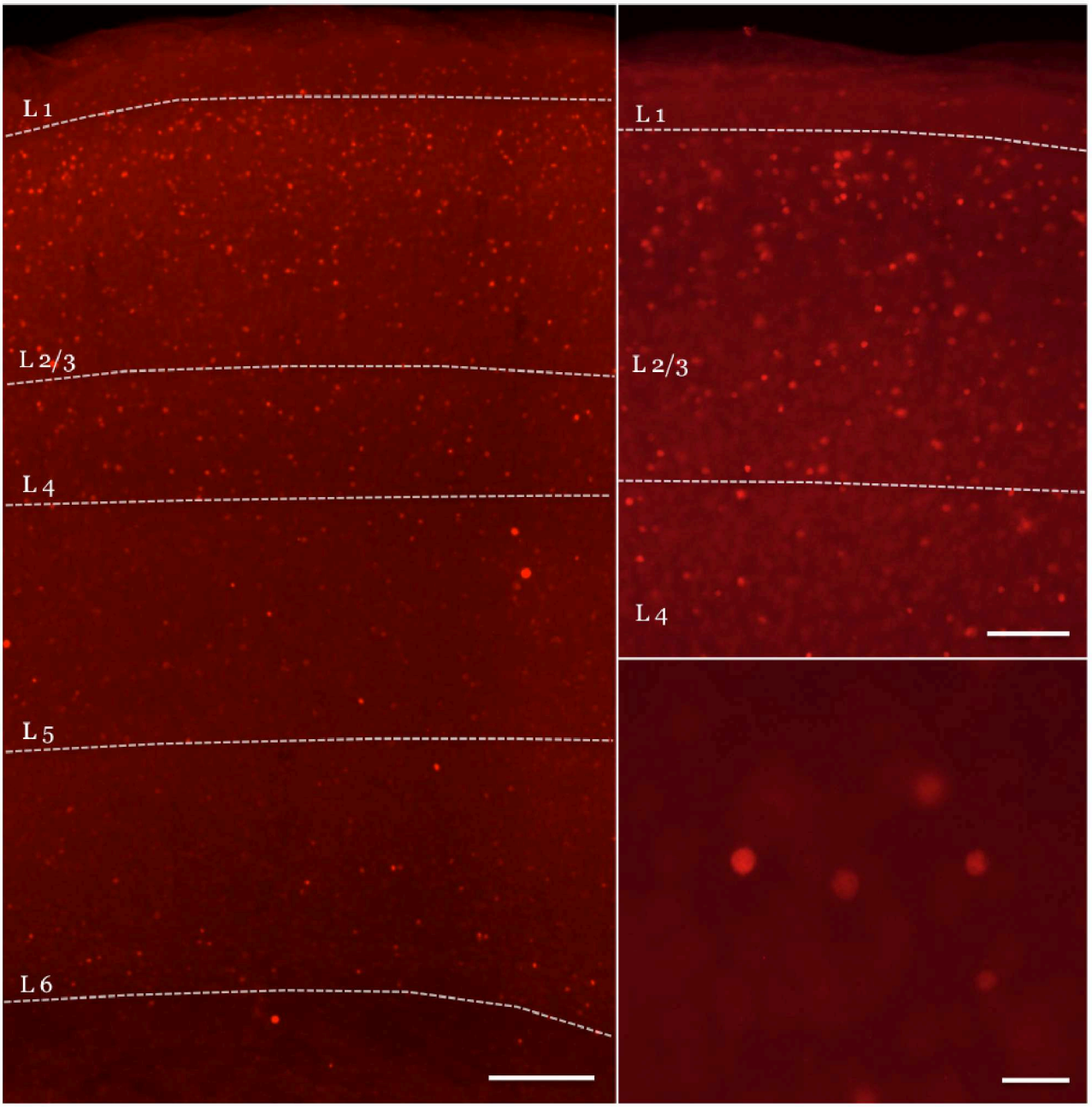

S.Fig.9. Distribution of Prox-1 across different layers in rat barrel cortex. *Fluorescence images of Prox-1 conjugated to Alexa Fluor® 647 acquired at different magnifications.* ***(Left)*** *An overview of Prox-1 distributed through different layers at 40-fold magnification. Scale bar: 150 µm.* ***(Right, top)*** *100-fold magnification of the superficial layers showing differential distribution. Scale bar: 100 µm.* ***(Right, bottom)*** *400-fold magnification of L4 Prox-1 positive neurons. Scale bar: 20 µm.*

S. table 1. Morphological parameters extracted using the Neurolucida explorer program by MicroBrightField.

Parameters describing the soma

Soma perimeter (μm)	Perimeter of the soma
Soma area (μm^2)	Area of the soma
Soma aspect ratio	Degree of flatness of the soma
Soma compactness	$\sqrt{4/\pi}$ * Area / Max diameter
Soma form factor	$4/\pi$ * Area / $(\text{perimeter})^2$
Soma roundness	$(\text{Compactness})^2$

Parameters describing the axon

Axon length (μm)	Total length for all branched structures of an axon
Axon nodes	Total number of axonal nodes
Surface area (μm^2)	Computed by modelling each piece of axonal branch as a frustum
Axon node density	Total axonal length / total axonal nodes
Total segments	Total number of the axonal line segments
Segment length average (μm)	Average of total axonal segment length
Segment length standard deviation (μm)	Standard deviation of total axonal segment length
Tortuosity average	Average of tortuosities measured for each axonal segment. Tortuosity = [Actual length of the segment] / [Distance between the endpoints of the segment]
Tortuosity standard deviation	Standard deviation of the tortuosities measured for each axonal segment
Tortuosity nodes average	Average of tortuosities measured for each axonal nodes. Tortuosity nodes = [Distance along process] / [Straight line distance]
Tortuosity nodes standard deviation	Standard deviation of the tortuosities measured for each axonal nodes
Torsion ratio	(Length of axonal process) / (Length of axonal process after applying the fan in projection)

K-dim	Describes how axonal structure fills space. Morphological dissimilarities can be identified with significant K-dim differences
Planar angle average	Average of polar angles of all axonal nodes. The polar angle is the change in direction from one branch to the next branch
Planar angle standard deviation	Standard deviation of polar angles of all axonal nodes
Local angle average	Average of local angles of all axonal nodes. The local angle is the change in direction using the line segments closest to the node
Local angle standard deviation	Standard deviation of local angles of all axonal nodes
Spline angle average	Average of spline angles of all axonal nodes. The local angle is the change in direction in the tangents that are taken at the ends of the cubic splines
Spline angle standard deviation	Standard deviation of spline angles of all axonal nodes
Sholl sections	Number of sholl sections containing axonal processes
Sholl length at 100 μm	Total length of axonal segments at 100 μm / total axonal length
Sholl length at 200 μm	Total length of axonal segments at 200 μm / total axonal length
Sholl length at 300 μm	Total length of axonal segments at 300 μm / total axonal length
Sholl length density (μm)	Total axonal length / number of axonal sholl sections
Sholl node density	Total axonal nodes / number of axonal sholl sections
Area (μm^2)	Area of the 2-D convex polygon created by connecting the tips of the distal axonal segments
Perimeter (μm)	Perimeter of the 2-D convex polygon created by connecting the tips of the distal axonal segments
Volume (μm^3)	Volume of the 3-D convex polygon created by connecting the tips of the distal axonal segments
Surface area (μm^3)	Surface area of the 3-D convex polygon created by connecting the tips of the distal axonal segments

Parameters describing the dendrites

Dendrite number	Total number of dendrites

Dendrite length	Total length for all branched structures of dendrites
Dendrite mean length	Total dendritic length / number of dendrites
Dendrite nodes	Total number of dendritic nodes
Dendrite node density	Total dendritic length / total dendritic nodes
Surface area (μm^2)	See total surface area of axon
Total segments	See total axonal segments
Segment length average (μm)	See axonal segment length average
Segment length standard deviation (μm)	See axonal segment length standard deviation
Tortuosity average	See axonal tortuosity average
Tortuosity standard deviation	See axonal tortuosity standard deviation
Torsion ratio	See axonal torsion ratio
K-dim	See axonal K-dim
Polar angle average	See axonal polar angle average
Polar angle standard deviation	See axonal Polar angle standard deviation
Local angle average	See axonal local angle average
Local angle standard deviation	See axonal local angle standard deviation
Spline angle average	See axonal spline angle average
Spline angle standard deviation	See axonal spline angle standard deviation
Sholl sections	See axonal sholl sections
Length at 50 μm	Total length of dendritic segments at 50 μm / total dendritic length
Length at 100 μm	Total length of dendritic segments at 100 μm / total dendritic length
Length at 150 μm	Total length of dendritic segments at 150 μm / total dendritic length
Sholl length density (μm)	See axonal sholl length density
Sholl node density	See axonal sholl node density
Area (μm^2)	See axonal area
Perimeter (μm)	See axonal perimeter
Volume (μm^3)	See axonal volume
Surface area (μm^3)	See axonal surface area

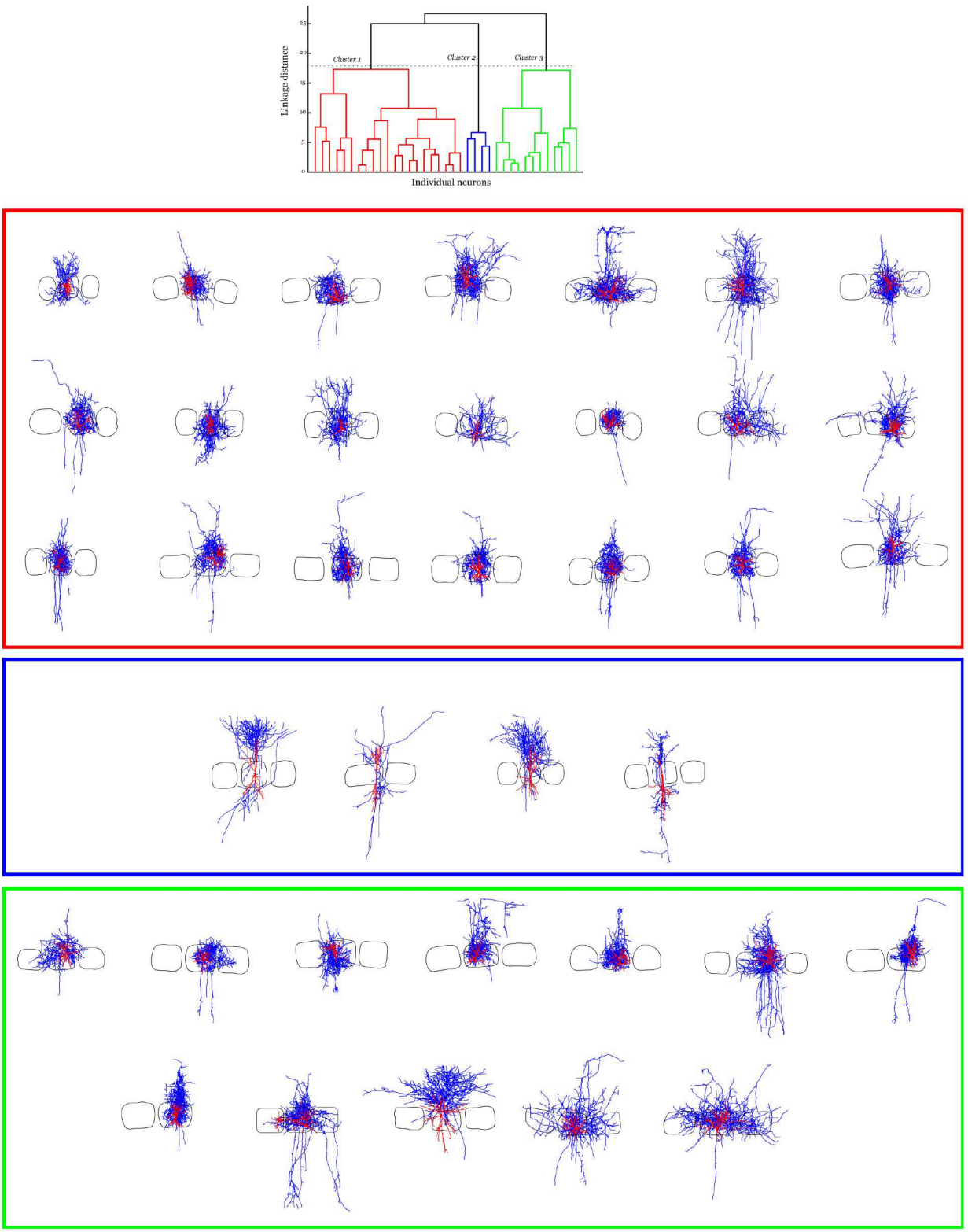

S.Fig.10. Morphological clusters of nFS interneurons based on the parameters described in S.table.1. *Using hierarchical unsupervised cluster analysis based on 64 morphological parameters, L4 nFS interneurons were classified into 3 groups. This classification is entirely different from the classification made using axonal and dendritic projection pattern as parameters (refer main text). Cluster 1 and 3 showed a combination of different axonal projection patterns, therefore resulting in a classification which is not*

Acknowledgments

I would like to express my immense gratitude to my PhD supervisor, Prof. Dr. Dirk Feldmeyer who is indeed my doctoral father. He shared with me his experiences and knowledge in the field of research which inspired me to follow high quality research. I learnt a lot of valuable qualities from him, such as dedication, determination, passion for science. I am very much indebted to his constant support throughout my doctoral work.

I owe my deepest thanks to Prof. Dr. Björn Kampa for being my second supervisor and for his endless support in several situations. I would like to extend my thanks to Prof. Dr. Frank Müller and Prof. Dr. Ted Abel for their timely help and valuable discussions.

I would like to thank Dr. Guanxiao Qi for introducing me to patch-clamp technique, who was always available to help me in everything he could. I would like to thank him very much for his collaboration in the paired recording project. Special thanks to Werner Hucko, without whose effort in histological staining, it would be impossible to visualise neurons under microscope, which helped me a lot in doing high quality morphological reconstructions. He was always available to help us with any technical problem in the laboratory. I would like to extend my thanks to Dr. Manuel Marx, who helped me a lot in imaging techniques, administrative work, and was always available for any kind of help.

For making my PhD days pleasant and enjoyable and for creating a nice working atmosphere in the lab, I would like to thank my lab members - Dr. Guanxiao Qi, Dr. Manuel Marx, Dr. Gabriele Radnikow, Werner Hucko, Dr. Claudia Barz, Dr. Jiali Tang, Chao Ding, Danqing Yang, Dr. Haijun Wang, Ramya Rama, and Jawad Jawadi. I would also like to thank all my friends outside the lab, especially Mahendran, Neethu, Kanchan, Poorni, Shampali and Judith who were there for me during my thick and thin.

I would like to thank International Research Training Group - 1328, Aachen for supporting me financially during three years of my PhD work.

Finally, I would like to thank my family, Sivarajan, Nagaretnam, Kishore, Priya and my Swiss family, Doris, Pascal, and my partner Marc Emmenegger for having faith in me and their constant encouragement and support during the whole process of finishing this thesis. To them, I dedicate this thesis.

Curriculum Vitae

Personal details

Name	Vishalini Sivarajan
Date of birth, place	25.01.1987, in Chennai
Email	vishalini.sivarajan@rwth-aachen.de
Nationality	Indian
Marital status	Single

Education

Since October 2012	PhD student in the group of Prof. Dr. Dirk Feldmeyer, RWTH Aachen University, Germany
2007 - 2009	M.Sc. Neuroscience, University of Madras, India *Dissertation*: Neuroprotective effects exerted by bone marrow derived mesenchymal stem cells on neurons subjected to oxidative stress
2004-2007	B.Sc. Zoology, Women's Christian College, Manonmanian Sundaranar University, India

Research Positions

August 2015 - December 2015	Visiting researcher in the group of Prof. Dr. Ted Abel, University of Pennsylvania, Philadelphia, USA
July 2012 - March 2013	Research assistant in the group of Prof. Dirk Feldmeyer, RWTH Aachen University, Germany
January 2011 - June 2012	Research assistant in the group of Prof. Dr. Alexander Gail, Deutsches Primatenzentrum, Goettingen, Germany
July 2009 - October 2010	Research assistant in the group of Prof. Dr. Neeraj Jain, National Brain Research Centre, Gurgaon, India

Awards

- International Research Training Group - 1328 Scholarship funded by Deutsche Forschungsgemeinschaft (DFG) for the completion of PhD at the RWTH Aachen University from April 2013 to March 2016

- Best Poster Award at the Neurovision conference in the category 'Connectivity and Networks' held in Forschungszentrum Juelich on September 26, 2014
- University Rank II for Master's degree in Neuroscience at the University of Madras for the year 2007-09
- University Rank IV for Bachelor's degree in Zoology at the Manonmaniam Sundaranar University for the year 2004-07

Conferences

- Poster presentation at the BaCoFun meeting held in Amsterdam, The Netherlands on May 19-21, 2016
- Poster presentation at the Society of Neuroscience (SfN) held in Chicago, USA on October 17-21, 2015
- Oral presentation at the Barrels meeting XXVIII held in Chicago, USA on October 15-16, 2015
- Poster presentation at the Gordon Research Conference held in Maine, USA on August 16-21, 2015
- Oral presentation at the Gordon Research Seminar held in Maine, USA on August 14-15, 2015
- Poster presentation at the Neurovision conference held in Forschungszentrum Juelich on September 26, 2014